2008-01-01

Development of Fiber Bend Loss Edge Filter

Pengfei Wang

Technological University Dublin

Development of Fiber Bend Loss Edge Filter

A thesis

submitted for the degree of Doctor of Philosophy

by

PENGFEI WANG, *MSc*

School of Electronic and Communications Engineering

Faculty of Engineering

Dublin Institute of Technology

Supervisors: Dr. Gerald Farrell and Dr. Yuliya Semenova

Dublin, Ireland

November, 2008

To my mother, my wife with all my love

In memory of my father

Abstract

This PhD thesis addresses several aspects of macrobending loss in single-mode optical fibers. The context for the work is the development of an edge filter for a rapid wavelength measurement system. Based on scalar approximation theory and the beam propagation method, a simulation platform is developed and used to predict the macrobending loss of singlemode fiber with single or multiple coating layers.

A single-mode step index fiber macrobending loss edge filter is investigated theoretically in terms of baseline loss, discrimination range and polarization dependent loss (PDL). The theoretical analysis is supported by a range of experimental investigations and results. The bend loss characteristics of a conventional SMF28 based edge filter are investigated. The bend loss characteristics of a high bend loss fiber based edge filter are also investigated for comparison. It is shown that while the high-bend loss fiber based filter requires significantly fewer bend turns and exhibits a lower PDL, temperature dependence can be a major issue. A fiber selection method, specifically for an edge filter application, is reported and using this method a fiber is selected for a fiber bend loss edge filter that shows significantly improved spectral response (measured baseline loss is 5.09 dB and discrimination range is 17.42 dB) coupled to a lower average PDL and simpler fabrication technique.

A theoretical model for macrobending-induced temperature dependent loss (TDL) for a fiber with dual coating layers is presented, with good agreement demonstrated between theoretical calculations and experimental results. The impact of temperature on two examples of an all-fiber based edge filter is also

investigated theoretically and experimentally and using the developed model, it is shown that it is possible to predict the impact of temperature variations on an all-fiber based edge filter. The effect of temperature on polarization dependent loss is presented theoretically and experimentally as well.

The impact of fiber manufacturing tolerances is also investigated and it is shown that variations in the numerical aperture and fiber core radius can have significant impact on the spectral response of an edge filter. A simple bend radius tuning technique is proposed to mitigate the effect of fiber manufacturing tolerances.

A complete methodology for the design of a fiber based edge filter is presented, starting with the task of selecting suitable fibers and then considering the design of a fiber bending loss edge filter. Through the comparison of the performances of two previously developed types of fiber edge filters, as an example, a Corning SMF28e fiber with 900 μm jacket is selected as a tradeoff between SMF28 and 1060XP fiber and an edge filter design is undertaken.

Finally, a subsidiary objective of this thesis is to explore novel applications for macrobending fiber based optical sensing devices. In this context, a macrobending fiber based refractometer sensor is studied theoretically, and a new theoretical model based on a 3-dimensional full-vectorial finite difference beam propagation method for accurately predicting the fiber bending loss is also presented.

Declaration

I certify that this thesis which I now submit for examination for the award of PhD, is entirely my own work and has not been taken from the work of others save and to the extent that such work has been cited and acknowledged within the text of my work.

This thesis was prepared according to the regulations for postgraduate study by research of the Dublin Institute of Technology and has not been submitted in whole or in part for an award in any other Institute or University.

The work reported in this thesis conforms to the principles and requirements of Institute's guidelines for ethics in research.

The Institute has permission to keep, to lend or to copy this thesis in whole or in part, on condition that any such use of the material of the thesis be duly acknowledged.

Signature 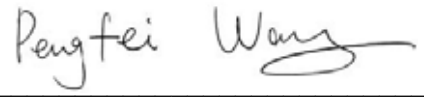 _____ Date___26/11/2008_____

Candidate

Acknowledgements

The work presented in this thesis has been carried out within the Photonics Group, at the Applied Optoelectronics Center of the Dublin Institute of Technology.

There are numerous people without whose support this thesis would be impossible. Firstly I would like to express the most sincere gratitude to my supervisor, Dr. Gerald Farrell for giving me this opportunity to further my education. I also want to thank him for all his guidance, support and patience during my doctoral studies, and for allowing me the freedom to pursue my own ideas and interests. I am deeply indebted to Dr. Yuliya Semenova and Dr. Qian Wang for their guidance, comments, encouragement and willingness to serve as my associate supervisors.

A special thank goes to the Center's Manager, Mr. Thomas Freir, for his assistance in technical writing, project management and the many valuable discussions that facilitated my research. It was a great honor to work with you in the past three years.

I would like to also extend my sincere thanks to all the faculty, staff and students in the Applied Optoelectronics Center and the School of Electronic and Communications Engineering for their friendship, technical assistance, and support. Without their efforts and support, I would never have continued my academic development at the Dublin Institute of Technology. The pleasure was mine to meet and work with these people.

The Optical fiber Research Departments of Corning and Nufern Ltd. in the United State of America kindly provided us with data and many of the fiber

samples used in the measurements. This is acknowledged and highly valued. I also want to gratefully acknowledge the financial support of Enterprise of Ireland for the work.

Finally I would like to express my gratitude to my deepest love, my wife, for her help, support and encouragement in every aspect of my life and to my parents and sister, who raised me and trust me with their endless love. Especially, for my father, who has contributed his life to the family and was one of those extraordinary people who will never be forgotten in my life. His life was like a sunbeam that lit up the world around me, now I can bask in the rainbow of the memories that I'll nurture in the years ahead. My thoughts are always with you!

List of publications arising from research

Journal papers

1. **P. Wang**, G. Farrell, Y. Semenova, G. Rajan, "*Investigation of Polarization Dependent Loss for a Macrobending Loss Sensitive Singlemode Fiber*," **Microwave and Optical Technology Letters**, accepted for publication.
2. **P. Wang**, Y. Semenova, G. Rajan, T. Freir and G. Farrell, "*The temperature dependence of polarization dependent loss for a macrobending singlemode fiber based edge filter*," **IEEE Photonics Technology Letters**, accepted for publication.
3. **P. Wang**, G. Rajan, G. Farrell, Y. Semenova, "*Temperature dependence of a macrobending edge filter based on a high-bend loss fiber*," **Optics Letters**, Vol. 33, No. 21, pp. 2470-2472, 2008.
4. **P. Wang**, G. Farrell, Y. Semenova, G. Rajan, "*Influence of fiber manufacturing tolerances on the spectral response of a bend loss based all-fiber edge filter*," **Applied Optics**, Vol. 47, No. 16, pp. 2921-2925, 2008.
5. **P. Wang**, Y. Semenova, G. Farrell, "*Temperature dependence of macrobending loss in all-fiber bend loss edge filter*," **Optics Communications**, Vol. 281, pp. 4312-4316 , 2008.
6. **P. Wang**, G. Farrell, Q. Wang and G. Rajan, "*An Optimized Macrobending-Fiber-Based Edge Filter*," **IEEE Photonics Technology Letters**, Vol. 19, No. 15, pp. 1136-1138, 2007.
7. **P. Wang**, Q. Wang, G. Farrell, et. al., "*Investigation of Macrobending Losses of Standard Single Mode Fiber with Small Bend Radii*," **Microwave and Optical Technology Letters**, Vol. 49, No. 9, pp. 2133-2138, 2007.
8. Q. Wang, G. Rajan, **P. Wang** and G. Farrell, "*Resolution investigation of ratiometric wavelength measurement system*," **Applied Optics**, Vol.46, No.25, pp. 6362-6367, 2007.
9. Q. Wang, G. Rajan, G. Farrell, **P. Wang**, et al., "*Macrobending fiber loss filter, ratiometric wavelength measurement and application*," **Measurement Science and Technology**, Vol. 18, pp. 2082-3088, 2007.

10. Q. Wang, G. Farrell, **P. Wang**, G. Rajan and T. Freir, "*Design of Integrated Wavelength Monitor based on a Y-branch with an S-bend Waveguide*," **Sensors and Actuators A**, Vol.134, No.2, pp.405-409, 2007.
11. Q. Wang, G. Rajan, **P. Wang** and G. Farrell, "*Polarization dependence of bend loss for a standard singlemode fiber*," **Optics Express**, Vol.15, No.8, pp. 4909-4920, 2007.
12. Q. Wang, G. Farrell, T. Freir, G. Rajan and **P. Wang**, "*Low-cost Wavelength Measurement based on a Macrobending Singlemode Fiber*," **Optics Letters**, Vol. 31, No. 12, pp. 1785-1787, 2006.

Journal papers under review

13. **P. Wang**, G. Farrell, Y. Semenova, "*A generalized design process for fiber bend loss based edge filters for a wavelength measurement system*," Submitted to **Applied Optics**. Manuscript ID: 106080.

Conference proceeding papers

1. **P. Wang**, G. Farrell, Y. Semenova, Q. Wang, A. M. Hatta and G. Rajan, "*Accurate theoretical prediction for singlemode fiber macrobending loss and bending induced polarization dependent loss*," Optical Sensors 2008, Proceedings of SPIE, Vol. 7003, pp. 7003Y1-7003Y13, 2008.
2. **P. Wang**, Y. Semenova, G. Farrell, "*A Macrobending Singlemode Fiber Based Refractometer: Proposal and Design*," Oral Presentation at the IOP Photon 08 Conference, Edinburgh, 26-28th August 2008.
3. Q. Wang, G. Rajan, **P. Wang** and G. Farrell, "*Resolution of Ratiometric System for Wavelength Measurement*," SPIE Europe: Optics and Optoelectronics, Prague, March 2007.
4. **P. Wang**, Y. Semenova, G. Farrell, "*A macrobending fiber based temperature sensor with a bending radius tuning*," SPIE Defense, Security and Sensing, Florida, accepted, Manucript ID: DSS09-DS205-10.

Contents

List of Figures

List of Tables

Chapter 1

Introduction

This chapter introduces the background, motivation and objectives of the research, and an overview of the thesis layout is included.

1.1 Background to the research

The measurement of an unknown wavelength is a common operation for many optical systems. Examples include wavelength monitoring in multichannel dense wavelength division multiplexing (DWDM) optical communication systems and optical sensing systems based on fiber Bragg grating (FBG) or on Fabry–Perot (FP) filters.

DWDM requires accurate control of each channel's wavelength, so wavelength measurement becomes indispensable in accurate setting and maintaining of an individual transmitter's wavelength [1, 2].

Fiber-sensing technology has reached qualitatively new performance levels with the development of FBG filters [3]. Such FBG and FP filters based optical sensing systems can convert a range of detectable measurands, such as temperature, strain or pressure, etc, into a central wavelength shift of a reflection peak and such techniques have been extensively investigated in recent years. However, the technique requires a wavelength demodulation system to detect the wavelength shift of reflected light, which is crucial in the successful implementation of the optical sensing system.

1.1.1 Wavelength measurement using an edge filter in a ratiometric power measurement scheme

There are numerous wavelength-measurement schemes and among them the ratiometric detection scheme [4-7], which undertakes wavelength measurement by means of a signal-intensity measurement, has a simple configuration and offers the potential for high-speed measurement as compared with methods such as wavelength scanning based active measurement schemes. A ratiometric detection scheme employs an edge filter and utilizes the transition region of the filter's spectral transmission response. The edge filters can be based on bulk thin film filters [4], biconical fiber filters [6], fiber gratings [7], multimode interference couplers [1], directional couplers [2], etc.

In this thesis, a simple all-fiber ratiometric wavelength measurement scheme is proposed and demonstrated in which a macrobending singlemode fiber is employed as an edge filter. By comparison with existing active wavelength scanning techniques [6, 7], it has a simple configuration, requires no mechanical movement and offers a potential for high-speed measurement. This all-fiber wavelength measurement technique offers useful advantages such as ease of fiber interconnection, mechanical stability, and low polarization dependence as compared with ratiometric systems involving bulk filters or integrated optical waveguide based filters.

For macrobending singlemode fiber, most of the previously published investigations focused on how to predict and lower the bend loss, which is regarded as an adverse effect for light transmission [8-10]. There are also some studies employing bent fibers as optical sensing elements. The

wavelength dependence of a bending fiber was reported in some studies [11, 12], but there have been very few investigations that employ this wavelength dependent characteristic for practical applications, for example as a part of a wavelength demultiplexer [13]. In this thesis, using simple surface processing, a macrobending standard singlemode fiber is developed as an edge filter and used in a ratiometric wavelength measurement system. By comparison with existing ratiometric wavelength measurement schemes based on a wavelength division coupler or biconical fiber filter, a macrobending fiber based edge filter has a lower fabrication cost while offering a flexible spectral response and measurable wavelength range, through the adjustment of the length of the macrobending section.

1.1.2 Spectral requirements for an edge filter in a wavelength measurement application

Previous investigations [6, 7] of a ratiometric detection scheme have mainly focused on different types of edge filters, and there have been few investigations concerning the transmission response of the edge filter. Defining the transmission response, specifically the wavelength range and slope of the transition region, is the preliminary work in the design of these edge filters for wavelength measurement.

Figure 1 (a) shows a schematic configuration for a ratiometric wavelength measurement system employing a fiber bending loss edge filter. The input signal is split into two equal signals. One passes through a reference arm (lower arm) and the other passes through the fiber bending loss edge filter (upper arm). A photodiode is placed at the end of each arm. By measuring the ratio of the electrical outputs of the two photodiodes, one

can determine the wavelength of the input signal, assuming a suitable system calibration has taken place.

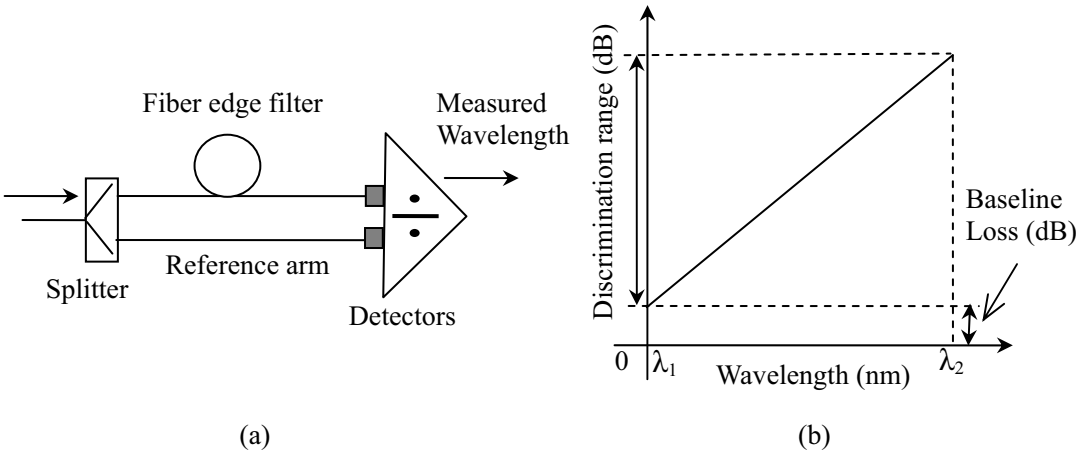

Figure 1. (a) Schematic structure of bending fiber based wavelength measurement; (b) Spectral response of fiber bending loss edge filter.

The bend loss wavelength characteristic of the filter is a critical issue. As shown in Fig. 1(b), a bend loss based edge filter operates over a wavelength range from λ_1 with a progressively larger attenuation as the wavelength increases from λ_1 to λ_2. The two key parameters for specifying an edge filter are the baseline loss and discrimination range. The baseline loss is defined as the loss of the filter at λ_1, while the discrimination range is the difference between the attenuation at λ_1 and λ_2.

For the wavelength measurement application that underpins the research described in this thesis, a low transmission loss at wavelength λ_1 with a suitable discrimination range that matches the wavelength measurement range is required. For the purpose of the research described in the thesis, the wavelength range is from 1500 nm to 1600 nm, which overlaps the major optical communications and sensing wavelength windows.

Intuitively, from Fig. 1b, the slope of the transmission response for the

edge filters should be as large as possible to ensure a high resolution for the measurement system given the limited precision of power detectors. However, in practice, an acceptable slope of the bend loss is determined by the signal-to-noise ratio of the input signal [14]. Assuming a limited precision of power detectors, such a ratiometric system was analyzed theoretically by Wang et al in the context of the limited signal-to-noise ratio (SNR) of the input signal, and it was shown that for a given measurable wavelength range from 1500 to 1600 nm, the acceptable slope of the edge filter is determined due to the noise of the input signals [14]. The noise of the photodetectors also plays an important role in determining the resolution of the ratiometric wavelength measurement system, i.e., the minimal wavelength shift that the system can detect, which is an important specification in the evaluation of the measurement performance. In further work by Wang et al [15], a wavelength measurement system involving the source, the edge filter, and the photodiodes was modeled. In that work both the theoretical and experimental results indicated that the limited SNR of the signal source, the noise of the photodetectors, and the other noise sources, such as receiver shot and thermal noise in the ratiometric system, have a significant impact on the selection of the spectral response for the edge filter used.

1.1.3 Characteristics of a fiber bending loss edge filter

For a macrobending fiber based edge filter employed in a wavelength measurement system, both the polarization dependence and temperature dependence of macrobending loss have a significant influence on the

transmission spectrum over the whole wavelength range, and thus affect the accuracy of wavelength measurement [16, 17].

In general polarization dependence in optical communications and sensing systems is mostly caused by fiber bending, angled optical interfaces, dichroism and oblique reflection, and it always degrades the performance of fiber based communications or sensing systems. For the polarization dependence of macrobending loss, the difference in the refractive index between the polymer coating layer and the cladding layer is much higher by comparison to that between the cladding and core. The reflectance of the radiated field occurring at the interface between the coating layer and cladding layer differs for different polarization states [16], which can lead to polarization dependence of the bend loss due to the coupling between the reflected radiated field and the quasi-guided fundamental mode. In this thesis, the polarization dependence of macrobending singlemode fiber edge filters is investigated theoretically and experimentally.

For temperature dependent loss, temperature changes can adversely affect the fiber macrobending loss and thus can have a significant influence on a wavelength measurement system. Temperature dependence is commonly described as a function of the different thermal expansion coefficients (TEC) and thermo-optic coefficients (TOC) of the fiber materials. As is well known, the refractive index of an optical material depends on temperature and wavelength. For silica material, the refractive index varies with the temperature as a result of lattice deformations in the silica matrix structure. For a fiber polymer coating material, the variation of the refractive index is induced by the amplitude of vibrations of polymer

molecules and results in the translation and distortion of the cross-linked network within the polymer long molecule structure. In this thesis, the influence of temperature on the bend loss and polarization characteristics of the macrobending singlemode fiber based edge filters is investigated both theoretically and experimentally. The theoretical model takes into account the influence of the temperature dependent parameters, such as TOC and TEC on the refractive index of the bending fiber layers and their physical dimensions.

1.1.4 Theoretical background of fiber bending loss

The total loss of a bending fiber includes the pure bending loss and transition loss caused by mismatch between the quasi-mode of the bending fiber and the fundamental mode of the straight fiber. The pure bending loss is investigated in this thesis and for a single mode fiber with a bending length L, it has the form [18]:

$$L_s = 10\log_{10}\left(\exp(2\alpha L)\right) = 8.686\alpha L \qquad (1.1)$$

where α is an bending loss factor, which is determined by the fiber structure, bending radius and input wavelength. Most theoretical investigations about fiber bend loss are focused on calculation of this bending loss factor.

The simulation of fiber bending loss began in 1970s. D. Marcuse [19] first developed the basic model for predicting the bending loss of optical waveguide/fiber assuming a core-infinite cladding structure in a cylindrical coordinate system. The analytical expression for calculating the fiber bend loss coefficient α with an infinite cladding can be expressed as follows:

$$2\alpha = \frac{\sqrt{\pi}\kappa^2 \exp\left[-\frac{2}{3}\left(\gamma^3 / \beta_g^2\right)R\right]}{e_v \gamma^{2/3} V^2 \sqrt{R}\mathrm{K}_{v-1}(\gamma a)\mathrm{K}_{v+1}(\gamma a)} \tag{1.2}$$

where $e_v = 2$, a is the radius of fiber core, R is the bending radius, β_g is the unperturbed propagation constant of the straight-fiber fundamental mode, $\mathrm{K}_{v-1}(\gamma a)$ and $\mathrm{K}_{v+1}(\gamma a)$ are the modified Bessel functions and V is the well known normalized frequency, which can be defined as:

$$V = \frac{2\pi a \cdot NA}{\lambda} \tag{1.3}$$

and κ, γ can be defined as follows:

$$\kappa = \sqrt{n_1^2 k^2 - \beta_g^2} \tag{1.4}$$

$$\gamma = \sqrt{\beta_g^2 - n_2^2 k^2} \tag{1.5}$$

where $k = 2\pi / \lambda$ is the vacuum wavenumber at the wavelength of λ and n_1, n_2 is the refractive index of the fiber core and cladding, respectively.

The model has several limitations: 1) it can only be used for predicting the bending loss with a core-infinite coating structure; 2) it cannot be employed for calculating the reinjected field arising from reflections at the cladding-coating interface.

A practical fiber usually contains more than a single cladding layer. It also has one or two coating layer(s) which offer mechanical protection. The existence of the coating layer will produce a so-called whispering-gallery mode* for a bending fiber due to the reflection of radiated field at the

* In the previous published work [20, 25], the term "whisper-gallery mode" has been used to describe the interference between the reflections and fundamental core modes, however, in opinion of some researchers, the term "cladding mode" could be used to describe such interference occurring at the region of the fiber cladding. In this thesis, "whispering-gallery mode" is utilized for consistency with the published papers.

interface between the cladding and coating layer(s). In order to consider the effect of this reflection on the bending loss, some more complex models concerning the bending loss factor α have been proposed. Three different formulas have been developed in the literatures [9, 12, 20], respectively and they all are based on the perturbation theory. As a starting point for the scalar approximation method, in 1985, a perturbation theory for analyzing the LP_{on} mode of a circular fibre by a quasi-degenerate field was built by C. Vassallo [21]. The perturbation formula can be expressed as:

$$2\gamma_a \delta\gamma \iint \psi_a^2 dxdy = {2\pi R_{pert} \psi_a(\rho)^2} \Big/ {K_0(\kappa\rho)} \tag{1.6}$$

where γ_a is the propagation constant of the straight-fiber fundamental mode, $\delta\gamma$ is the a linear function of the perturbing field, ψ_a is the scalar field in the fundamental core mode, ρ is the fiber core radius, R_{pert} is an effective reflection coefficient.

Based on the scalar approximation method developed above, I. Valiente and C. Vassallo [20] presented a new approach for calculating bending losses in coating singlemode weakly guiding optical fibers. The scalar field can be expressed with two parts as follows:

$$\Psi(x,y) = \begin{cases} \sum_{p=1}^{N} \left\{ C_p Bi[X_{2,p}(x)] + R_p Ai[X_{2,p}(x)] \right\} \cos\beta_p y & a \le x \le x_h \\ \sum_{p=1}^{N} D_p \left\{ Bi[X_{3,p}(x)] - iAi[X_{3,p}(x)] \right\} \cos\beta_p y & b \le x < \infty \end{cases} \tag{1.7}$$

Assuming that bending takes place in the *x*-plane, β_p is the real root of the conjugate variable for the Fourier transform in the restricted narrow *y*-region (see Figure 1 in I. Valiente and C. Vassallo, 1989 [20]) and it can be expressed as: $\beta_p = (2p-1)\pi/2h$, (where *p* is positive integer, *p*=1, 2, …); *h*

is defined as an imaginary factor on the y axis in the cylindrical system, which can define the boundary (x_h) between the scalar field of the cladding mode and that of the fundamental mode on the x axis. The bend loss coefficient α is expressed as an imaginary part here:

$$\alpha = -\mathrm{Im}\left[\frac{\pi \cdot \Psi_R(0,0)}{\gamma_0 \cdot \int \Psi_0^2 dxdy}\right] \tag{1.8}$$

where γ_0 is the propagation constant of straight fiber LP_{01} mode.

A simple formula for the bend loss factor α was presented by Hagen Renner [9],

$$\alpha = \alpha_0 \frac{2\sqrt{Z_2 Z_1}}{(Z_2 + Z_1) - (Z_2 - Z_1)\cos(2\theta_0)} \tag{1.9}$$

where $Z_q = -\left(2k2n_q^2/R\right)^{2/3} X_q(x_2,0)$, $q = 1,2$; $\theta_0 = \frac{2}{3}\left[-X_1(x_2,0)\right]^{3/2} + \frac{\pi}{4}$

and $X_q(x_2,0) = \left(\frac{R}{2k^2 n_q^2}\right)^{2/3}\left[\beta^2 - k^2 n_q^2\left(1 + \frac{2x}{R}\right)\right]$.

In Formula (1.9), α_0 is determined by the calculated bend loss factor based on the previous simple model (1.2) and (1.8). This simple formula (1.9) was derived based on some approximations. A more complex but reliable and effective formula which considered the conjugate variable of the Fourier transform has been presented [12]:

$$2\alpha = \frac{2\kappa^2}{\beta V^2 K_1^2(x_1\gamma)} \int_0^\infty \frac{\exp[-x_1\sqrt{\gamma^2+\zeta^2}]}{\sqrt{\gamma^2+\zeta^2}} \cdot \frac{Ai[X_1(0,\zeta)]}{Bi[X_1(x_1,\zeta)]} \frac{\sqrt{\chi_1\chi_2}}{\left[\chi_1 \cos^2\theta(\zeta) + \chi_2 \sin^2\theta(\zeta)\right]} d\zeta \tag{1.10}$$

where $X_q(x,\zeta)=\left(\frac{R}{2k^2n_q^2}\right)^{2/3}\left[\beta^2+\zeta^2-k^2n_q^2(1+\frac{2x}{R})\right]$, ζ is the conjugate variable for the Fourier transform, and can be treated as a deformation of β_p mentioned in formula (1.7), $\chi_q=\left(\frac{2k^2n_q^2}{R}\right)^{2/3}\left[-X_q(x_2,\zeta)\right]$, $\theta(\zeta)=\frac{2}{3}[-X_1(b,\zeta)]^{3/2}+\frac{\pi}{4}$, and A_i and B_i are Airy functions.

These expressions, from (1.8) to (1.10), accurately describe bend loss for a fiber with only one coating layer. However, most existing common fibers have more than one coating layers or the fiber itself is a multiple cladding structure, such as the Corning (Corning Inc., New York) standard singlemode fiber-SMF28 which has core, cladding, inner coating and outer coating layers. Recent studies suggest that a fiber designed with multiple claddings could have a low bending loss, for example a fiber with a refractive index profile of depressed and elevated ring structure [22]. Therefore, a model for predicting bend loss for a fiber with multiple cladding or coating layers is considered in this thesis based on perturbation theory, which can be used for modeling and design of multi-cladding or coating fiber devices involving or utilizing bend loss.

Based on the same scalar approximations made in Ref. [9] and [12], the field in the cladding layers of the bending fiber satisfies the equation:

$$\frac{d^2\tilde{\psi}_q(x,\zeta)}{dx^2}+\left[k^2n_q^2\left(1+\frac{2x}{R}\right)-\beta_0^2-\zeta^2\right]\tilde{\psi}_q(x,\zeta)=0 \qquad (1.11)$$

where $\tilde{\psi}_q(x,\zeta)$ is the Fourier transformation of the field in cladding along y-axis. $n_q\,(q=1,2...N)$ is the refractive index of cladding layer and β_0 is the propagation constant of the straight fiber. With Eq. (1.11) we have

$$\psi_q(x,y)=\frac{1}{2\pi}\int_{-\infty}^{+\infty}\left[D_q(\zeta)B_i\left(X_q\right)+H_q(\zeta)A_i\left(X_q\right)\right]\exp(-i\zeta y)d\zeta \quad (1.12)$$

where $X(x,\zeta)=\left(\frac{R}{2k^2n_q^2}\right)^{2/3}\left[\beta^2+\zeta^2-k^2n_q^2\left(1+\frac{2x}{R}\right)\right]$. B_i and A_i are Airy functions. In order to calculate the bend loss factor, we have to calculate the coefficients $D_q(\zeta)$ and $H_q(\zeta)$ in each cladding layer. At the outermost layer, there is a relationship between $D_N(\zeta)$ and $H_N(\zeta)$: $H_N(\zeta)=-iD_N(\zeta)$. For two arbitrary adjacent layers, according to field-continuous boundary conditions, we have

$$\begin{cases}D_j(\zeta)B_i\left[X_j(x_j,\zeta)\right]+H_j(\zeta)A_i\left[X_j(x_j,\zeta)\right]=D_{j+1}(\zeta)B_i\left[X_{j+1}(x_j,\zeta)\right]+H_{j+1}(\zeta)A_i\left[X_{j+1}(x_j,\zeta)\right]\\ D_j(\zeta)B_i'\left[X_j(x_j,\zeta)\right]+H_j(\zeta)A_i'\left[X_j(x_j,\zeta)\right]=D_{j+1}(\zeta)B_i'\left[X_{j+1}(x_j,\zeta)\right]+H_{j+1}(\zeta)A_i'\left[X_{j+1}(x_j,\zeta)\right]\end{cases} \quad (1.13)$$

Therefore, $\begin{bmatrix}D_1(\zeta)\\H_1(\zeta)\end{bmatrix}=\begin{bmatrix}M_{11}&M_{12}\\M_{21}&M_{22}\end{bmatrix}\begin{bmatrix}D_N(\zeta)\\H_N(\zeta)\end{bmatrix}$, when considering all the cladding layers. The relationship between $D_1(\zeta)$ and $H_1(\zeta)$ is obtained as $D_1(\zeta)=\frac{M_{11}i+M_{12}}{M_{21}i+M_{22}}H_1(\zeta)=GH_1(\zeta)$.

According to the boundary condition at the interface between the core layer and inner cladding layer, again one has

$$D_1(\zeta)B_i\left[X_2(x_1,\zeta)\right]+H_1(\zeta)A_i\left[X_2(x_1,\zeta)\right]=\frac{\pi}{\sqrt{\gamma^2+\zeta^2}}\exp\left(-a\sqrt{\gamma^2+\zeta^2}\right) \quad (1.14)$$

Therefore, $$H_1(\zeta)=\frac{\pi}{\left(GB_i\left[X_1(x_1,\zeta)\right]+A_i\left[X_1(x_1,\zeta)\right]\right)\sqrt{\gamma^2+\zeta^2}}\exp\left(-a\sqrt{\gamma^2+\zeta^2}\right)$$

and according to the perturbation theory, the bend loss factor can be calculated by

$$2\alpha=-2\frac{\kappa^2}{2\pi\beta V^2K_1^2(a\gamma)}\mathrm{Im}\left(\int_{-\infty}^{\infty}H_1(\zeta)A_i\left[X_2(0,\zeta)\right]d\zeta\right) \tag{1.15}$$

Our developed modeling platform can be utilized to not only investigate the design of a novel fiber bending loss edge filter, but also can take account of the effect of 1) temperature influence involving in the thermal optical coefficient on the size of fiber each layer and thermo-optic coefficient on the refractive index of fiber material; 2) different polarization states involving in the different boundary condition in equation (1.13) and 3) fiber tolerance involving in the given manufacturing tolerance range.

In most previous published papers [8, 9, 12, 20, 23-24], the effective bend radius (wavelength dependent correction factor*) was employed to achieve good agreement between the modeled results and the experimental results due to the effect of fiber bending stress on refractive index profile. Experimental results have shown that the fiber effective bend radius mostly depends on the fiber structure and the wavelength used, e.g., for different fiber parameters, $R_{eff}\approx 1.23R_{\exp}$ in Ref. [20], while $R_{eff}\approx 1.27R_{\exp}$ in Ref. [24]. For different wavelengths, the effective bend radius changes between 1.269 at 1350 nm up to 1.334 at 1600 nm in Ref. [8]. However, it is shown in a previously published investigation of Corning standard singlemode fiber-SMF28 fiber bend loss [25] with a dual coating layer, that the effective

* In the opinions of some researchers, the effective bend radius should be is referred to as a "calibration factor". However, in this thesis, the term "wavelength dependent correction factor" is used to maintain consistency with the published work that forms the basis of this thesis.

bend radius was not required in the theoretical models.

To take account of the fact that fiber stress can cause a refractive index change, in the previous publications using the calculation method proposed in Ref. [12], a good agreement between modeled and experimental data was by utilizing an effective bend radius equal to 1.325 times to the real bend radius for a wavelength of 1480nm. The major difference between the research presented in this thesis and the previous investigations is the fiber type. Previously published investigations of fiber bend loss have been focused on some special fibers (particularly fibers with small numerical apertures) rather than standard single mode fibers (SMF28). For example, the parameter V^* of the fiber LB1000 employed in Ref. [12] is 1.68 at a wavelength of 1480 nm. However, for the SMF28 used in this research the corresponding fiber parameter V is about 2.123. These differences between fibers are suggested as the reason for the difference between the results in Ref. [25] and those in previous publications.

1.2 Motivation and the objectives of the research

The numerous wavelength measurement schemes in existence can be divided into passive wavelength measurement schemes and active wavelength measurement schemes. Most of the existing passive schemes [4], employing wavelength sensitive optical devices, have a simple configuration and offer high-speed measurement, but suffer from a limited resolution due to associated problems with the use of bulk-optic filter/collimation components

---

* V is the well known normalized frequency, which can be defined as: $V = \frac{2\pi a \cdot NA}{\lambda}$, where a is the core radius of the fiber, NA is the numerical aperture, and λ is the wavelength.

and associated alignment stability or a limited wavelength range due to the spectral characteristics of the employed optical devices. Active schemes [7], mainly using wavelength-scanning technologies, which can achieve high resolution and a wide range, require much more complicated configurations and have a low measurement speed as compared to the passive schemes. A classic commercial instrument measuring the wavelength of light involves an interferometer or a monochromator, suffering from high cost and inherently slow measurement speed due to the mechanical motion involved.

The core aim of this research and thesis is to:

Develop an effective modeling platform for singlemode fiber bend loss which can deal with a variety of fiber types and to utilize this modeling platform to investigate the design of a novel fiber bending loss edge filter, taking account of the effect of temperature, polarization and fiber tolerance

The primary application of the edge filter is within a passive all-fiber wavelength measurement scheme, but it should be noted that other applications also exist, such as laser blocking in Raman spectroscopy applications [26] and light projection for reconstructing the 3D surface of objects positioned in a camera [27]. This novel fiber bending loss edge filter is based on a different mechanism than existing fiber filters, such as FBG and thin-film filters. It uses the wavelength dependent characteristic of the fiber bending loss which is a function of the fiber cross-sectional refractive index profile, bending radius and the length of the bend.

Investigations about macrobending loss of fibers started in the 1970s [28]. Since then, most of the investigations are focused on how to predict the

bending loss for a given optical singlemode fiber with macrobending, which is regarded as an adverse effect in optical communications and sensing applications. There have been very few investigations which employ this wavelength dependent characteristic for practical sensing applications. The research described in this thesis investigates a fiber bending loss based edge filter and introduces this novel fiber filter into a wavelength ratiometric measurement system for the first time, with the objective of allowing for the design of measurement systems which offer high-speed with a good resolution and low fabrication cost. In addition, such a singlemode fiber based wavelength measurement system offers other advantages such as low cost, ruggedness, vibration insensitivity, and portability.

The insights and conclusions generated by the research can also support the development of new macrobending loss based optical sensing devices, such as temperature, strain, displacement, refractive index sensing applications in the future work. The objectives of the research are as follows:

- Develop a robust and reliable theoretical model based on scalar approximation theory for predicting the macrobending loss behaviour of singlemode fibers, to include:

    a). Investigate existing approximated models; modeling the bending loss of a step-index fiber with multiple cladding layers.

    b). Construct an experimental setup for measuring bending loss.

    c). Verify the models with existing standard or custom fibers.

d). Study the effect of bending strain on the bending loss; investigate the elastooptical effective bend radius used in conventional modeling.

- Compare the relative merits and performance in a macro bend edge filter of coated fiber, bare fiber and custom manufactured fibres.
- Investigate both temperature and polarization dependence for a fiber bending loss edge filter.
- Develop a design method for the fiber bend loss edge filter.

    a). Develop effective simulation programs; utilize global simulation techniques.

    b). Develop fiber bend loss filter with step-index singlemode fibers, considering the polarization dependent and temperature dependent loss.

    c). Choose a suitable customized fiber or an existing commercial fiber type.

    d). Consider the effect of fiber manufacturing tolerances on the parameters of the edge filter.

- Investigate fiber macrobending loss as a mechanism for new optical sensor types with a view toward future work.

1.3 Research methodology

This section provides a brief overview of the methodology employed in this research. The methodology employed throughout the research undertaken

typically consisted of a sequence of related steps 1 to 5 thus:

1). **Carry out an analytic and theoretical study, utilizing existing published knowledge as a foundation.**

Such studies were undertaken a number of times over the course of the research, most frequently involving an investigation of the basic theoretical solutions for analyzing the macrobending loss of fiber devices with multiple cladding layers or multiple coating layers. The studies utilized as a foundation the existing published knowledge and as outcomes provided a suitable analytic model for use in computer based simulations.

2). **Develop appropriate models and carry out computer simulations.**

Based on the analytic and theoretical studies on the prediction of fiber macrobending loss in Step 1, appropriate computer based models were developed to simulate macrobending loss under a variety of conditions. The computer programmes used were based on custom source code in Matlab mixed with Compaq Visual Fortran, performed on a personal computer with an Intel Pentium 4 processor with a clock speed of 3.0 GHz, 1 GB RAM and 80 GB hard disk storage.

3). **If required, investigate and trial fiber modification methods needed for experimental verification.**

In some cases the analytic models and simulations in Step 1 and 2 were based on using fibers where some special processing step was

assumed, beyond simple wrapping of the fiber on a mandrel. Before moving on to experimental verification in Step 4, in some cases techniques to modify fibers had to be developed, most commonly fiber etching and the application of absorption layers. The chemical commonly used in the silica fiber etching process was hydrofluoric (HF) acid. Etch depth is a function of time and the typical duration of the etching process was from 5 to 30 minutes. Important issues in HF etching are health and safety. An acrylic material based absorbing layer[*] was employed on the surface of the bare fiber cladding or fiber coating in the experiments, to reduce the impact of whispering gallery modes, so as to improve the spectral response.

4). **Develop an experimental setup and use this setup to compare and verify the predictions of the model/simulations with real world results.**

While each experimental investigation involved a customized setup, in practice a common core for an experimental setup was constructed at an early stage and adapted and added to as required. A block diagram of the common core experimental setup is shown in Figure 2. The singlemode bend fiber is wrapped to form bend loops around a series of precisely dimensioned metal mandrels, with each mandrel providing a different usable diameter. The bend fiber was connected to a tunable laser source and an optical spectrum analyzer for getting the output signal. Both the tunable laser and optical

[*] In the opinion of some researchers, the "absorbing layer" should be renamed as the "attenuating layer", because attenuation is a more general term which covers the gradual loss in intensity of any kind through a medium. A bare fiber with an absorbing layer can be treated as core-infinite cladding structure, and radiation propagating in the infinite cladding effectively undergoes attenuation. However, in order to retain consistency with the published papers that form the basis of this thesis, the term "absorbing layer" is used.

spectrum analyzer are controlled by a computer with a Labview program. In addition, an optional polarization controller can be added between the tunable laser and bend fiber for changing the polarization dependent states of the input signal and an optional temperature controller can be used to change the temperature of the bend fiber.

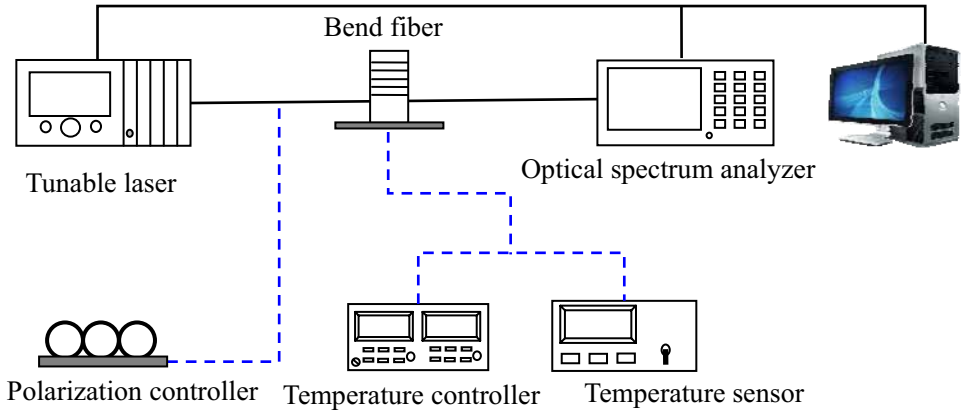

Figure 2. Block diagram for the common core of experimental setup used in the research.

5). Refine the model based on the experimental results and then repeat these steps to refine the agreement between the model and experiments.

This step is critical and involves an in-depth examination in the first instance of the disparities between the modeled/simulated results and the experimental results, including an assessment of the likely sources of error and measurement limitations. In a number of cases the disparities led to fundamental revisions of the analytic model, For example, the scalar approximation theory [9] for predicting macrobending loss is built on a base of perturbation theory [12]. The disparity between the theoretical model and experimental results

showed that the conjugate variable for the Fourier transform [12] needs to be further refined in the model. The disparity also shows that the single coating model [9, 12] needs to be extended to become a multiple coating layer model. Refinements were also made to the experimental setup, for example correcting the experimental bend radius used to include the fiber radius.

1.4 Layout of thesis

This thesis consists of a series of linked journal publications prepared within the duration of the PhD research period. The publications are all first author publications by the author of this thesis. As the research was carried on within a research group, there are several authors for each publication. A signed statement from all the co-authors is included in Appendix A, confirming that the first author undertook all aspects of the research described in each paper, including preparation and submission of the paper, with the support and advice of the co-authors.

Chapter 1 is an introduction chapter which introduces the motivation and research objectives and outlines the whole structure of the thesis.

Chapter 2 presents basic theoretical and experimental analyses of macrobending losses for standard singlemode fiber-Corning SMF28, and provides a fundamental simulation platform for predicting the macrobending loss of singlemode fiber utilizing a scalar approximation method. It also provides a foundation for the calculation of polarization dependent loss and temperature dependent loss in Chapter 3 and 4.

Chapter 3 presents an analysis of the polarization dependent loss

characteristics of a high-bend loss singlemode fiber, Nufern 1060XP, for an edge filter application. The theoretical analysis is based on the scalar approximation theory. The experimental results demonstrate a good agreement with the theoretical calculations and both the theoretical and experimental results show that the fiber coating layers have a significant influence on the polarization sensitivity of bend loss.

Chapter 4 analyzes the temperature dependent loss for the fiber bending loss edge filters, which is based on SMF28 and 1060XP fiber, respectively. Temperature dependencies are calculated by the scalar approximation theory. The experimental results show a good agreement with the proposed theoretical models. For an SMF28 or 1060XP fiber based edge filter, it is clear that temperature variations will significantly impact the accuracy of wavelength measurements. The proposed theoretical method can be used to evaluate the performance of a fiber-macrobending-based edge filter as a function of ambient temperature for high-speed wavelength measurements and also for fiber based temperature sensing applications. Furthermore, the effect of temperature on polarization dependent loss is also investigated theoretically and experimentally.

Chapter 5 presents analysis of the influence of fiber manufacturing tolerances on the all-fiber bending loss edge filter. It is shown that the manufacturing tolerances of the fiber physical parameters, such as bend radius and NA, have a significant influence on the fiber bending loss spectral response of the fiber-based edge filter. A theoretical model, validated by experimental results, is used to determine the changes in key spectral parameters for an edge filter, resulting from changes within their

manufacturing tolerance range, for both the bending radius and NA. Finally it is shown that a bending-radius tuning during fabrication of such filters is a means of mitigating the effect of manufacturing variations.

Chapter 6 presents a complete methodology for the design of a fiber based edge filter, starting with the task of selecting suitable fibers and then considering the design of fiber bending loss edge filter. Through the comparison of the performances of two previously developed types of fiber edge filters, as an example a Corning SMF28e fiber with 900 μm jacket is selected as a tradeoff between SMF28 and 1060XP fiber and an edge filter design is undertaken.

Chapter 7 summarizes the main conclusions and key results of this thesis and presents a brief overview of future research work. Reference is made to a publication (contained in the Appendix B) by the author of this thesis to a new theoretical model based on a 3-dimensional full-vectorial finite difference beam propagation method for accurately predicting the fiber bending loss. Finally a subsidiary objective of this thesis is to explore novel applications for macrobending fiber based optical sensing devices. In the course of simulation and measurements of macrobending losses for singlemode fibers, a range of temperature, refractometric, displacement and strain sensing applications with a high resolution were discovered based on a macrobending fiber. Such sensing applications form the basis of future work and reference is made to the Appendix C to the thesis to another publication by the author of this thesis on a macrobending fiber based refractometer sensor, presented as a good example of the application of bend loss to optical sensing.

1.5 References

[1]. B. Mason B, S. P. DenBaars and L. A. Coldren, “Tunable sampled-grating DBR lasers with integrated wavelength monitors,” IEEE Photon. Technol. Lett. Vol. 10 pp. 1085–1087, 1998.

[2]. J. J. Lepley and A. S. Siddiqui, “Primary referenced DWDM frequency comb generator,” IEE Proc. Optoelectron. Vol. 146, pp. 121–124, 1999.

[3]. A. D. Kersey, M. A. Davis, H. J. Patrick, M. Leblanc, K. P. Koo, C. G. Askin, M. A. Putnam, and E. J. Friebele, “Fiber grating sensors,” J. Lightwave Technol. Vol.15, pp.1442–1463, 1997.

[4]. S. M. Melle, K. Liu, and R. M. Measures, “A passive wavelength demodulation system for guided-wave Bragg grating sensors,” IEEE Photonics Technol. Lett. Vol. 4, pp. 516–518, 1992.

[5]. M. A. Davis and A. D. Kersey, “All fiber Bragg grating strain sensor demodulation technique using a wavelength division coupler,” Electron. Lett. Vol. 30, pp. 75–76, 1994.

[6]. A. B. L. Ribeiro, L. A. Ferreira, M. Tsvekov, and J. L. Santos, “All-fiber interrogation technique for fiber Bragg sensors using a biconical fiber filter,” Electron. Lett. Vol. 32, pp.382–383, 1996.

[7]. Y. Liu, L. Zhang, and I. Bennion, “Fabricating fibre edge filters with arbitrary spectral response based on titled chirped grating structures,” Meas. Sci. Technol. Vol. 10, pp. L1–L3, 1999.

[8]. B. Sharma, A. -H. Al-Ani and S. J. Halme, “Constant-curvature loss in monomode fibers: an experimental investigation,” Appl. Opt. Vol. 23, pp. 3297-3301, 1984.

[9]. H. Renner, “Bending losses of coated single-mode fibers: a simple approach,” J. Lightw. Technol., Vol. 10, pp. 544-551, 1992.

[10]. N. Healy and C. D. Hussey, “Minimizing bend loss by removing material inside the caustic in bent single-mode fibers,” Appl. Opt. Vol. 45, pp. 4219-4222, 2006.

[11]. R. Morgan, J. S. Barton, P. G. Harper, and J. D. C. Jones, “Wavelength dependence of bending loss in monomode optical fibers: effect of the fiber buffer coating,”Opt. Lett. Vol. 15, pp. 947-949, 1990.

[12]. L. Faustini and G. Martini, “Bend loss in single-mode fibers,” J. Lightw.

Technol., Vol. 15, pp. 671-679, 1997.

[13]. A. J. Harris, P. A. Shrubshall, and P. F. Castle, “Wavelength Demultiplexing Using Bends in a Single-Mode Optical Fiber,” J. Lightw. Technol., Vol. 6, pp. 80–86, 1988.

[14]. Q. Wang, G. Farrell and T. Freir, "Study of transmission response of edge filters employed in wavelength measurements", Applied Optics, Vol. 44, pp. 7789-7792, 2005.

[15]. Q. Wang, G. Rajan, P. Wang and G. Farrell, "Resolution investigation of ratiometric wavelength measurement system," Applied Optics, Vol.46, pp. 6362-6367, 2007.

[16]. Q. Wang, G. Rajan, P. Wang and G. Farrell, “Polarization dependence of bend loss for a standard singlemode fiber”, Optics Express, Vol.15, pp.4909-4920, 2007.

[17]. P. Wang, Y. Semenova, G. Farrell, "Temperature dependence of macrobending loss in all-fiber bend loss edge filter," Optics Communications, Vol. 281, pp. 4312-4316 , 2008.

[18]. A. J. Harris and P. F. Castle, “Bend loss measurement on high numerical aperture single-mode fibers as function of wavelength and bend radius,” J. Lightwave Technol. Vol. LT-4, No. 1, pp. 34-40, 1986.

[19]. D. Marcuse, “Curvature loss formula for optical fibers,” J. Opt. Soc. Am., Vol. 66, No. 3, pp. 216-220, 1976.

[20]. I. Valiente and C. Vassallo, “New formalism for bending losses in coated single-mode optical fibers,” Electron. Lett., Vol. 25, No. 22, pp. 1544-1545, 1989.

[21]. C. Vassallo, “Perturbation of an LP mode of an optical fiber by a quasi-degenerate field: a simple formula,” Opt & Quantum Electron., Vol. 17, pp. 201-205, 1985.

[22]. S. Tomljenovic-Hanic, D. A. P. Bulla, A. Ankiewicz and J. D. Love, “Multiple-cladding fibers with reduced bend loss,” J. Opt. Soc. Am. A, Vol. 24, No. 4, pp. 1172-1176, 2007.

[23]. K. Nagano, S. Kawakami and S. Nishida, “Change of the refractive index in an optical fiber due to external forces,” Appl. Opt. Vol. 17, No. 13, pp. 2080-2085, 1978.

[24]. Y. Murakami and H. Tsuchiya, “Bending Losses of Coated Single-Mode

Optical Fibers," IEEE J. Quantum Electron., Vol. QE-14, No. 7, pp. 495-501, 1978.

[25]. Q. Wang, G. Farrell, and T. Freir, "Theoretical and experimental investigations of macro-bend losses for standard single mode fibers," Opt. Exp., Vol. 13, No. 12, pp. 4476-4484, 2005.

[26]. http://www.interferencefilters.co.uk/ShortPassEdgeFilterRange.htm, Access data: 02rd November 2008.

[27]. S. H. Chang, H. Deng, J. Fuller, A. Farsaie and L. Elkins, "An adaptive edge detection filter for light stripe projection (LSP) in surface reconstruction," Proc. SPIE, Vol. 5302, pp. 1-8, 2004

[28]. D. Marcuse, "Curvature loss formula for optical fibers," J. Opt. Soc. Am. Vol. 66, pp. 216-220, 1976.

Chapter 2

Macrobending loss of step-index singlemode fiber

The primary aim of this research is to develop an effective modeling platform for singlemode fiber bend loss which can deal with a variety of fiber types and to utilize this modeling platform to investigate a novel fiber bending loss edge filter. This chapter contributes to achieving this aim by presenting the fiber bend loss model and defining the real root of conjugated variable on the Fourier transform, which can be utilized to predict the bend loss of fiber with single or multiple cladding/coating layers along with effectively reducing the computation time.

This chapter presents a basic theoretical and experimental analysis of macrobending losses for standard singlemode fiber - Corning SMF28 and provides a fundamental simulation platform for predicting the macrobending loss of a step-index singlemode fiber utilizing a scalar approximation method. It also underpins the theoretical foundation for the prediction of polarization dependent loss and temperature dependent loss in Chapters 3 and 4.

The model presented in this chapter has a specific focus on the effects of whispering gallery modes. In order to verify the effectiveness of the model, three different cases for bending fiber are investigated experimentally. The agreement between calculated and measured results suggests a major conclusion that the reflection occurring at the interface between the cladding and coating layer or the cladding layer and air has a significant influence on the bend loss. Such an

influence has been taken account of in the developed theoretical models throughout the entire thesis.

Bending fiber with a smaller bend radius is useful for bending fiber based sensing applications, particularly, when it is developed as an optical probe with a full or half loop structure, an example of which is briefly presented in the Appendix C. Therefore, it is necessary to investigate the characteristics of macrobending loss of standard singlemode fiber with small bend radii.

Investigation of Macrobending Losses of Standard Single Mode Fiber with Small Bend Radii*

Keywords: Fiber macrobending loss, single mode fiber, whispering gallery mode

Abstract: An investigation of macrobending loss characteristics of a standard singlemode fiber (SMF28) for small bend radii is presented theoretically and experimentally, which includes the bend loss of the SMF28 with coating layers and the bare SMF28 after stripping the coating layers and chemical etching of partial cladding. The significant influence of reflection occurring at the interface between the cladding and coating layer or the cladding layer and air on the bend loss is investigated theoretically and experimentally.

2.1 Introduction

Optical fiber has been used in a range of optical sensing applications involving microbending or macrobending [29-34]. Examples include displacement sensing

* P. Wang, Q. Wang, G. Farrell, G. Rajan, T. Freir, J. Cassidy, "Investigation of Macrobending Losses of Standard Single Mode Fiber with Small Bend Radii," Microwave and Optical Technology Letters, Vol. 49, No. 9, pp. 2133-2138, 2007.

[29], pressure sensing [30, 32], wavelength referencing sensing [31], temperature sensing [34], and so on. Theoretical investigations about macrobending loss of fibers started in 1970s. The models developed by D. Marcuse [35, 36] treated the fiber as a core-infinite cladding structure. For the core-cladding-infinite coating structure, a number of theoretical modeling and corresponding experimental investigations of macrobending loss have been presented in Refs. [37-41], which considered the impact of the whispering-gallery mode (WGM) caused by the reflection of the radiated field at the interface between the cladding and coating layer. Previous published investigations of fiber bend losses have been focused on some special fibers (particularly fibers with small numerical apertures) rather than standard single mode fibers (such as SMF28), which are widely used in optical communications [37-40].

Recently, the macrobending loss properties of SMF28 (bend radius ranges from 8.5 to 12 mm) were investigated theoretically and experimentally and optimized as an edge filter for wavelength measurements [42, 43]. However, a bending fiber with a smaller bend radius, e.g., substantially less than 10 millimeters, is useful for sensing applications, particularly when the fiber bend is optimized as a small optical probe. Therefore, it is necessary to study the characteristics of macrobending loss with smaller bend radii. In practice, after stripping the polymer coating layers, the bare fiber is easily broken without any protection. To reduce the bending induced internal stress and allow for smaller bending fiber structures, the fiber cladding is etched partially by using HF acid, which will be presented in Sec. 2.4.

A thorough investigation of the fiber bend loss with small bend radii is presented theoretically and experimentally, which includes: 1) theoretical

modeling analysis for fiber bend loss; 2) macrobending loss of the SMF28 with coating layers; 3) macrobending loss for the bare SMF28 fiber after stripping the coating layers (core-cladding structure only) and partially etching the cladding layer; 4) macrobending loss of the bare etched SMF28 fiber after coating with an absorbing layer. The theoretical results agree with the measured bend losses for SMF28 with or without polymer coating layers. Through comparison between the first two cases and the third case, it is found that the whispering-gallery modes caused by reflection at the interface between the cladding and coating layer (case 1) or between the cladding layer and air (case 2) have a significant impact on the bend loss.

2.2 Theoretical modeling for fiber bend loss

There are different approaches developed for the prediction of the macrobending loss of singlemode fibers with coatings [38-40]. For example, a theoretical model based on weak perturbance of the guide field has been presented in Ref. [38-40]. Fig. 3 illustrates the cross section of a bend fiber with a core-cladding-infinite coating layer structure. Based on the weak-guidance approximation theory, when the fiber is bent the Fourier transform scalar field in the cladding and infinite coating regions in both x and y-direction can be expressed as a Fourier series following [38]:

$$\Psi(x,y)=\begin{cases}\sum_{p=1}^{N}\left\{C_p Bi[X_{2,p}(x)]+R_p Ai[X_{2,p}(x)]\right\}\cos\beta_p y & a\le x\le x_h\\ \sum_{p=1}^{N}D_p\left\{Bi[X_{3,p}(x)]-iAi[X_{3,p}(x)]\right\}\cos\beta_p y & b\le x<\infty\end{cases} \tag{2.1}$$

Assuming that bending takes place in the x-plane, β_p [*] is the conjugate variable

[*] The details of theoretical models can be found in Section 1.1.4 (Page 25-31).

for the Fourier transform in the restricted narrow *y*-region, and β_p could be expressed as: $\beta_p = (2p-1)\pi/2h$ (p is positive integer, p=1, 2, …), and h is defined in Fig. 3. In our calculations, it is found that the calculated bend loss differs with the h value. A simple and practical method to find out a suitable h-value can be: 1) assume the refractive index of the coating to equal to that of the cladding, i.e., core-infinite cladding structure, 2) calculate the bend loss with the above method and the method developed by D. Marcuse in Ref. [35], separately under different bending radii. 3) determine a suitable h-value so that the two results match.

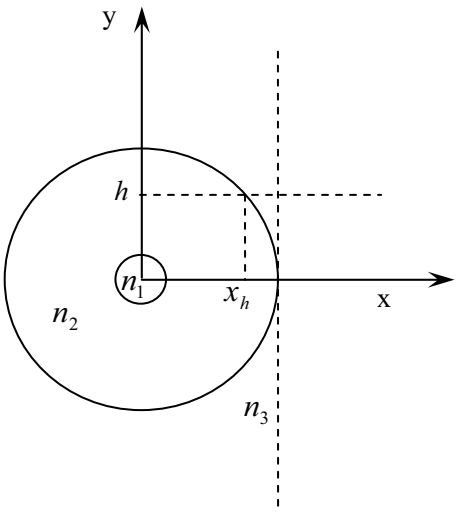

Figure 3. The cross section view of the bend fiber with core-cladding-infinite coating structure.

Table 1. Parameters of the standard Corning SMF28 fiber; (the refractive index values are defined at a wavelength of 1550 nm)

SMF28 fiber	**Refractive index**	**Radius (μm)**
Core	n_1=1.4504	a=4.15
Cladding	n_2=1.4447	b=62.5
Inner coating	n_3=1.4786	c=95
Outer coating	n_4=1.5294	d=125

For the Corning standard SMF28 fiber considered in this paper, the refractive indices (for wavelength 1550 nm) and radii of the core, cladding and coating layers are shown in Table 1.

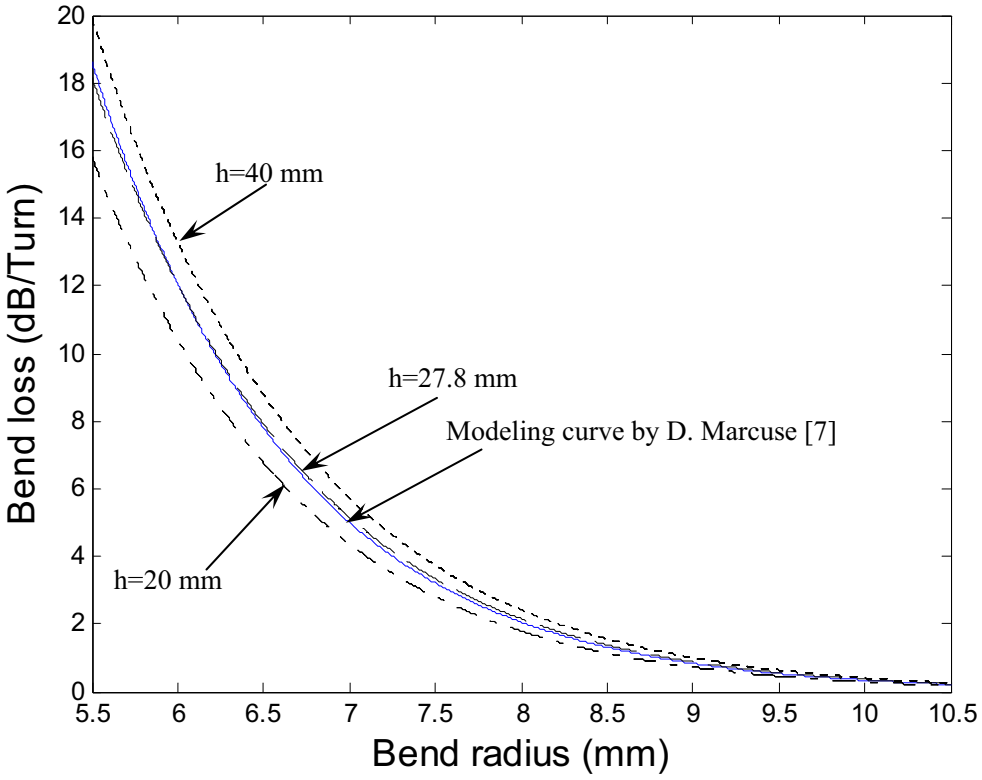

Figure 4. Theoretical modeling bend loss curves from Ref. [35] (solid line) and Ref. [38] (the dashed line is with h=27.8 mm; the dash-dot line is with h=20 mm; the dotted line is with h=40 mm) for SMF28 fiber with different bend radii at the wavelength is 1500 nm.

Fig. 4 shows the calculated fiber bend loss results from Ref. [35] and Ref. [38] for standard SMF28 fiber. For illustration values of h equal to 20 μm, 27.8 μm, and 40 μm for the y-direction are shown. From Fig. 4, one can see that the calculated result with h=27.8 μm (dashed line) from Ref. [38] is in agreement with the modeling result (solid line) from Ref. [35] and this yields a suitable value of h in the formula (2.1).

2.3 Fiber bend loss with coating layers

As mentioned in the introduction, the existence of the coating layer(s) will produce a so-called whispering-gallery mode for a bending fiber due to the reflection of the radiated field at the interface between the cladding layer and the coating layer. Previous published investigations of fiber macrobending loss have developed a series of formulas for the calculation of fiber macrobending loss, and when the effect of the coating layer is included the formulas presented in Ref. [38-40] are used. In this experiment, the singlemode fiber was wrapped on a mandrel consisting of multiple sections, each providing a different usable diameter. The bending fiber was connected to a tunable laser and an optical spectrum analyser. The bend losses of SMF28 fiber with an absorbing layer (to remove the reflection occurring at the interface between the coating layer and air) were measured for the bending radii range from 6 to 8.5 mm when the wavelength is 1500 and 1600 nm, respectively (see Fig. 5a and Fig. 5b).

One can see that as the bend radius increases, the non-monotonic decrease of both the experimental and theoretical results of the bend loss confirms the impact of a strong WGM influence caused by the coating layer as mentioned above. In Fig. 5, the modeling results agree well with the experimental data for a bend radius in the range from 7 to 8.5 mm. When the bend radius gets smaller, the agreement between the theoretical and experimental results decreases. One reason is that in the experiment for such cases, the bend loss is highly sensitive to the bend radius, e.g., the discrimination is about 40 dB between the bend radius 5.5 and 6 mm in Fig. 5b, however, in practice it is difficult to control the bend radius precisely.

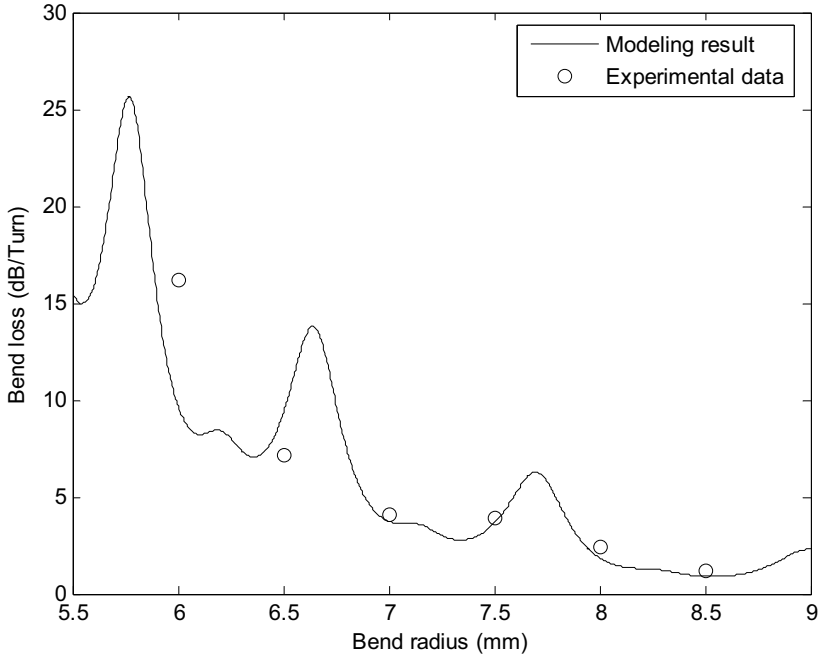

(a)

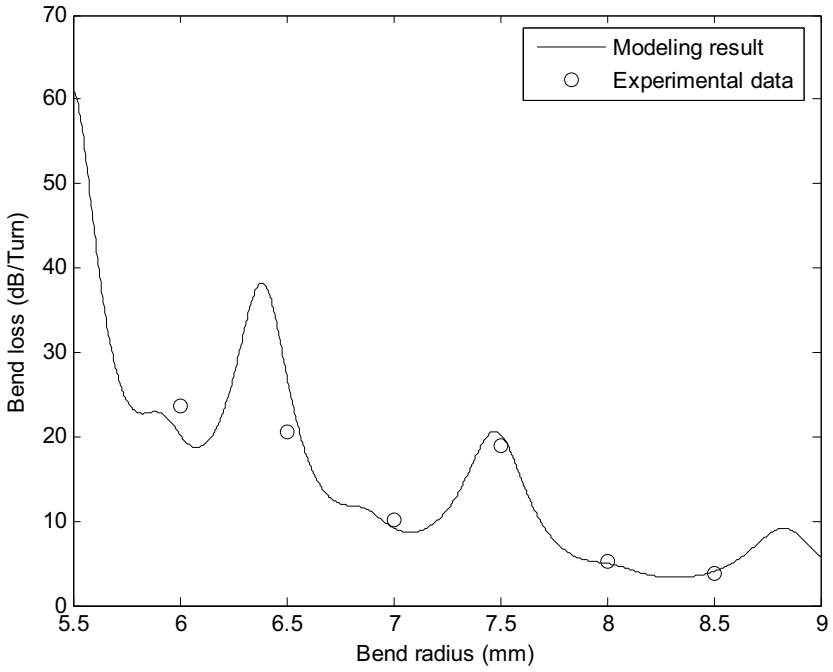

(b)

Figure 5. Modeling and measured macrobending losses for bend radius ranging from 6 to 8.5 mm at wavelength a) 1500 nm b) and 1600 nm.

2.4 Bend loss of a bare SMF28 after stripping coating layers and partially etching the cladding layer

In our experiments, the SMF28 fiber coatings were stripped by hot concentrated sulfuric acid (H_2SO_4, wt >95%, ~200^oC). It is found that the fiber is easily broken even when the bend radius is smaller than 10 mm. To reduce the bending stress and retain the mechanical flexibility of bare fiber, the fiber cladding is etched partly by using hydrofluoric (HF) acid. After the etching process using HF acid and cleaning by acetone and alcohol, the diameter of thinned-cladding fiber was about 61 μm, measured by a high-precision screw micrometer. Both the bare SMF28 and the thinned-cladding fiber as seen under a microscope are shown in Fig. 6.

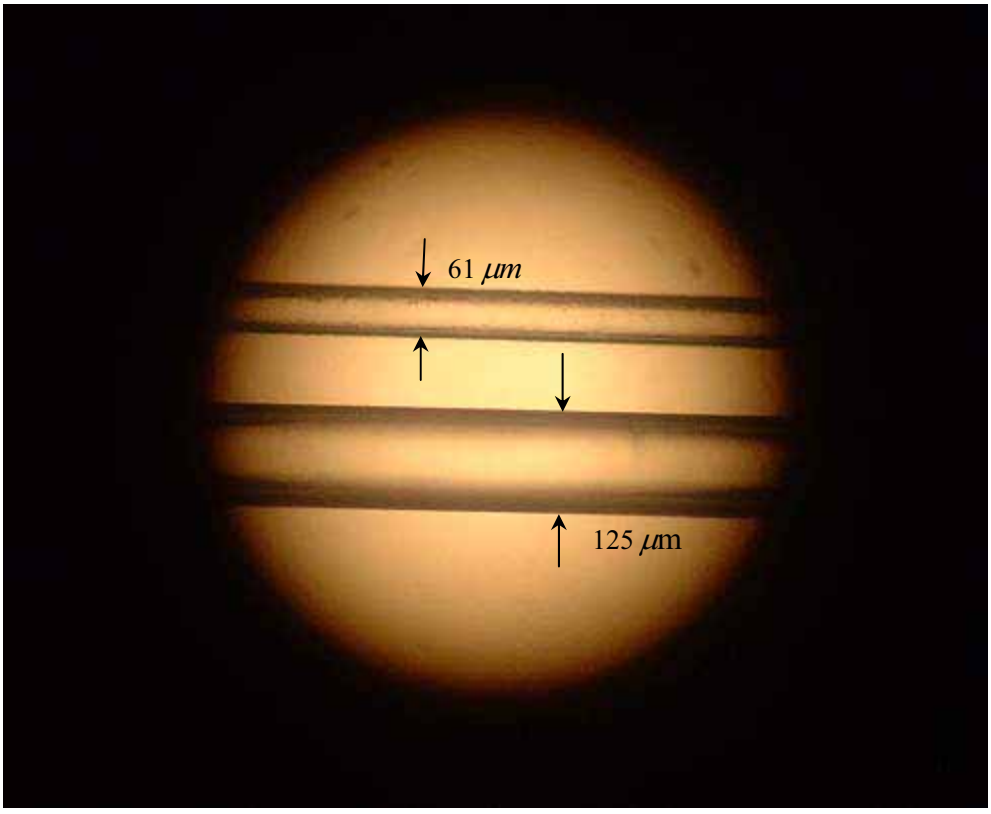

Figure 6. Photograph of etched thinned-cladding fiber contrasting against standard stripped bare SMF28 optical fiber

We measured the bend loss of the bare SMF28 fiber with a diameter of 61 μm, for a bend radius of 5.5, 6.0, and 6.5 mm (the bend length is one turn), in the wavelength range from 1500 to 1600 nm, and corresponding results are presented in Fig. 7. For this case, the reflection of the radiated field at the interface between the cladding layer and air has a significant impact on the bend losses. When the bending etched fiber without an absorbing layer coated at the outside, the radiated light is reflected back at the interface between the cladding layer and air. The reflected light is coupled with the propagating light within the core. As distinct from the first case presented in section 2.3, where the radiated field is reflected at the interface between the cladding and coating layer, the reflection occurring in the case of etched fiber is much stronger due to the significant refractive index difference between the cladding and air (the etched fiber can be regarded as a multimode fiber when the cladding is treated as the core and the air is the cladding). Because of the strong reflection and recoupling, which can be seen from the simulation results by e.g., the beam propagation method, there is no single quasi-guided mode propagating within the core as the case of bending fiber with a polymer coating. This is why the measured bend loss presented in Fig. 7 seems “unusual”, for example, from Fig. 7, one can see that the bend loss at 5.5 mm which increases with wavelength to one at 6.5 mm which decreases, whilst at 6mm the loss peaks at 1540 nm.

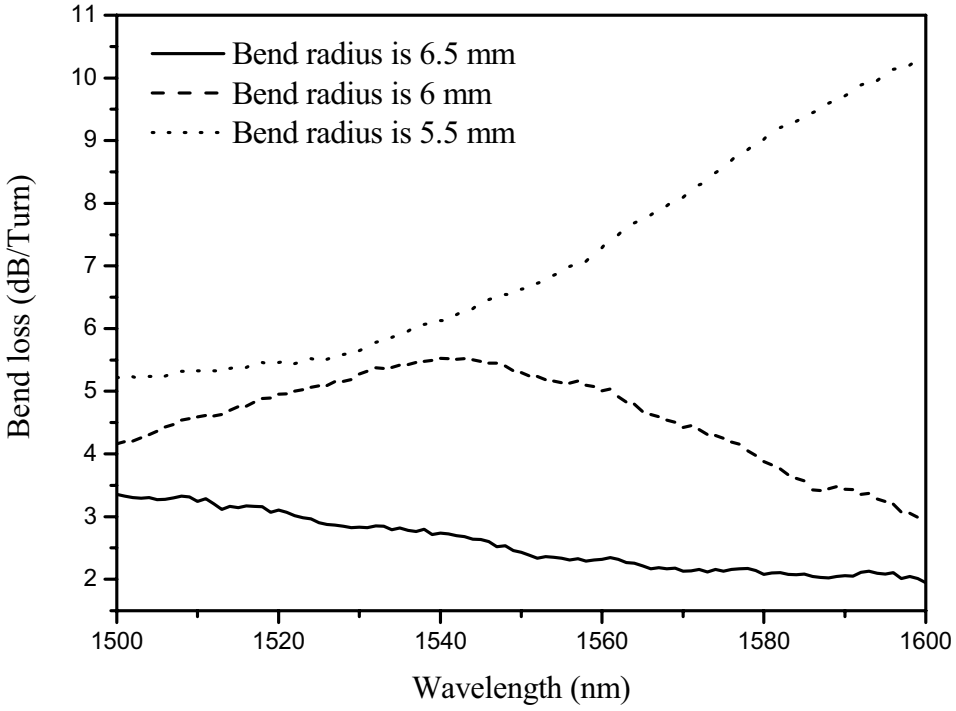

Figure 7. Measured bend loss results of thinned-cladding SMF28 fiber without absorbing layer in wavelength ranging from 1500 to 1600 nm for bend radius is 5.5, 6.0, and 6.5 mm.

It should be noted that modeling of the behavior of the bare etched fiber using the technique outlined in section 2.2 is not possible. This can be explained as follows, for the case of core-cladding-infinite coating presented in the above section, in which the refractive index of coating layer is higher than that of the cladding there is only a single quasi-guided mode propagating in the bending fiber. However, for the bare etched SMF28, the refractive index of the cladding layer is higher than that of the surrounding air and the whole fiber can be regarded as a multimode fiber. The numerical beam propagation method shows the reflected field by the interface of cladding layer and air is strongly coupled with the guided mode within the fiber core along the direction of propagation. No single quasi-guided mode is observed as the case of core-cladding-coating structure (where the refractive index of coating is much higher than that of the

cladding layer). For this case, the existing analytical expressions shown in section 2.2 are not suitable for modeling.

2.5 Bend loss for the core-cladding-absorbing layer structure

To remove the impact of the reflection at the interface between the cladding and air the bare thinned-cladding fiber was coated with an absorbing layer. This case is approximately equivalent to a core-infinite cladding structure and the analytical expression for calculating the fiber bend loss with an infinite cladding developed by D. Marcuse [35, 36] is used.

In the experiment, the etched section coated with absorbing layer, was bent to form a small 360^{o} bend in free space, with the fiber overlapped in a "knot-like" fashion for mechanical stability, and the ends of fiber were connected with a tunable laser and an optical spectrum analyzer, respectively. The operating process is the same as the experiment which has been described earlier in Section 2.4. The theoretical and experimental macrobending loss curves versus wavelength range from 1500 to 1600 nm for bend radius of 6.5 and 6 mm are presented in Fig. 8a and Fig. 8b, respectively, from which one can see that the theoretical bend loss agrees with the experimental results. As a comparison, the measured bend losses of bare SMF28 in Fig. 7 are also presented. The difference of bend loss between the two cases, i.e., bare SMF28 and the bare SMF28 with an absorbing layer, shows that the reflection occurring at the interface between the cladding layer and air has a significant effect on the bend loss.

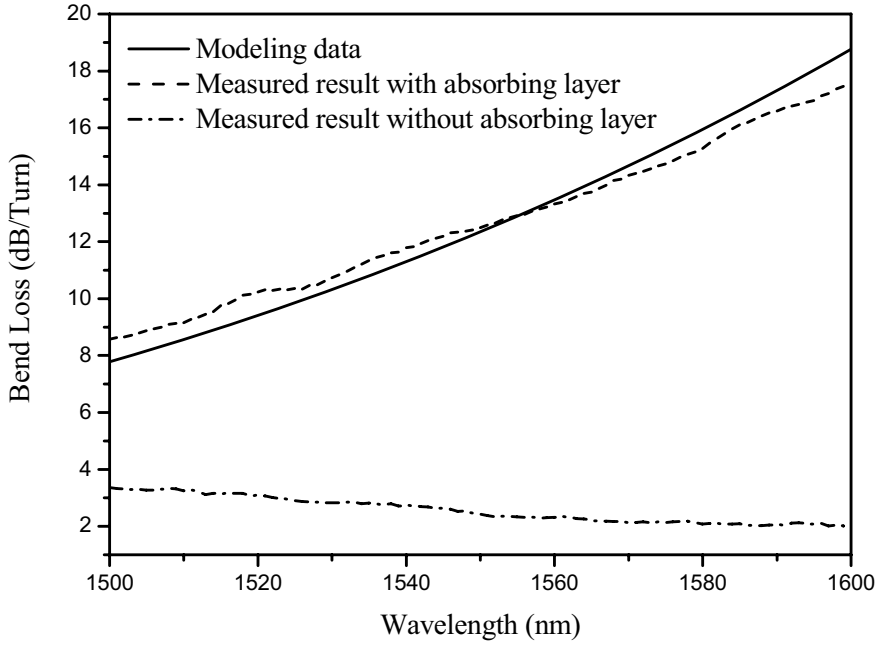

(a)

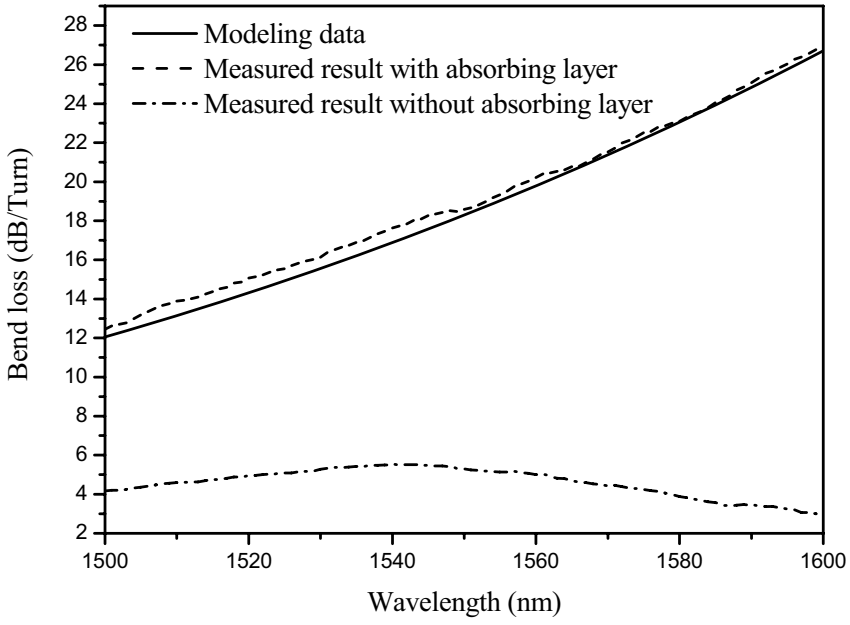

(b)

Figure 8. Measured and modeling bend loss results for thinned-cladding fiber at wavelength range from 1500 nm to 1600 nm with bend radius is a) 6.5 mm b) and 6 mm with and without absorbing layer.

2.6 Conclusion

In conclusion, we have presented a thorough theoretical and experimental investigation of the macrobending loss characteristics of a standard singlemode fiber with small bend radii, which includes theoretical modeling analysis for fiber bend loss, for SMF28 with coating layers and the bare SMF28 after stripping the coating layers and chemical etching of partial cladding. Both experimental and theoretical results have demonstrated the impact of reflection occurring at the interface between the cladding and coating layer or the cladding layer and air on the bend loss.

2.7 References

[29]. N. Lagakos, T. Litovitz, P. Macedo, R. Mohr, and R. Meister, Multimode optical fiber displacement sensor, Appl Opt 20 (1981), 167-176.

[30]. N. Lagakos, J. H. Cole, and J. A. Bucaro, Microbend fiber-optic sensor, Appl Opt 26 (1987), 2171-2180.

[31]. M. T. Wlodarczyk, Wavelength referencing in single-mode microbend sensors, Opt Lett 12 (1987), 741-743.

[32]. R. C. Gauthier and C. Ross, Theoretical and experimental considerations for a single-mode fiber-optic bend-type sensor, Appl Opt 36 (1997), 6264-6273.

[33]. Y. Jeong, S. Baek, B. Lee, S. Choi, and K. Oh, Macrobend sensor via the use of a hollow-core splice fiber: theory and experiments, Opt Eng 41 (2002), 1815-1820.

[34]. S. H. Nam, and S. Yin, High-Temperature Sensing Using Whispering Gallery Mode Resonance in Bent Optical Fibers, IEEE Photon Technol Lett 17 (2005), 2391-2393.

[35]. D. Marcuse, Curvature loss formula for optical fibers, J Opt Soc Am 66 (1976), 216-220.

[36]. D. Marcuse, Bend loss of slab and fiber modes computed with

diffraction theory, IEEE J Quantum Electron 29 (1993), 2957-2961.

[37]. C. Vassallo, Perturbation of an LP mode of an optical fiber by a quasi-degenerate field: a simple formula, Opt & Quantum Electron 17 (1985), 201-205.

[38]. I. Valiente and C. Vassallo, New formalism for bending losses in coated single-mode optical fibers, Electron Lett 25 (1989), 1544-1545.

[39]. H. Renner, Bending losses of coated single-mode fibers: a simple approach, J Lightwave Technol 10 (1992), 544-551.

[40]. L. Faustini and G. Martini, Bend loss in single-mode fibers, J Lightwave Technol 15 (1997), 671-679.

[41]. Y. Powell-Friend, L. Phillips, T. George, and A. Sharma, A simple technique for investigating whispering gallery modes in optical fibers, Rev Sci Instrum 69 (1998), 2868-2870.

[42]. Q. Wang, G. Farrell, and T. Freir, Theoretical and experimental investigations of macro-bend losses for standard single mode fibers, Opt Exp 13 (2005), 4476-4484.

[43]. Q. Wang, G. Farrell, T. Freir, G. Rajan, and P. Wang, Low-cost Wavelength Measurement based on a Macrobending Singlemode Fiber, Opt Lett 31 (2006), 1785-1787.

❖ Comments by the author on Chapter 2

I. In this chapter, equation (2.1) is employed to resolve the value of *h*, which is very important in defining the real root of the conjugate variable of the Fourier transform in the y-direction, and which can be used for the bend loss simulation in the Faustini model. In the previously published work [40, 42] , it is shown that for the bending fiber with a core-cladding-infinite coating structure, the measured experimental results have a good agreement with the Faustini model, hence in this chapter, the Faustini model is employed for bend loss prediction of a singlemode fiber, along with a defined *h* value.

II. It should be noted that the sampling interval for the measured data is set by

the limited step size of radius of the metal mandrel and thus the measured data sampling interval is significantly lower than the modeling data sampling interval.

It could be argued that the peaks in the modeled data are not valid as they are not always supported by measured data points. However, other authors [40, 42] have demonstrated the existence of the peaks in the relationship between bend loss and bend radius and wavelength. It is therefore asserted by the author that the modeled peaks are valid and that the lack of measured data points in certain instances to support the existence of peaks is simply a result of the unavoidable disparity between the sampling interval of the measured data and the modeled data. Future work can resolve this issue by fabricating a larger number of mandrel diameters which can be utilized in the experiments. For example, 0.1 mm interval of diameter while this level of mandrel diameter accuracy can improve the scope and quality of this research, though our data have shown good agreement between model and measurement results at 1 mm interval.

Chapter 3

Polarization dependent loss of high-bend loss based edge filter

A primary aim of this research is to develop an effective modeling platform for singlemode fiber bend loss which can deal with a variety of fibers and to utilize this modeling platform to investigate the design of a novel fiber bending loss edge filter, taking account of the effect of temperature, polarization and fiber tolerance.

It is well known that the polarization dependent loss induced by macrobending has a significant influence on the measurable accuracy of fiber edge filter for wavelength measurement application. This chapter contributes to achieve this aim by presenting the theoretical prediction of fiber polarization dependent loss model by solving different boundary conditions and verifying this model by experiments.

For weakly guiding* singlemode optical fibers, the scalar approximation of the wave equation works well for the analysis of the light propagation. Theoretical and experimental results supporting this have been presented in Chapter 2. The reflectance of the radiated field occurring at the interface between the coating layer and cladding layer differs for different polarization states, which can lead to polarization dependence for the bend loss due to the coupling between the reflected radiated field and the quasi-guided fundamental mode and

* Weakly guiding singlemode fiber is the singlemode fiber with a small refractive index difference between fiber core and cladding.

furthermore will impact on the accuracy of wavelength measurement. All previously published investigations on the polarization dependent loss for a singlemode fiber were carried out based on a beam propagation method or finite difference method [*]. However, both beam propagation method and finite difference method are time consuming on a personal computer, as they demand large amounts of processing power

This chapter presents an analysis of the polarization dependent loss of high-bend loss singlemode fiber, Nufern 1060XP, for an edge filter application. The experimental results are in a good agreement with the theoretical calculations. Both the theoretical and experimental results show that the fiber coating layers have a significant influence on the polarization sensitivity of bend loss.

3.1 An Optimized Macrobending-Fiber-Based Edge Filter[+]

Keywords: Macrobending loss, fiber edge filter, 1060XP fiber

Abstract: An optimized all-fiber edge filter is developed, based on a one-turn macrobending bare fiber structure. The discrimination range (DR) is 16.32 dB over a wavelength range from 1500 to 1600 nm, which can be employed for wavelength measurement applications. It offers a simpler structure compared to the previously developed macrobending fiber loss edge filters, without an increase in the polarization dependent loss (PDL).

---

[*] R. Scarmozzino, A. Gopinath, R. Pregla, and S. Helfert, "Numerical techniques for modelling guided-wave photonic devices," IEEE J. Sel. Top. Quantum Electron., Vol. 6, pp. 150-162, 2000.
[*] M. S. Stern, "Semivectorial polarized finite difference method for optical waveguides with arbitrary index profiles," IEE Proceedings, Vol. 135, pp. 56-63, 1988.
[+] P. Wang, G. Farrell, Q. Wang and G. Rajan, "An Optimized Macrobending-Fiber-Based Edge Filter," IEEE Photonics Technology Letters, Vol. 19, No. 15, pp. 1136-1138, 2007.

3.1.1 Introduction

Fiber bend loss (BL) has been investigated widely for optical sensing and optical communication applications [44, 45], and recently, a macrobending standard singlemode fiber (SMF28) was investigated theoretically and experimentally and optimized as an edge filter for wavelength measurement applications using a bend radius circa 10 mm with multiple turns and a total fiber length about 1~2 meters [46-48]. Both theoretical and experimental results have shown that the polymer coating layer of SMF28 can not only affect the BL but also has a significant influence on the polarization dependence [49]. To remove this influence, a direct method is to strip the coating layers and utilize the bare fiber. However, bare SMF28 fiber after stripping is easily broken due to the mechanical stress. To reduce the bending induced internal stress, etching of the fiber cladding partially by chemicals is a possible solution [50], but it increases the fabrication difficulty and cost.

The formation of more compact structure for the fiber BL edge filter is one of our aims. A more compact structure is an advantage in many applications, for example in a handheld wavelength measurement instrument. To obtain the desired transmission spectrum with a shorter fiber bend length for fiber BL edge filter applications, a type of BL sensitive fiber could be employed, where the normalized frequency V [*] should be lower. Therefore, in this letter an alternative BL sensitive fiber (1060XP) is considered compared to SMF28 fiber. The macrobending loss behavior of bare 1060XP fiber will be presented in this letter, along with consideration of the optimal design of a fiber BL edge filter. Finally

[*] V is the well known normalized frequency, which can be defined as: $V = \frac{2\pi a \cdot NA}{\lambda}$, where a is the core radius of the fiber, NA is the numerical aperture, and λ is the wavelength.

the PDL behaviour of bare 1060XP fiber (using a single turn structure) with an optimal bend radius is also presented. Our investigation involves: 1) modeling BL; 2) the design of a BL edge filter and 3) experimental verification. The numerical theoretical modeling agrees with the measured results for the BL of 1060XP fiber with a correction factor of 1.298 at a wavelength of 1550nm. Through examination of the PDL behavior of bare 1060XP fiber with an absorbing layer, it is found that the BL of bare 1060XP fiber with absorbing layer can achieve a marginally better PDL behavior than an equivalent SMF28 based edge filter, with a more compact structure.

3.1.2 Modeling and Optimal Design

Theoretical investigations about macrobending loss in optical fibers started in the 1970s. The models developed by D. Marcuse [51] treated the optical fiber as a core-infinite cladding structure. While an infinite cladding structure is not possible in practice, a bare fiber coated with an absorbing layer is approximately equivalent to a core-infinite cladding structure. In this investigation an absorbing layer is used over a conventional finite cladding and thus the analytical expression for calculating the fiber BL with an infinite cladding developed by D. Marcuse [51] can be used.

For standard Corning SMF28 and 1060XP fiber, the corresponding parameters are shown in TABLE 2:

Table 2. Parameters of the standard corning SMF28 and 1060XP fiber; (the refractive index values are defined at a wavelength of 1550 nm).

Parameter of fiber	1060XP	SMF28
Refractive index of fiber core	1.46313	1.4504
Refractive index of fiber cladding	1.45642	1.4447
Diameter of fiber core	5.3 ± 0.5 μm	8.3 ± 0.5 μm
Diameter of fiber cladding	125 ± 0.5 μm	125 ± 0.5 μm
NA (Numerical Aperture)	0.14	0.1285
V (Normalised frequency)	1.5035	2.1611

In previously published papers [52-54], to fit the calculated BLs with experimental results, a so-called effective bend R_{eff} has been used, which was different from the actual (experimental) bend radius R_{exp}. An effective bend radius is needed to allow for the change in refractive index of silica glass induced by bending axial stress. In practice it is represented as a wavelength dependent elastooptic correction factor relating R_{eff} *and* R_{exp}. For example in [54] for LB1000 fiber the correction factor is 1.325 at a wavelength of 1480 nm. It is also known that the exact correction factor value is wavelength dependent [52]. As shown in the Fig. 9, the BL of bare 1060XP fiber with an absorbing layer (to remove the reflection occurring at the interface between the cladding layer and air) was measured for a bending radii range from 8.5 to 14.5 mm when the operating wavelength is 1550 nm. For comparison, the calculated BLs (with/without a corresponding correction factor) are also presented in Fig. 9. It is evident that the results are incorrect if the correction factor is not used in modeling BL for bare 1060XP fiber with absorbing layer as compared to the measured results. The selection of 1.298 as the correction factor at 1550 nm was determined from an error analysis which compared the theoretical and

experimental values over the range of bend radii employed. The correction factor varies with wavelength and while it is not practical to determine the value of the correction factor at all wavelengths, it was determined at 10 nm intervals over the wavelength range of interest between 1500 and 1600 nm. The correction factor as a function of wavelength is shown in Fig. 10.

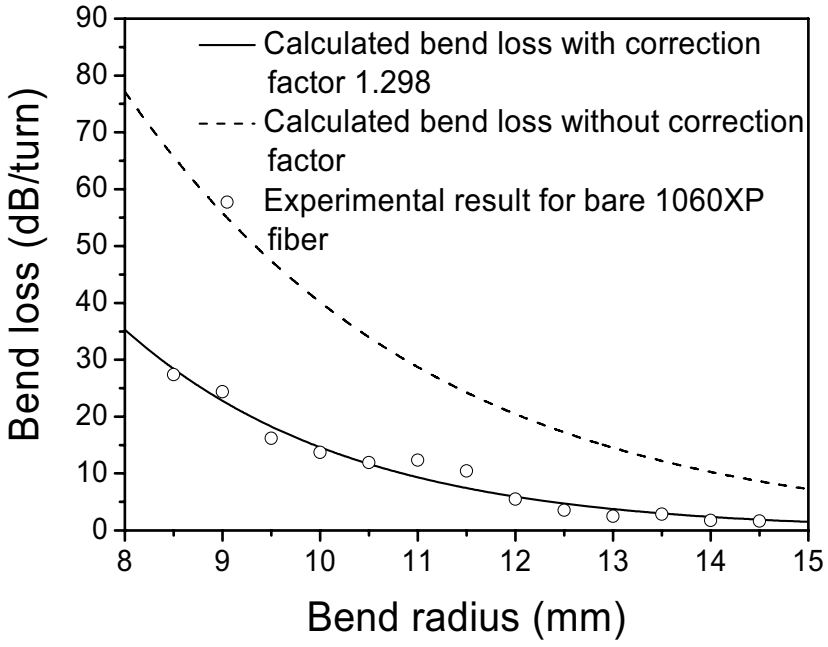

Figure 9. Modeling with (solid line) and without (dashed line) correction factor, and measured macrobending losses for bend radius ranging from 8.5 to 14.5 mm at a wavelength of 1550 nm.

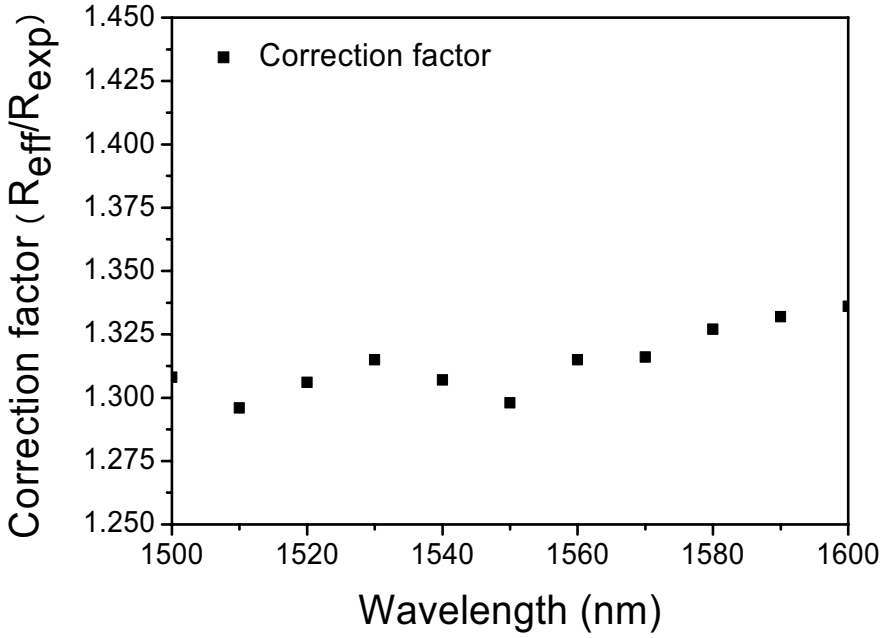

Figure 10. Correction factor as a function of wavelength.

An ideal edge filter provides a strong monotonically increasing wavelength dependent attenuation (DR) from a given start wavelength to an end wavelength, with a low inherent attenuation (baseline loss) at the start wavelength. In this case wavelength measurement over the range from 1500 nm to 1600 is envisaged. Thus there needs to be a low baseline loss (BL at the wavelength 1500 nm with the correction factor of 1.308) along with a desired DR (the difference in BL between 1500 and 1600 nm, with corresponding correction factors of 1.308 and 1.336, respectively) as shown in [48].

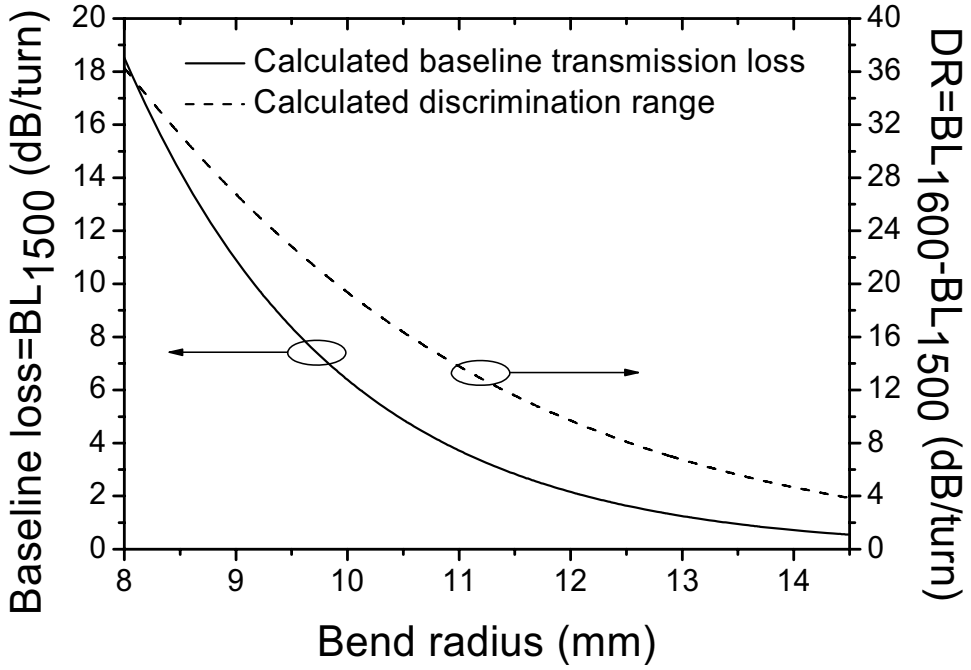

Figure 11. Calculated baseline loss (BL at the wavelength of 1500 nm with the correction factor of 1.308) and discrimination versus different bend radius.

Based on the theoretical formulas presented in [51], Fig. 11 shows the calculated baseline transmission loss and DR as a function of bend radius for bare 1060XP fiber with an absorbing layer, with correction factors applied as appropriate. The curves in Fig. 11 simplify the design of a fiber BL based edge filter using a single turn of 1060XP fiber. In experiments, it is found that bare 1060XP fiber is easily broken when the bend radius is smaller than 10 mm. To reduce the bending stress and retain the mechanical reliability, bend radii less than 10 mm should be avoided. For a given fiber BL edge filter, the aim is to use Fig. 11 to select a working bend radius where the baseline loss is not excessive, while still retaining a reasonable DR. Using Fig. 11 it is possible to tradeoff higher baseline losses for an improved discrimination, but in a wavelength measurement application [48] while higher discrimination can improve

measurement resolution, the consequent higher baseline loss will reduce the overall signal levels available for detection, decreasing measurement accuracy due to noise. Furthermore there is a limit on the discrimination which can be used. In [46] we showed that due to the limited Signal-to-Noise Ratio (SNR) of the input signal, the measured ratio at wavelengths where the edge filter attenuation is highest (toward the upper end of the measurable wavelength range) diverged from the value expected given the transmission response of the edge filter. Effectively this places an upper limit on the allowable maximum attenuation in the edge filter and thus the discrimination. For the experimental investigation in the next section, a bend radius of 10.5 mm was chosen which provides a reasonable baseline loss of 4.86 dB and a DR of 16.32 dB.

3.1.3 Experimental results and discussion

Experimentally, the bare section coated with an absorbing layer, was bent to form a small 360^{o} bend in free space, with a bend radius of 10.5 mm, with the bare fiber crossover point protected by a short polymer jacket to improve mechanical stability (see Fig. 12). The ends of fiber were connected to a tunable laser and an optical spectrum analyzer, respectively, to determine the value of the macrobending loss.

The theoretical and experimental macrobending loss curves over the wavelength range from 1500 to 1600 nm for a bend radius of 10.5 mm are presented in Fig. 13. There is very good match between the calculated modeling and experimental data. The experimental transmission spectrum shows a suitable macrobending loss characteristic which matches the design predictions well, in that the measured baseline transmission loss is about 5.23 dB at the wavelength

of 1500 nm and the measured DR is circa 16.33 dB from 1500 to 1600 nm. These values compare well with those achieved for SMF28 fiber [48], but with the advantage that only one fiber turn is required in this case, instead of 22 turns for the SMF28 case. The divergence between the experimental and theoretical results may be caused by: 1) the experimental accuracy of the bend radius (both baseline loss and DR are sensitive to the bend radius as shown in Fig. 11) and 2) the application of a correction factor at a limited number of wavelength intervals (10 nm) in the calculation of BL.

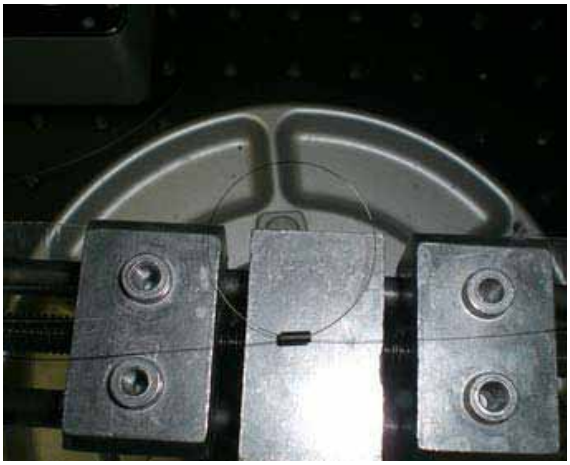

Figure 12. Photograph of bend bare 1060XP fiber coated absorbing layer.

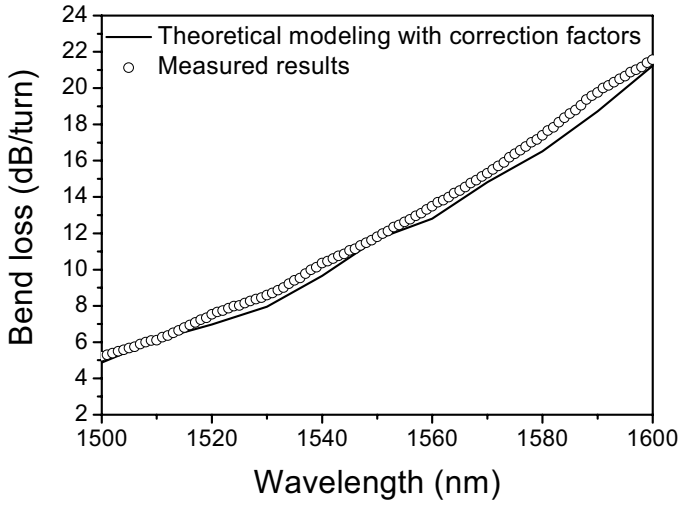

Figure 13. Calculated and measured macrobending results for bare bend 1060XP fiber with absorbing layer when the bend radius is 10.5 mm, the fiber length is single turn.

PDL is also an important parameter for a fiber BL edge filter [49]. For bent bare 1060XP fiber coated with an absorbing layer, the calculated PDL is very small in the fiber core-infinite cladding structure (about the 10^{-12}dB* with the bend radius of 10.5 mm). In Fig. 14, the experimental PDL versus wavelength over the range from 1500 to 1600 nm with bend radius of 10.5 mm for bare 1060XP fiber coated with an absorbing layer. As a comparison, the measured PDL results of SMF28 fiber with coating and absorbing layer is also presented in Fig. 14. As shown in Fig. 14, the minimum PDL is 0.0359 dB at the wavelength of 1550nm, and the average value of PDL experimental results of bare 1060XP fiber is 0.0922 dB, lower than 0.1072 dB of PDL average value of SMF28 fiber which was presented in [49].

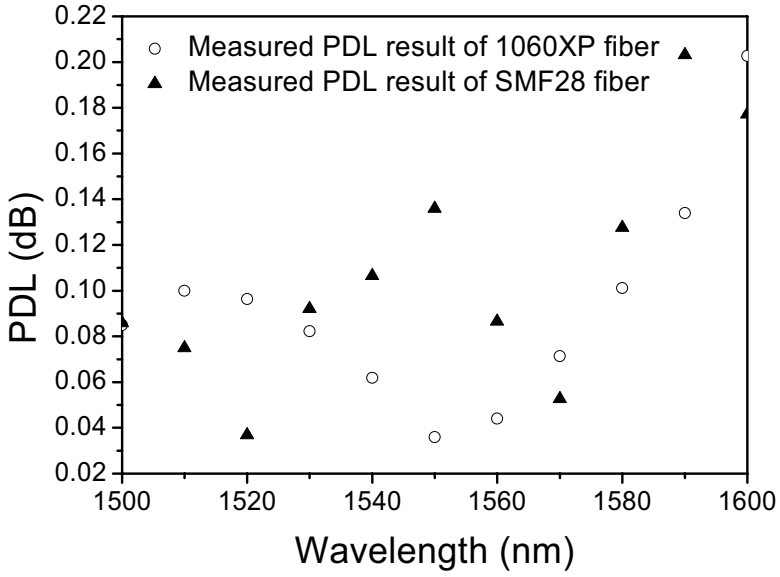

Figure 14. Measured PDL in wavelength ranging from 1500nm to 1600 nm for bare 1060XP fiber coated absorbing layer(circles) and SMF28 fiber with coating and absorbing layers(solid triangle).

The divergence between the experimental and theoretical PDL results for

* The inclusion of the value 10^{-12} dB is an error in the published paper and should be ignored as a noise level of 10^{-3} dB would be more reasonable assessment of the actual data.

1060XP fiber is most likely caused by the imperfect absorbing layer material coated on the bare fiber cladding surface. If this layer is not absorbing all the radiation from the core at the bend then partial radiation will reflect from the fiber cladding-air boundary and recouples with the fundamental propagation mode, resulting in changes the polarization states of fundamental mode. It should be noted that there is about 0.02dB variation exists in the wavelength measurements due to the SNR of tunable laser source, and it effects the PDL measurement result as well. Overall we can conclude that the use of 1060XP fiber, to allow for the implementation of compact single turn fiber BL edge filter does not compromise PDL performance by comparison with SMF28 fiber.

3.1.4 Conclusion

In conclusion, an optimal design of fiber macrobending loss based edge filter for BL sensitive fiber (1060XP) is presented, and the experimental macrobending loss data has a good agreement with the proposed theoretical modeling. Compared with the performance of standard SMF28 fiber presented previously, both theoretical and experimental results have shown that the bend bare 1060XP fiber with an absorbing layer is more compact and is suitable for the fiber BL edge filter applications.

3.1.5 References

[44]. S. H. Nam, and S. Yin, “High-Temperature Sensing Using Whispering Gallery Mode Resonance in Bent Optical Fibers,” IEEE Photon. Technol. Lett., Vol. 17, No. 11, pp. 2391-2393, 2005.

[45]. M. D. Nielsen, N. A. Mortensen, M. Albertsen, J. R. Folkenberg, A. Bjarklev, and D. Bonacinni, “Predicting macrobending loss for large-mode area photonic crystal fibers,” Opt. Express, Vol. 12, No. 8, pp. 1775-1779,

2004.

[46]. Q. Wang, G. Farrell and T. Freir, "Study of transmission response of edge filters employed in wavelength measurements," Appl. Opt., Vol. 44, No.36, pp. 7789-7792, 2005.

[47]. Q. Wang, G. Farrell and T. Freir, "Theoretical and experimental investigations of macro-bend Losses for standard single mode fibers," Opt. Express, Vol.13, No.12, pp. 4476-4484, 2005.

[48]. Q. Wang, G. Farrell, T. Freir, G. Rajan and P. Wang, "Low-cost Wavelength Measurement based on a Macrobending Singlemode Fiber," Opt. Lett., Vol. 31, No. 12, pp. 1785-1787, 2006.

[49]. Q. Wang, G. Rajan, P. Wang, and G. Farrell, "Polarization Dependence of Bend Loss for a Standard Singlemode Fiber," Opt. Express, Vol. 15, No. 8, pp. 4909-4920, 2007.

[50]. P. Wang, Q. Wang, G. Farrell, G. Rajan, T. Freir and J. Cassidy, "Investigation of Macrobending Losses of Standard Single Mode Fiber with Small Bend Radii," Microw. Opt. Techn. Lett., to be published.

[51]. D. Marcuse, "Curvature loss formula for optical fibers," J. Opt. Soc. Am. Vol. 66, No. 3, pp. 216-220, 1976.

[52]. A. B. Sharma, A. -H. Al-Ani and S. J. Halme, "Constant-curvature loss in monomode fibers: an experimental investigation," Appl. Opt. Vol. 23, No. 19, pp. 3297-3301, 1984.

[53]. H. Renner, "Bending losses of coated single-mode fibers: a simple approach," J. Lightw. Technol., Vol. 10, No. 5, pp. 544-551, 1992.

[54]. L. Faustini and G. Martini, "Bend loss in single-mode fibers," J. Lightw. Technol., Vol. 15, No. 4, pp. 671-679, 1997.

3.2 Investigation of Polarization Dependent Loss for a Macrobending Loss Sensitive Singlemode Fiber*

Keywords: Polarization dependent loss, macrobending loss, singlemode fiber, 1060XP fiber

Abstract: An investigation of the polarization dependent loss (PDL) of macrobending loss sensitive single fiber (1060XP) is presented theoretically and experimentally. The experimental results are in good agreement with the modeling outcomes. Through the comparison of experimental results of PDL between 1060XP fiber with coatings and bare 1060XP fiber, it is shown that the fiber coating has significant impact on the PDL of bend loss sensitive singlemode fiber.

3.2.1 Introduction

PDL has been investigated as an important issue in many fiber-optic communication applications [55-58]. Polarization dependence is mostly caused by fiber bending, dichroism and oblique reflection, and it always increases the error rate in fiber-optic transmission systems. Recently, fiber macrobending loss of standard Corning SMF28 singlemode fiber was investigated theoretically and experimentally and was optimized as an all-fiber edge filter for a rapid wavelength measurement application [59]. Low polarization dependence in the macrobending loss transmission spectrum is a requirement for such an all-fiber ratiometric wavelength measurement system. However, the structure of an

* P. Wang, G. Farrell, Y. Semenova, G. Rajan, "Investigation of Polarization Dependent Loss for a Macrobending Loss Sensitive Singlemode Fiber," Microwave and Optical Technology Letters, accepted for publication.

SMF28 fiber based edge filter is complex from a theoretical perspective for modeling and in addition an SMF28 fiber based filter requires a significant number of turns of fiber, for example, 22 turns with a bend radius of 11 mm [59], because SMF28 is bend loss insensitive. Therefore, the optimal design of a more compact fiber edge filter would benefit from using a bend loss sensitive singlemode fiber, and in [60], we proposed a bend loss sensitive singlemode fiber, 1060XP, for this purpose.

This paper presents the results of a thorough investigation of the PDL behavior of 1060XP fiber with different bend radii, including: 1) calculation of the correction factor of a bent 1060XP fiber with coating and absorbing layers; 2) theoretical modeling and PDL measurements of a bent 1060XP fiber, with coating and absorbing layers; 3) PDL measurements of bare bent 1060XP fiber with an absorbing layer. Through comparison of PDL results between 1060XP fiber with and without a coating, the fiber coating layer is shown to have significant effect on PDL performance.

3.2.2 Correction factor for bent 1060XP fiber with coating and absorbing layers

It is well known, when optical fiber is bent, that the presence of the coating layer(s) produces a so-called whispering-gallery mode due to the reflection of the radiated field at the interfaces of cladding-coating and coating-air layers. To reduce the whispering-gallery modes, the 1060XP fiber employed in this investigation is coated with an absorbing layer, and the fiber can thus be treated as a fiber core-cladding-infinite coating structure, as depicted in Fig. 15; where the *z*–axis is the direction of light propagation.

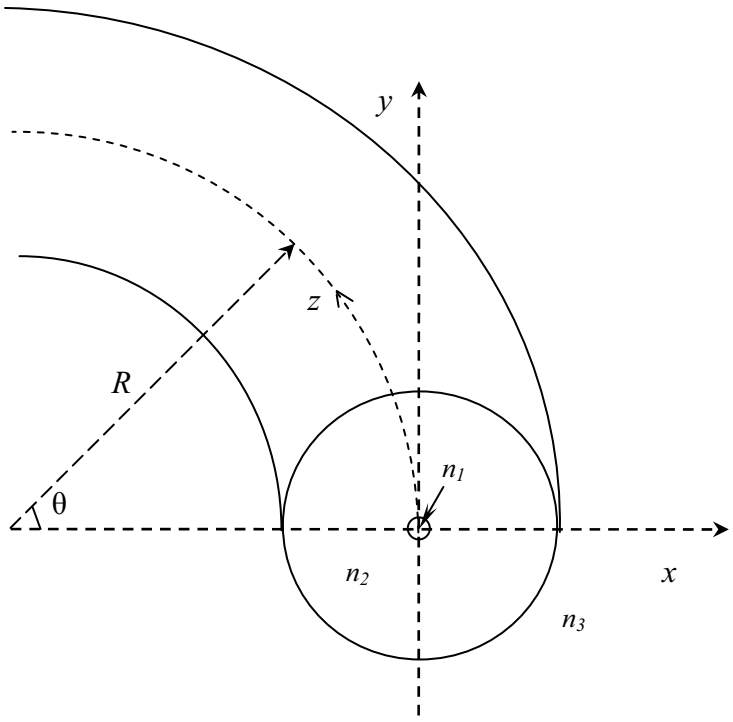

Figure 15. Cross section of bent fiber with core-cladding-infinite coating structure.

For 1060XP fiber, selected properties are listed in Table 3:

Table 3. Parameters of 1060XP fiber (refractive index values defined at 1550nm wavelength)

Parameters of 1060XP fiber	
Refractive index difference (between fiber core and cladding)	0.0067
Refractive index of primary coating	1.4975
Refractive index of secondary coating	1.5068
Diameter of fiber core	5.3 ± 0.3 μm
Diameter of fiber cladding	125 ± 0.5 μm
Diameter of primary coating	195 μm
Diameter of secondary coating	245 μm
NA (Numerical Aperture)	0.14
V (Normalized frequency)	1.5035

Following the weak-guidance approximation theory [61], when the fiber is bent, the Fourier transform scalar field in the cladding and infinite coating regions (q=2, 3) in y-direction can be expressed as:

$$\frac{d^2\bar{\psi}_q(x,\zeta)}{dx^2}+\left[k^2n_q^2(1+\frac{2x}{R})-\beta_0^2-\zeta^2\right]\bar{\psi}_q(x,\zeta)=0 \tag{3.1}$$

where ζ is the conjugate variable for the Fourier transform in y-direction. Following solution by an inverse Fourier transform of the y-field, formula (3.1) can be treated as [62]:

$$\psi_q(x,y)=\frac{1}{2\pi}\int_{-\infty}^{+\infty}\left[D_q(\zeta)B_i(X_q)+H_q(\zeta)A_i(X_q)\right]\cdot\exp(-i\zeta y)d\zeta \tag{3.2}$$

where $X(x,\zeta)=\left(\frac{R}{2k^2n_q^2}\right)^{2/3}\left[\beta^2+\zeta^2-k^2n_q^2(1+\frac{2x}{R})\right]$, and B_i and A_i are Airy functions, respectively. For any two adjacent layers, given the continuous boundary conditions of the field, the adjacent fields for the TE mode (polarization direction is x-z direction in Fig. 15) is given by [63]:

$$\begin{cases}D_q(\zeta)B_i[X_q(x_q,\zeta)]+H_qA_i[X_q(x_q,\zeta)]=D_{q+1}(\zeta)B_i[X_q(x_{q+1},\zeta)]+H_{q+1}A_i[X_q(x_{q+1},\zeta)]\\ D_q(\zeta)B_i'[X_q(x_q,\zeta)]+H_qA_i'[X_q(x_q,\zeta)]=D_{q+1}(\zeta)B_i'[X_q(x_{q+1},\zeta)]+H_{q+1}A_i'[X_q(x_{q+1},\zeta)]\end{cases} \tag{3.3}$$

By solving the boundary condition using perturbation and scalar approximation theory, the bend loss coefficient of the TE mode, defined as α_{TE}, can be calculated.

In prior work [64, 65], an "effective bend radius" (R_{eff}) was introduced to fit the theoretically calculated bend losses to experimentally measured values. R_{eff} is related to the measured bend radius (R_{exp}) by a wavelength-dependent elasto-optic correction factor that accounts for the change in refractive index induced by axial bending stress [65]. Fig. 16 shows TE-mode bend loss results

for 1060XP fiber coated with an absorbing layer (to remove reflections at the air-coating interface) measured when bend radius was systematically varied between 8.5 and 12.5 mm, at 1550 nm. Figure 16 also shows the theoretically calculated bend-loss values, both uncorrected (*i.e.*, R_{eff} = 1) and best-fit. Reasonable agreement between theoretical and experimental results is achieved with R_{eff}(1550 nm) = 1.283. Consequently, it is suggested that the correction factor of 1.283 at 1550 nm might be employed in the theoretical macrobending loss calculation of 1060XP fiber.

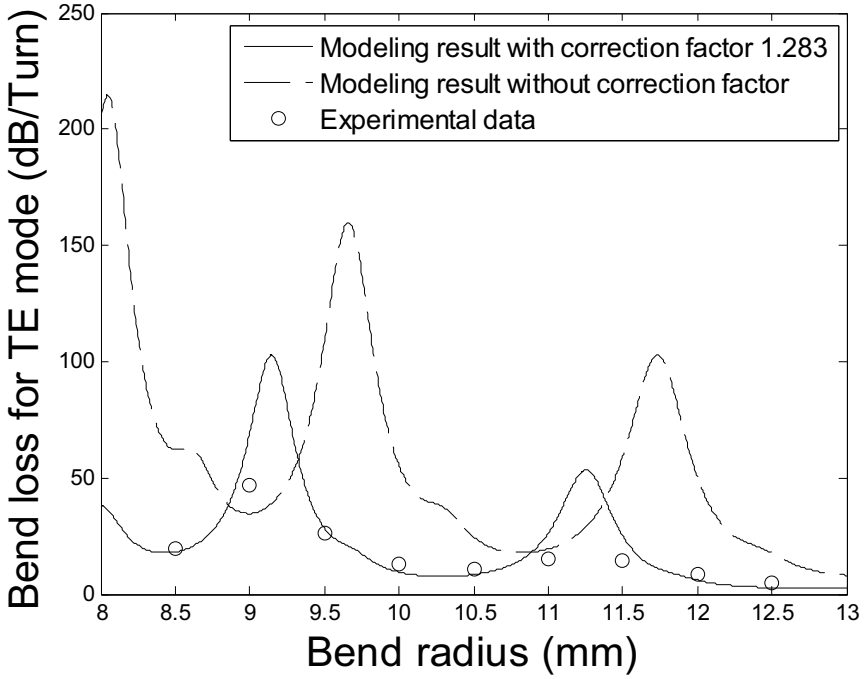

Figure 16. Calculated and measured macrobending loss for different bending radii at 1550 nm.

However, a bend loss based fiber edge filter is designed to cover a range of wavelengths. The correction factor varies with wavelength and while it is not practical to determine the value of the correction factor at all wavelengths, it was determined at 10 nm intervals over the wavelength range of interest between

1500 and 1600 nm. The correction factor as a function of wavelength is shown in Fig. 17.

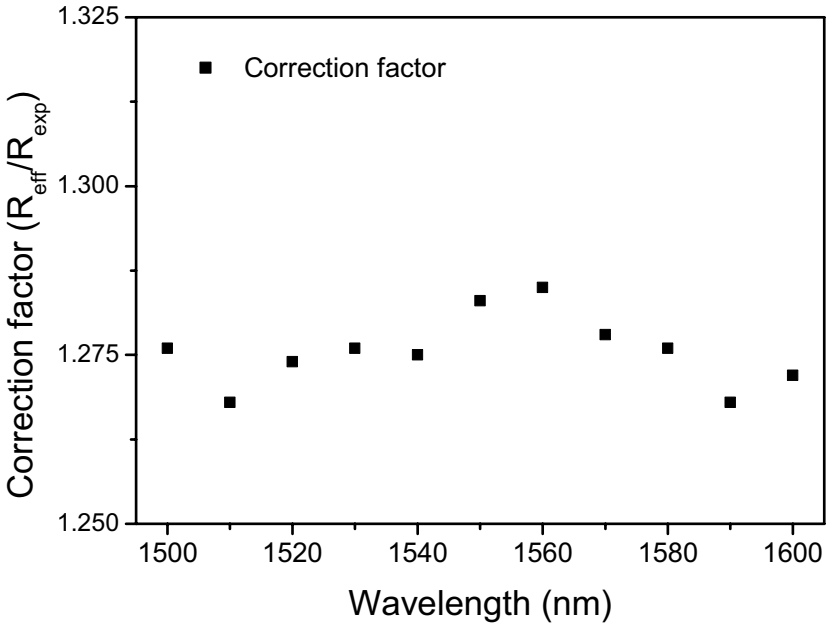

Figure 17. Correction factor as a function of wavelength.

3.2.3 Theoretical modeling and experiments for the PDL of a bent 1060XP fiber with coating and absorbing layers

To solve the different boundary conditions between the fiber's adjacent layers (q=2, 3), the adjacent fields for the TM mode (polarization direction is y-z direction in Fig. 15) can be expressed as following:

$$\begin{cases} D_q(\zeta)B_i[X_q(x_q,\zeta)] + H_q A_i[X_q(x_q,\zeta)] = D_{q+1}(\zeta)B_i[X_q(x_{q+1},\zeta)] + H_{q+1}A_i[X_q(x_{q+1},\zeta)] \\ \frac{1}{n_q^2}\left\{D_q(\zeta)B_i'[X_q(x_q,\zeta)] + H_q A_i'[X_q(x_q,\zeta)]\right\} = \frac{1}{n_{q+1}^2}\left\{D_{q+1}(\zeta)B_i'[X_q(x_{q+1},\zeta)] + H_{q+1}A_i'[X_q(x_{q+1},\zeta)]\right\} \end{cases} \tag{3.4}$$

Therefore, the bend loss coefficients, α_{TE} and α_{TM}, and the bend loss values, BL_{TE} and BL_{TM}, of the TE and TM modes can be calculated. To better characterize the polarization sensitivity of the bend loss, an absolute value of PDL can be defined by $PDL = \left|BL_{TE} - BL_{TM}\right|$. In our previous work [60], it was

found that PDL can induce variations in the transmission spectrum, and affect the accuracy of the measured wavelength.

To verify the modeling results, experimental PDL measurements were carried out using the apparatus shown in Fig. 18. In these experiments, the bending radius was controlled by wrapping the fiber around a variable-diameter mandrel, as shown in Fig. 18. Input from a tunable laser was polarization-controlled, and the TE and TM responses were measured using an optical spectrum analyser and associated data-collection software.

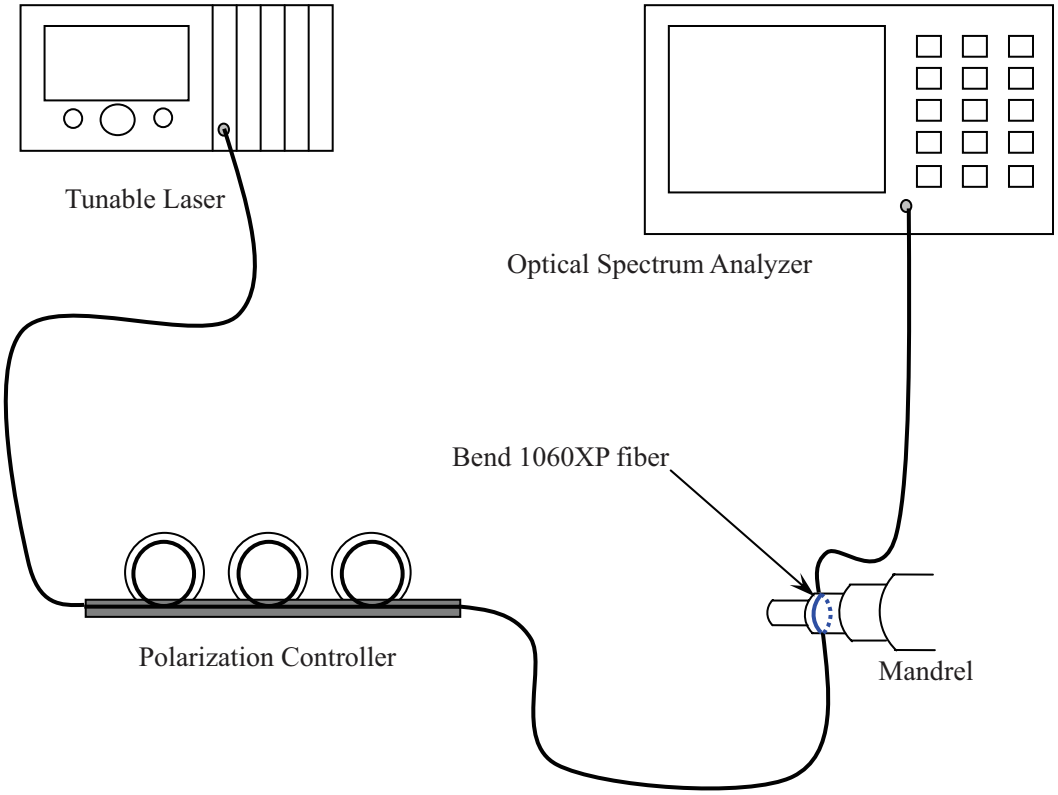

Figure 18. Schematic configuration of the experimental setup for PDL measurement[*].

[*] Tunable laser is a NETTEST OSICS ECL1560 external cavity laser, the Optical Spectrum Analyzer is an Agilent 86142B, while the polarization controller (THORLABS FPC560) is placed between the tunable laser and bending fiber to control the polarization state of the input signal to the bend filter.

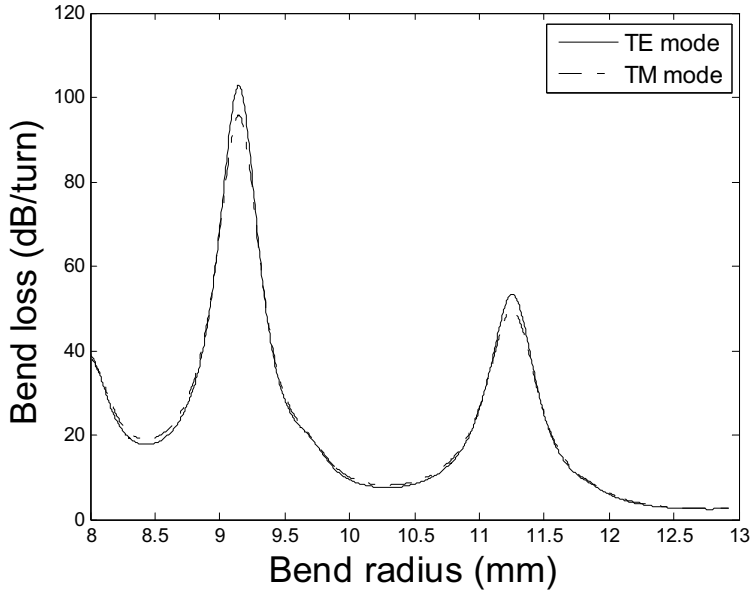

(a)

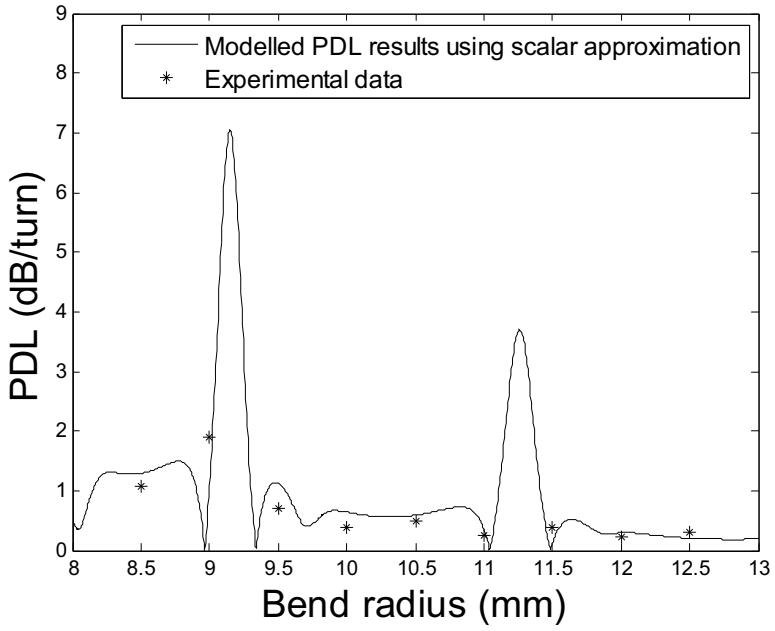

(b)

Figure 19. (a) Calculated bend loss for TE and TM mode for different bend radii (correction factor is 1.283 at 1550 nm wavelength); (b) theoretical and experimental differences in bend loss between TE and TM mode for 1060XP fiber with different bend radii.[*]

[*] In Figure 19, "dB/Turn" is employed to describe the power attenuation for a single loop structure based bending 1060XP singlemode fiber. From Figure 19(a), one can see circa 100 dB attenuation at the bend radius of 9.3 mm. It is important to point out that while a numerical model can produce attenuation values of this magnitude, it is not practically possible to measure such a large bend loss due to the accuracy and range limitations of the experimental setup.

As mentioned above using a scalar approximation of the wave equations for the analysis of light propagation in singlemode fiber, values of macrobending loss for the TE and TM modes are calculated as a function of bend radius and are presented in Fig. 19(*a*), while their difference value is shown in Fig. 19(*b*). The differences between calculated TE and TM mode bend losses are largest at the bend radii of 9.2 and 11.3 mm. Measured values are also shown and are generally in reasonable agreement with the calculated result. Occasional discrepancies between experimental and theoretical results in Fig. 19(*b*) are most likely caused by inaccuracy in measuring the bending radius and/or approximations made in calculating bend loss.

Fig. 20 shows the measured PDL values for 1060XP fiber at a 10.5 mm bend radius (single-turn); calculated results (using the correction factor obtained at 1550nm) are also shown. As mentioned in Sec. 3.2.2, PDL calculations employed correction factors at a limited number of wavelength intervals (10 nm) across the wavelength range 1500-1600 nm. Within this range, calculated and experimental results are in semi-quantitative agreement (with some random variations in the experimental data). The calculated results agree with experimental values more closely at 1500-1550 nm than at 1550-1600 nm. The discrepancy between the calculated PDL and measured results could be caused by approximations made in the calculations and/or by imperfect absorbing layer material coated on the fiber surface. If this layer does not absorb all the radiation from the core at the bend then some partial radiation will reflect from the fiber coating-air boundary and recouple with the fundamental propagation mode, resulting in changes to the polarization states of the fundamental mode.

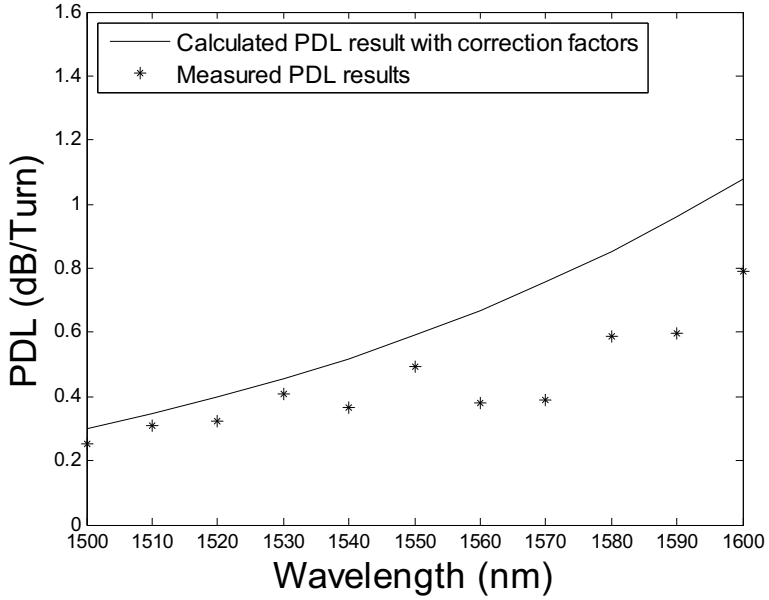

Figure 20. Experimental and calculated PDL values for fiber length of one turn and 10.5mm bend radius, across the wavelength range 1500-1600nm. (For calculated results, the correction factors measured which are presented in Fig. 17 are applied across this theoretical range.)

3.2.4 PDL of bare bent 1060XP fiber with an absorbing layer

According to the boundary equations (3.3) and (3.4), a stripped bare 1060XP fiber with an absorbing layer (q=1, 2), can be treated as a fiber core-infinite cladding structure, and the calculated PDL is virtually zero at a bend radius of 10.5 mm.

In the experiment, the bare fiber section coated with an absorbing layer using acrylic based material was bent to form a small 360^{o} loop in free space, with the bare fiber loop cross section protected by a polymer jacket for mechanical stability. The fiber ends were connected to a polarization controller and an optical spectrum analyzer, respectively. The measurement was undertaken as described in Sec. 3.2.3.

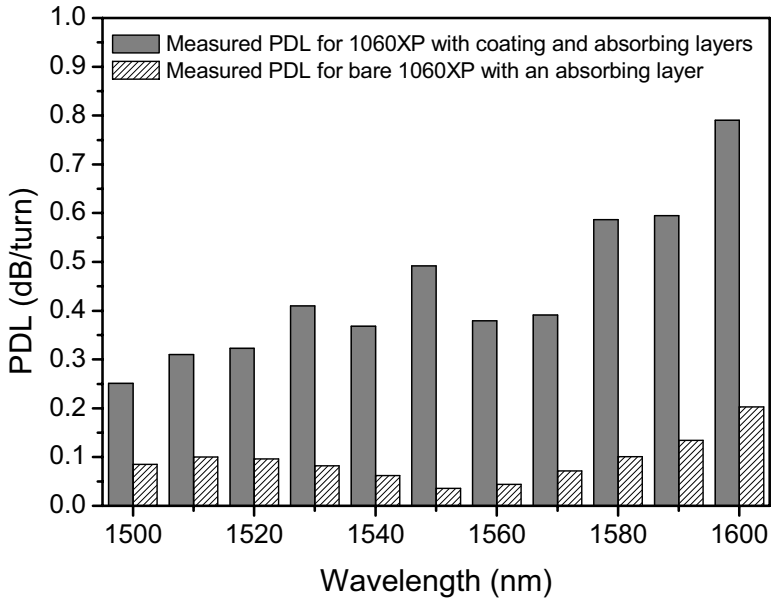

Figure 21. Measured PDLs for bend radius of 10.5 mm (one turn).

Experimental PDL values for bare 1060XP fiber with an absorbing layer are presented in Fig. 21. For comparison, measured PDL values for 1060XP fiber with coating and absorbing layers are also shown. PDL values for coated fiber are in general greater than for bare fiber. In Fig. 21, as mentioned in Ref. [61], the divergences between the experimental and theoretical PDL results for bare 1060XP fiber are most likely caused by imperfect in the absorbing layer material. In the PDL measurements, it should be noted that there is about 0.02 dB variation exists in the wavelength measurements due to the Signal-Noise-Ratio (SNR) of the tunable laser source, and it effects the polarization dependent loss measurement result as well. Overall we can conclude that the use of bare 1060XP fiber, for the implementation of a compact single-turn fiber edge filter, has a significantly better PDL performance by comparison with a 1060XP fiber with coating layer and absorbing layers.

3.2.5 Conclusion

In conclusion, both macrobending loss and PDL for bend loss sensitive fiber (1060XP) has been investigated theoretically and experimentally. Both theoretical and experimental results have shown that the coating layer has a significant influence on the polarization dependence of bend loss. It is suggested that the bent bare 1060XP fiber with an absorbing layer is more suitable for fiber bend loss edge filter applications.

3.2.6 Acknowledgement

The authors would like to thank Dr. Dan Kuehner for useful discussions and suggestions.

3.2.7 References

[55]. A. Mecozzi and M. Shtaif, The statistics of polarization-dependent loss in optical communication systems, IEEE Photon Technol Lett 14 (2002), 313-315.

[56]. R. M. Craig, Accurate Spectral Characterization of Polarization-Dependent Loss, J Lightwave Technol 21 (2003), 432-437.

[57]. L. Chen, Z. Zhang, X. Bao, Polarization dependent loss vector measurement in a system with polarization mode dispersion, Opt Fiber Technol 12 (2006), 251–254.

[58]. J. Q. Zhou, H. Dong, S. Aditya, Y.D. Gong, P. Shum, X. Guo, L. Ma, Two-states method for polarization dependent loss measurement, Opt Fiber Technol 13 (2007), 139–142.

[59]. Q. Wang, G. Farrell, T. Freir, G. Rajan and P. Wang, Low-cost wavelength measurement based on a macrobending single-mode fiber, Opt Lett 31 (2006), 1785-1787.

[60]. P. Wang, G. Farrell, Q. Wang and G. Rajan, An optimized macrobending-fiber-based edge filter, IEEE Photon Technol Lett 19 (2007),

1136-1138.

[61]. H. Renner, Bending losses of coated single-mode fibers: a simple approach, J Lightwave Technol 10 (1992), 544-551.

[62]. L. Faustini and G. Martini, Bend loss in single-mode fibers, J Lightwave Technol 15 (1997), 671-679.

[63]. Q. Wang, G. Farrell and T. Freir, Theoretical and experimental investigations of macro-bend Losses for standard single mode fibers, Opt Express 13 (2005), 4476-4484.

[64]. Y. Murakami and H. Tsuchiya, Bending losses of coated single-mode optical fibers, IEEE J Quantum Electron QE-14 (1978), 495-501.

[65]. A. B. Sharma, A. H. Al-Ani and S. J. Halme, Constant-curvature loss in monomode fibers: an experimental investigation, Appl Opt 23 (1984), 3297-3301.

❖ Comments by the author on Chapter 3

I. In previously published work [62, 63] involving bend loss predictions based on the scalar approximation method for the case of a fiber core-cladding-infinite coating structure, it is shown that significant peaks exist throughout the spectral responses. The reason can be explained as resonant couplings between the fundamental core mode and leaky cladding modes propagating near the cladding-coating interface. In a previous investigation (Q. Wang, et al., “Theoretical and experimental investigations of macro-bend Losses for standard single mode fibers”, Optics Express, Vol. 13, No.12, pp. 4476-4484, 2005), the agreement between modeled and experimental results at the bend loss peak position (especially for the wavelength of 1600 nm) have confirmed that the so-called whispering gallery mode, has an apparent effect on the bend loss characteristics so that loss peaks exist in the spectral response.

II. This chapter contains a range of experimental data results. In most cases the measurements were repeated multiple times to improve the accuracy of the measured data. It is therefore possible to illustrate and quantify the estimated experimental error existing in the published papers and by way of an example Figure 10 and Figure 17 are reproduced here with the addition of error bars.

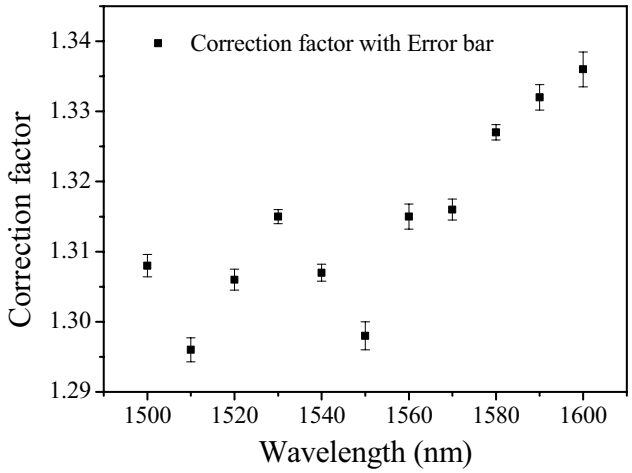

Figure 10. Correction factor with error bar as a function of wavelength for bare bending 1060XP fiber.

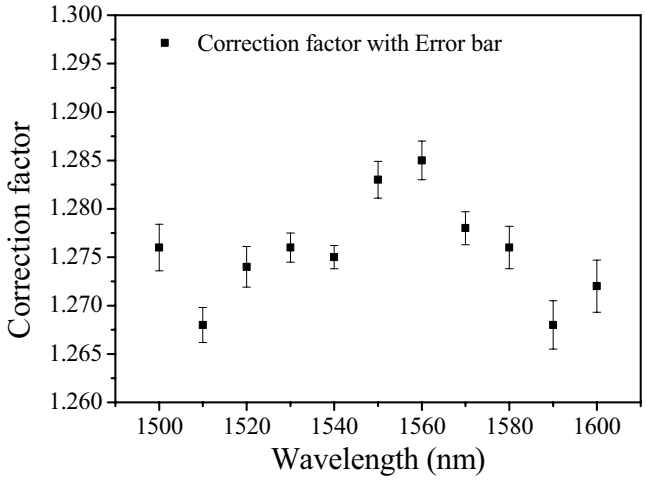

Figure 17. Correction factor with error bar as a function of wavelength for coated bending 1060XP fiber.

Chapter 4

Temperature dependence of fiber based edge filters

A primary aim of this research is to develop an effective modeling platform for singlemode fiber bend loss which can deal with a variety of fiber types and to utilize this modeling platform to investigate the design of a novel fiber bending loss edge filter, taking account of the effect of temperature, polarization and fiber tolerance.

It is well known that temperature changes the refractive index of fiber materials, and affects the refractive index profile of fiber as well, and results in a significant influence on the measurable accuracy of fiber edge filter for wavelength measurement application. This chapter contributes to achieve this aim by presenting the theoretical predictions of fiber temperature dependent loss models involving in the thermal expansion coefficients and thermo-optic coefficients of fiber material and verifying such models by experiments.

This chapter analyzes temperature dependent loss for a fiber bending loss edge filter based on a low bend loss fiber with multiple loops and a high bend loss fiber with a single loop structure. One theoretical model is developed for predicting the temperature dependence of low bend loss fiber with a structure consisting of a core-cladding inner-coating-outer-coating absorbing layer. Another model is developed for a stripped bare high bend loss fiber with core-cladding-absorbing layer structure. For both low bend loss and high bend loss fiber based edge filters, the experimental results show good agreement with

the proposed theoretical models. It is clear that temperature variations will significantly impact the accuracy of wavelength measurements. The proposed theoretical method can be used to evaluate the performance of a fiber-macrobending-based edge filter as a function of ambient temperature for high-speed wavelength measurements and also be of benefit in bend fiber based temperature sensing applications.

Previously developed theoretical models for calculating the temperature dependence of macrobending losses of singlemode fibers based on bend geometry considerations have demonstrated that whispering gallery modes propagating in the buffer coating of a singlemode fiber can lead to oscillations in the bending loss as a function of temperature. The period of such oscillations varies as a function of the bend geometry and the optical and physical properties of the buffer coating (such as the thermal expansion coefficient and thermo-optic coefficient). However, the bend geometry theory has limitations; for example, it predicts the bend loss accurately only for the core-cladding-coating-air fiber structure. It cannot be employed to predict the bend loss temperature behavior for the case of fiber coated with an absorbing layer, such as a fiber core-infinite cladding structure. Therefore, in this chapter, the theoretical model of temperature dependent loss is presented for the first time, which is based on a scalar approximation method, by using different thermal expansion coefficients and thermo-optic coefficients of the fiber core, cladding and coating layers, to allow for the prediction of temperature dependence. The temperature dependence of polarization dependent loss (PDL) for a macrobending standard singlemode fiber (SMF28) is also investigated both theoretically and experimentally. The experimental results show an overall agreement with the proposed theoretical

model over a temperature range from 0 to 70°C. An SMF28 based edge filter is used as an example regarding temperature dependent PDL performance.

4.1 Temperature dependence of macrobending loss in all-fiber bend loss edge filter*

Keyword: Temperature dependent loss, macrobending loss, singlemode fiber, SMF28, edge filter

Abstract: A theoretical model for macrobending-induced temperature dependent loss (TDL) for a standard singlemode fiber (SMF28) with dual coating layers is presented, with good agreement demonstrated between theoretical calculations and experimental results. The impact of temperature on two examples of an all-fiber based edge filter is also investigated theoretically and experimentally and using the developed model, it is shown that it is possible to predict the impact of temperature variations on an all-fiber based edge filter.

4.1.1 Introduction

It is well known that temperature change causes significant temperature dependent loss at a bend in a singlemode fiber. Temperature dependence for fiber macrobending loss has been presented in several published papers both theoretically and experimentally [66-69]. The fibers employed in most of the previous published works had a structure that consisted of a fiber core, cladding and a single coating layer.

The influence on bend loss of whispering gallery modes (WGMs) is an

* P. Wang, Y. Semenova, G. Farrell, "Temperature dependence of macrobending loss in all-fiber bend loss edge filter," Optics Communications, Vol. 281, pp. 4312-4316 , 2008.

important issue considered by many authors, with some publications considering the practical application of WGMs in developing an interferometric sensor [68, 69]. WGMs in bent optical fibers are excited when the radiating rays are reflected at interfaces such as the coating–air boundary or cladding–coating boundary. Such WGMs can recouple to the propagating mode in the fiber core and can result in wavelength dependent interference effects.

Most existing commercial standard singlemode fibers (such as SMF28) have two coating layers, which offer protection and stability to the fiber core and cladding. SMF28 fiber has been widely employed for optical communication and sensing. However, previously published investigations of the temperature dependent loss of bending fiber have been focused on the prediction of phase shift in the core modes induced by interference and no existing formulas have been presented for the modeling of theoretical temperature dependent loss of standard singlemode fiber with multiple coating layers. In this paper, the theoretical prediction of temperature dependent loss for an SMF28 fiber based on perturbation theory is presented for the first time.

One justification for the investigation is that recently macrobending singlemode fiber with an absorbing layer (such as SMF28 or 1060XP) has been investigated and optimized for use in a bend loss based edge filter for a rapid wavelength measurement system [70-72]. Changes in macrobending loss with temperature will alter the spectral responses of the fiber edge filter leading to inaccuracy in the measurement of wavelength.

For the bent SMF28 singlemode fiber employed in this paper, the existence of the coating layers produces WGMs for the bent fiber because of reflections at the interfaces at the boundaries of the cladding–coating, the inner and outer

coating layers and the coating–air layers. However, for a macrobending fiber based edge filter application, in order to maintain a quasi-linear filter transmission response with wavelength [70], an absorbing layer is required on the surface of the outer coating layer to absorb the radiated light in the outer coating and thus suppress the formation of WGMs at the coating–air interface. In the model the absorption layer is taken account of by assuming an infinite outer coating thickness.

In this paper, we report on both a theoretical and an experimental investigation of the bending induced temperature dependent loss of standard SMF28 singlemode fiber. The operating temperature is controlled within the range 0^{o}C to 70^{o}C, as the SMF28 polymer coatings would suffer degradation if the temperature is higher than 70^{o}C. The corresponding experimental results show a good agreement with the results of the theoretical modeling. Both the theoretical and experimental results suggest that both the thermal expansion coefficient (TEC) and thermo-optic coefficient (TOC) of the fiber materials have a significant influence on macrobending loss.

4.1.2 Modeling for temperature dependent loss of singlemode fiber with dual coating layers

As is well known, the refractive index of an optical material depends on temperature and wavelength. For silica material, the refractive index varies with the temperature as a result of lattice deformations in the silica matrix structure. For a fiber polymer coating material, the variation of the refractive index is induced by the amplitude of vibrations of polymer molecules and results in the translation and distortion of the cross-linked network within the polymer long molecule structure.

A series of theoretical formulations have been developed [73-77] for the prediction of the macrobending loss of singlemode fibers. For example, the theoretical modeling of fiber bending loss based on weak perturbance of the guide field for a multi-coating structure (such as SMF28) has been presented in Ref. [77], along with comparisons with the modeling of fiber macrobending loss which were presented in previous publications [73-76]. Based on the satisfactory agreement between the calculated and experimental results for SMF28 fiber in Ref. [77], the model presented in Ref. [77] is employed in this paper to predict the temperature dependent loss of bending SMF28 singlemode fiber.

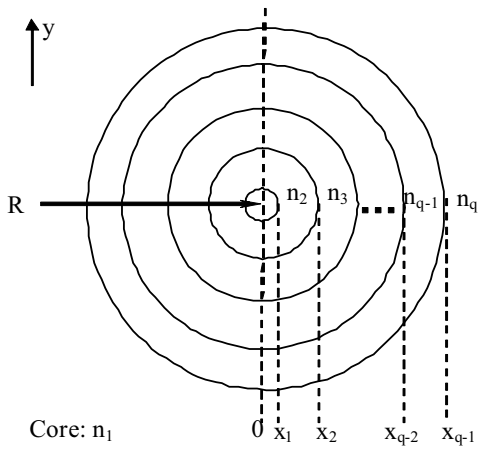

Figure 22. Cross-section of a bending fiber with multiple coating layers.

Fig. 22 gives the schematic cross-section of a bending fiber with multiple cladding or coating layers. The bending radius is denoted by R. For the q-th (q is a positive integer, q=1, 2, 3…) layer of fiber, its refractive index is n_q and the thickness is x_q-x_{q-1}. q=1 represents the core and q=2 represents the cladding layer.

As a starting point, the analysis in Ref. [75] is used, In Ref. [75], the fiber was assumed to consist of a core, cladding (q=2) and an infinite coating (q=3). When the fiber is bent, the Fourier transform scalar field in the cladding and infinite coating regions (q=2, 3) in the y-direction can be expressed as:

$$\nabla_t^2 \bar{\psi}_q(x,\zeta) + \left[k^2 n_q^2 (1+\frac{2x}{R}) - \beta_0^2 - \zeta^2 \right] \bar{\psi}_q(x,\zeta) = 0 \qquad (4.1)$$

where $\bar{\psi}_q(x,\zeta)$ is the Fourier transform along the *y*-direction of the transverse field component in region *q*; ζ is the conjugate variable for the Fourier transform in *y*-direction; n_q is the refractive index in region *q*; *k* is the well know wavenumber in vacuum at the wavelength λ, it can be expressed as $k = 2\pi/\lambda$; $\left(1+\frac{2x}{R}\right)$ is the correction factor for n_q^2 to take account of the change induced by the stress-optic effect; and β_0 is the complex propagation constant, the imaginary part of which is the bend loss coefficient. Following solution by an inverse Fourier transform of the y-field, equation (4.1) can be treated as [76]:

$$\psi_q(x,y) = \frac{1}{2\pi} \int_{-\infty}^{+\infty} \left[D_q(\zeta) B_i(X_q) + H_q(\zeta) A_i(X_q) \right] \cdot \exp(-i\zeta y) d\zeta \quad (4.2)$$

where $X(x,\zeta) = \left(\frac{R}{2k^2 n_q^2} \right)^{2/3} \left[\beta^2 + \zeta^2 - k^2 n_q^2 (1+\frac{2x}{R}) \right]$, and B_i and A_i are Airy functions, respectively. Both $D_q(\zeta)$ and $H_q(\zeta)$ are the Fourier spectra which were previously defined in Ref. [75]. For the outermost infinite layer, the relation between $D_q(\zeta)$ and $H_q(\zeta)$ can be defined as $H_q(\zeta) = -iD_q(\zeta)$. Thus by extending the model, for any two adjacent layers in the fiber structure, given the continuous boundary conditions of the field, the adjacent fields are given by [77]:

$$\begin{cases} D_q(\zeta) B_i[X_q(x_q,\zeta)] + H_q A_i[X_q(x_q,\zeta)] = D_{q+1}(\zeta) B_i[X_q(x_{q+1},\zeta)] + H_{q+1} A_i[X_q(x_{q+1},\zeta)] \\ D_q(\zeta) B_i'[X_q(x_q,\zeta)] + H_q A_i'[X_q(x_q,\zeta)] = D_{q+1}(\zeta) B_i'[X_q(x_{q+1},\zeta)] + H_{q+1} A_i'[X_q(x_{q+1},\zeta)] \end{cases} \qquad (4.3)$$

which has the form of $\begin{bmatrix} D_j(\zeta) \\ H_j(\zeta) \end{bmatrix} = \begin{bmatrix} M_{11} & M_{12} \\ M_{21} & M_{22} \end{bmatrix} \begin{bmatrix} D_{j+1}(\zeta) \\ H_{j+1}(\zeta) \end{bmatrix}$. Considering the core

and cladding layer, the relationship between $D_1(\zeta)$ and $H_1(\zeta)$ is obtained as the following:

$$D_1(\zeta) = \frac{M_{11}i + M_{12}}{M_{21}i + M_{22}} H_1(\zeta) = GH_1(\zeta) \tag{4.4}$$

Given the boundary condition at the interface between the core layer and cladding layer, then:

$$D_1(\zeta) B_i\left[X_2(x_1,\zeta)\right] + H_1(\zeta) A_i\left[X_2(x_1,\zeta)\right] = \frac{\pi}{\sqrt{\gamma^2+\zeta^2}} \exp\left(-a\sqrt{\gamma^2+\zeta^2}\right) \tag{4.5}$$

Therefore, $H_1(\zeta) = \dfrac{\dfrac{\pi}{\sqrt{\gamma^2+\zeta^2}} \exp\left(-a\sqrt{\gamma^2+\zeta^2}\right)}{GB_i\left[X_1(x_1,\zeta)\right] + A_i\left[X_1(x_1,\zeta)\right]}$ and finally according to perturbation theory the bend loss factor can be expressed as:

$$2\alpha = -2\frac{\kappa^2}{2\pi\beta V^2 K_1^2(a\gamma)} \mathrm{Im}\left(\int_{-\infty}^{\infty} H_1(\zeta) A_i\left[X_2(0,\zeta)\right] d\zeta \right) \tag{4.6}$$

This factor can be used for the calculation of bend loss for a fiber with one or more coating layers, and the above formulas are used in the investigation which follows of the temperature dependence of bending loss for SMF28 fiber.

In most previously published papers [74-76], the effective bend radius (a wavelength dependent correction factor) was employed to take account of stress induced refractive index changes in order to achieve a good agreement between the modeled results and the experimental results. However in our previously published work [77], the good agreement between the theoretical model and experimental results for Corning standard singlemode fiber-SMF28 showed that for this particular fiber, the so-called “effective bending radius” used to take account of macrobending stress, was not required. SMF28 is the fiber type employed in the investigations of temperature dependent loss in this paper. For

the theoretical model employed in this paper, to maintain generality, the stress-optic effect is included in the model and all formulas, but in applying the model for SMF28 fiber, the value of the correction factor is set equal to 1.

For the fiber used in this paper the key parameters at 20°C are shown in Table 4:

Table 4. Parameters of the standard corning SMF28 CPC6 dual coating singlemode fiber; (the refractive index values are defined at a wavelength of 1550 nm at the room temperature, about 20°C)

SMF28 fiber	Core	Cladding	Primary coating	Secondary coating
Refractive index	1.4504	1.4447	1.4786	1.5294
Radius (μm)	4.15	62.5	95	125
TEC α (K^{-1})	5.5×10^{-7}	5.5×10^{-7}	800×10^{-7}	$<100\times10^{-7}$
TOC β (K^{-1})	$\approx1\times10^{-5}$	$\approx1\times10^{-5}$	-2.9×10^{-4}	—

While most of the parameter values are published by the manufacturer of SMF28, some TEC and TOC values were extracted from Ref. [78].

With the parameters of TEC and TOC listed in the Table 4, the corresponding temperature dependent thickness and refractive index of each fiber layer at a temperature *T* can be expressed as:

$$x_T = \left(x_q - x_{q-1}\right)\cdot\alpha_q\cdot\Delta T \tag{4.7}$$

$$n_T = n_q\cdot\beta_q\cdot\Delta T \tag{4.8}$$

where x_q is the distance from the fiber core center to the *q*-th fiber layer boundary as shown in Figure 22; α_q is the TEC of the *q*-th layer of fiber material, β_q is the TOC of the *q*-th layer of fiber material and ΔT is the difference in temperature with respect to 20°C.

A bending singlemode SMF28 fiber with dual coating layers and an absorbing layer can be treated as core-cladding-primary coating-infinite coating structure. In the previous publications [73-77], it was found that radiation, which is launched from the fiber core at the bend enters the coating region(s) of the fiber and thus it is important in principle to consider the effect of absorption within the coating in modeling the behavior of a bent fiber. However in the theoretical model in this case, we assume an infinite outer coating thickness, which suppresses the evolution of strong WGMs that otherwise could arise at the coating-air interface, where the refractive index difference is 0.5294. Experimentally an absorbing layer is applied to the surface of the outer fiber coating to achieve the same effect. WGMs also evolve at the interface between the coatings, where there is a small refractive index change (0.0508). However the actual absorption coefficient of the coating layers is in any event very low. Given that the coating layers are 62.5 microns thick, the coating absorption loss is less than 0.02 dB at a wavelength of 1550 nm and is thus not considered significant enough for inclusion in the model.

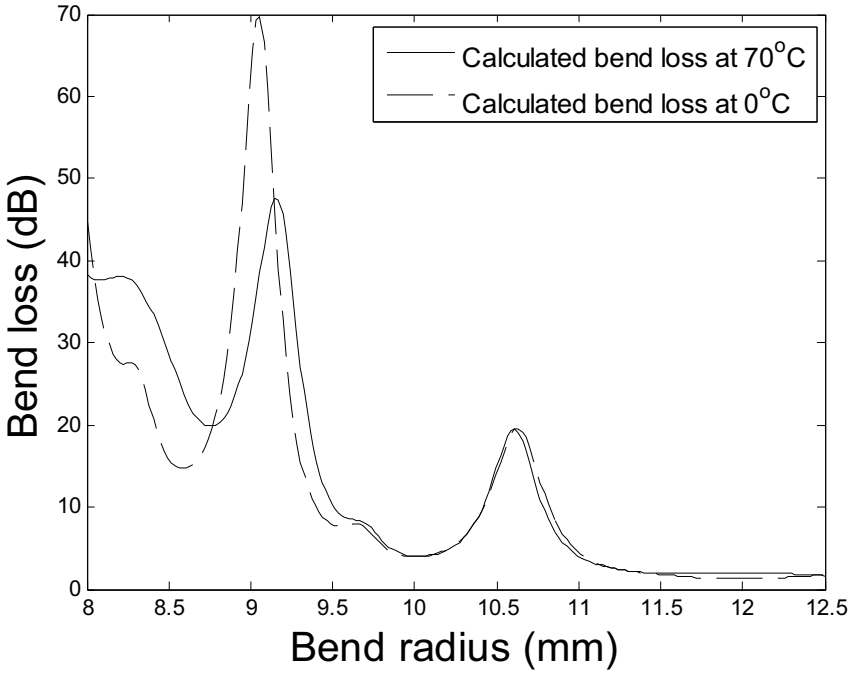

(a)

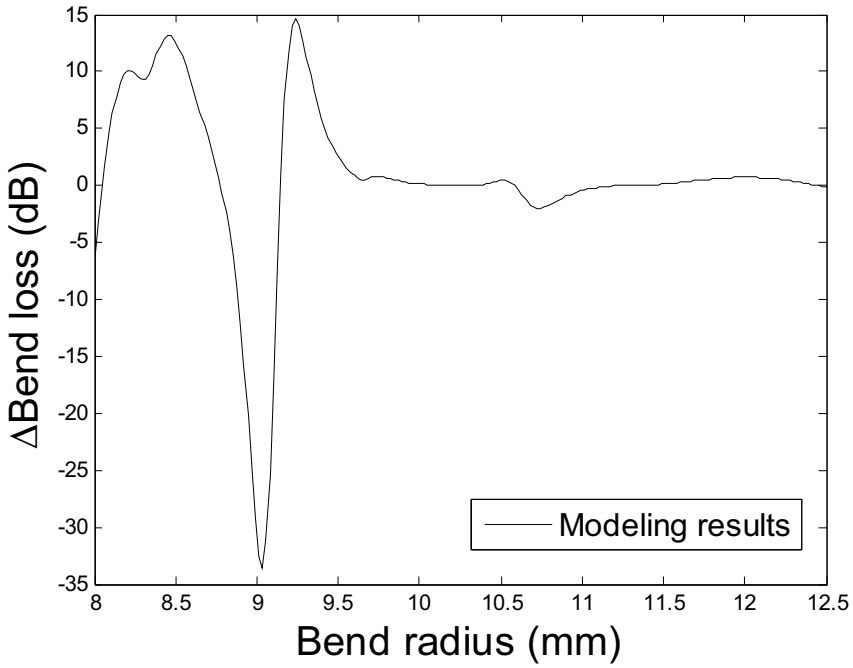

(b)

Figure 23. (a) Calculated macrobending loss for SMF28 fiber at the temperature of 0°C and 70°C, respectively; (b) Calculated result of difference of macrobending loss for SMF28 fiber between 0°C and 70°C at the wavelength of 1550 nm, the bending length is 10 turns.

In Figure 23 (*a*), the calculated bend losses are shown for two different

temperatures 0°C and 70°C. From this figure one can see that the bend loss at either temperature does not increase monotonically as the bending radius decreases. For example, bend losses for a bending radius of 9 mm are larger than those for a bending radius of 8.5 mm. This is due to the coherent coupling between the fundamental propagation mode and the reflected radiation from two interfaces: the cladding-inner coating interface and the inner coating-outer coating interface. These so-called whispering-gallery modes have a significant effect on the bend loss characteristics. The temperature dependent parameters TOC and TEC have a significant impact on the interference process and thus there are a significant changes in bend loss with temperature, which are also sensitive to the bend radius value, in particular below 9.5 mm. Overall a consequence of the fact that bend loss is not a monotonic function of bend radius is that when the temperature changes from 0°C and 70°C, the TDL at different bent radii (shown in Figure 23 (b)) displays significant variations in value and also changes sign.

Figure 23 (*b*) shows the calculated difference in macrobending loss for two temperatures, 0°C and 70°C, as a function of different bend radius ranging from 8 to 12.5 mm, where the bending fiber length is 10 turns and the wavelength is 1550 nm. The calculation was carried out by applying the corresponding TEC and TOC parameters of SMF28 fiber into the theoretical model described above. In Fig. 23 (*b*), one can also see that the calculated macrobending loss difference between 0°C and 70°C is very sensitive to the bend radius when the bend radius ranges from 8 to 9.5 mm due to the significant difference of bend losses between 0°C and 70°C presented in Fig. 23 (*a*). The maximal bend loss difference in Fig. 23 (*b*) is -32.67 dB for a bend radius of 9 mm.

4.1.3 Experimental results and discussion

Fig. 24 shows the experimental setup used for the measurement of temperature dependent loss; the SMF28 singlemode fiber is wrapped to form bend loops around a series of precisely dimensioned metal mandrels, with each mandrel providing a different usable diameter. The beginning and end of the bending fiber is fixed by a two-part epoxy to improve mechanical stability. The bending fiber was connected to a tunable laser and an optical spectrum analyser. The tunable laser has an output power range from +7 dBm to -7 dBm. Both the bending fiber with an outer absorbing layer and mandrel were attached to a thermoelectric Peltier cooler, which is controlled by a digital Temperature Controller (ITC 510, Thorlabs), while a digital resistance thermometer sensor probe is attached to the mandrel to accurately measure the temperature.

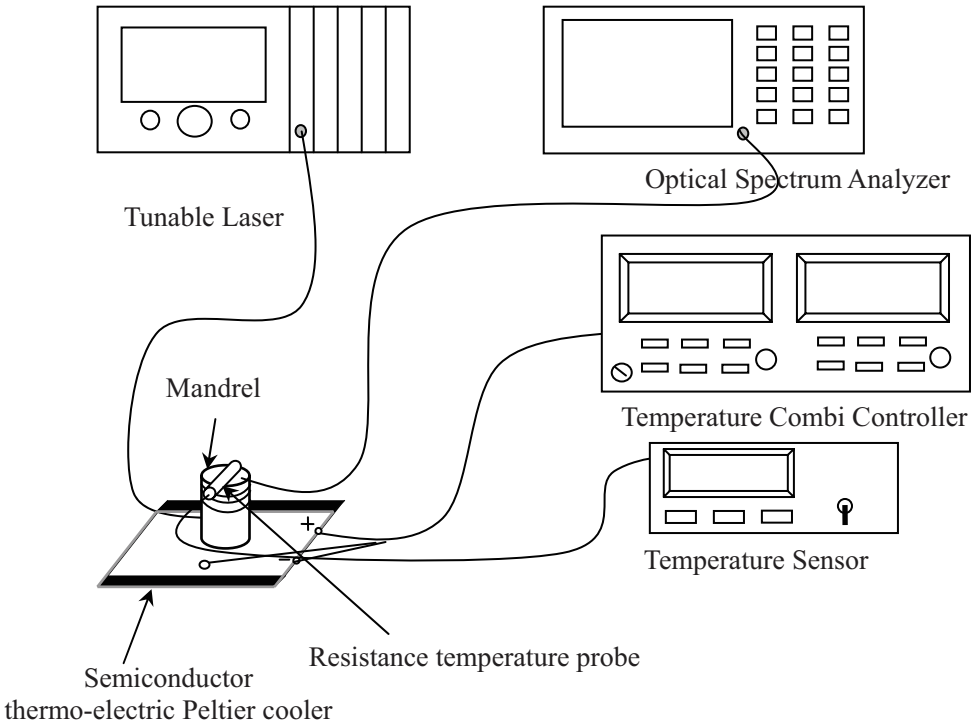

Figure 24. Experimental setup for measuring temperature dependent loss of macrobending fiber.

As presented in Ref. [66-68, 79], a bending singlemode fiber without an outer absorbing layer is attractive for applications such as thermo-optic interferometric sensing using the so-called whispering gallery mode, as fiber bends have a significant influence on the whispering gallery mode. However, a bending SMF28 fiber which does have an absorbing layer is needed in an all-fiber ratiometric wavelength measurement application [71, 77]. Thus the temperature dependent measurements of bending fiber are carried out with an absorbing layer to suppress the whispering gallery mode.

In order to better characterize the temperature dependent loss, the temperature dependent loss value is defined as the difference in bend loss between 0^oC and 70^oC thus:

$$TDL = BL_{70^oC} - BL_{0^oC} \tag{4.9}$$

Using this formula, the measurements of bend loss of the SMF28 are carried out for discrete bending radii ranging from 8 to 12 mm at a wavelength of 1550 nm at temperatures of 0^oC and 70^oC. In practice, because of the finite diameter of SMF28 fiber, the radius of the fiber should be treated as a part of bend radius, thus 0.125mm, the radius of SMF28 fiber, is added to each mandrel radius. In Fig. 25, both the theoretical modeling (solid line) and experimental temperature dependent loss results (star points) as a function of different bending radii are presented, from which one can see that the theoretical modeling of temperature dependent loss shows a reasonable agreement with the experimental results. The discrepancy between the calculated temperature dependent loss and measured results could be induced by the limited physical accuracy of each bend radius and the scalar approximation modeling of bending loss.

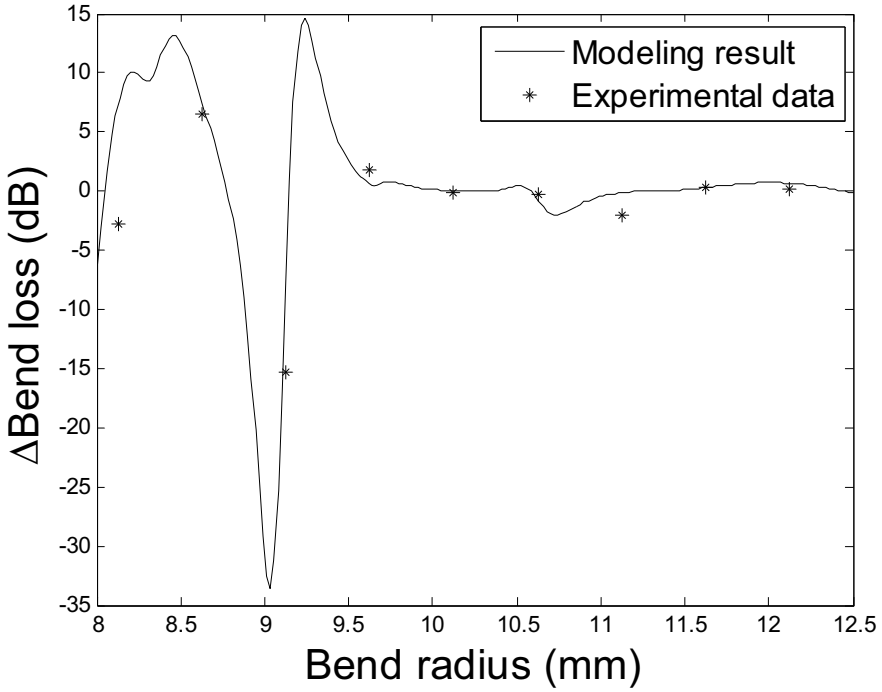

Figure 25. Calculated and measured bend loss of SMF28 as a function of bend radius at wavelength 1550 nm with a bending length of 10 turns.

The primary concern in this work is to study the impact of temperature on an all-fiber based edge filter. Using the model above, it is possible to predict the impact of temperature variations on an all-fiber based edge filter. We investigate this temperature dependence by measuring the bend loss for two different edge filters over the range 0^{o}C and 70^{o}C, in 5 ^{o}C increments. Both of the edge filters have bending radii equal to those which have been investigated in our previous publication [80]. The two cases of fiber edge filters are, case 1) a bending length of 10 turns (is 667.59 mm) for the bending radius of 10.5+0.125 mm and case 2) a bending length of 20 turns (is 1272.35 mm) for a bending radius of 10+0.125 mm,

In the measured bend loss results, both the transition loss which exists in the section between the bent section and the straight fiber, and the insertion loss which includes the interconnection loss and splicing loss, are deducted from the

total transmission loss to obtain the “pure” bend loss within the bent section.

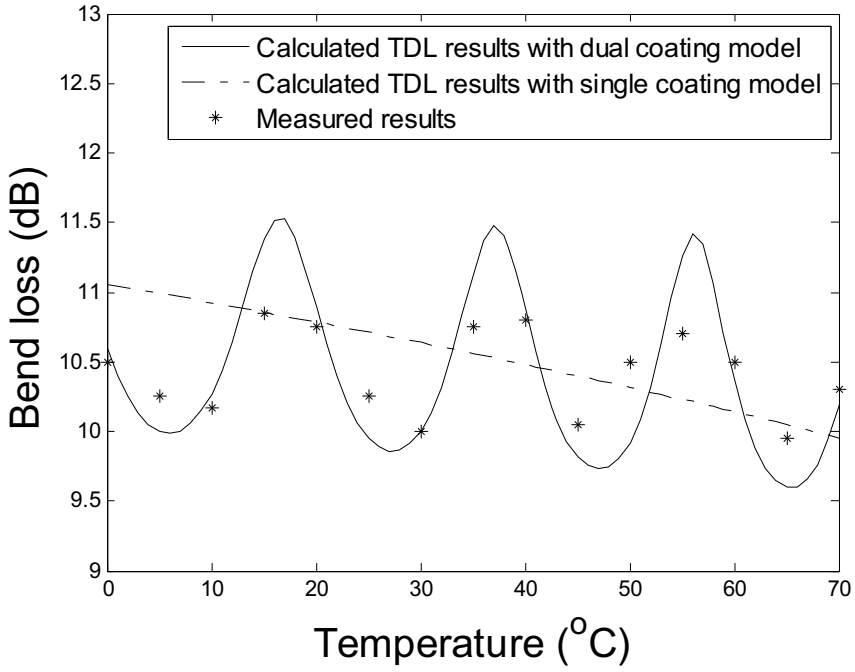

(a)

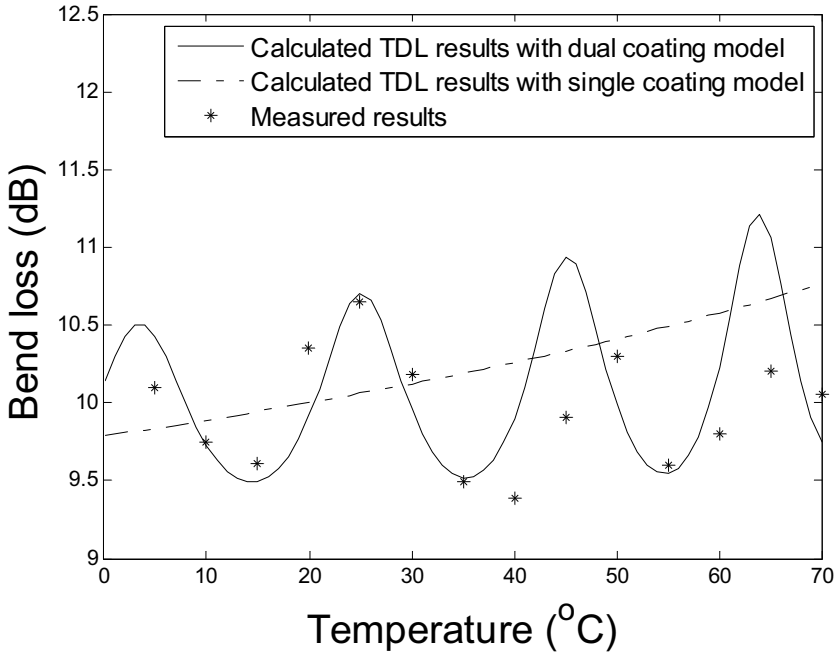

(b)

Figure 26. Modeled and measured macrobending loss results for temperature ranging from 0 to 70°C at a wavelength of 1550 nm, the bending radius is a) 10.5+0.125 mm with a bending length of 10 turns; b) 10+0.125 mm with a bending length of 20 turns.

In Figure 26 (*a*) and (*b*), the variation in the edge filter loss with temperature at 1550 nm is presented for two different bend radii/bend length combinations. The Figures show both experimental and modeled results for both single and dual coating layer models. The calculated TDLs using a dual coating layer model are in reasonable overall agreement with the experimental results. It is clear also that the single layer model, while it may be accurate at predicting loss at a fixed temperature of 20^{o}C, is not adequate for predicting the variation of loss with temperature. Also from Fig. 26 (*a*) and (*b*), one can see that wave-like variations exist in both modeled and measured temperature dependent loss results.

A physical interpretation of these results is as follows. In the theoretical model with single-coating layer, the fiber coating is assumed to be infinitely thick and hence the radiation entering the coating layer from the cladding propagates away from the fiber without any subsequent reflection. This explanation is consistent with the monotonic behaviour of the dashed-dot curves in Fig. 26 (*a*) and (*b*). In the theoretical model with dual-coating layer, the primary coating layer has a finite thickness and the secondary coating layer is assumed to be infinitely thick. Hence radiation entering the primary coating from the cladding is partially reflected at the first interface of the cladding-primary coating layer, and again at the second interface of the primary-secondary coating layer. The finite thickness of the primary coating layer combined with the index differences on either side form in effect a simple Fabry-Perot interferometer. Therefore as both the refractive index and thickness of the primary coating varies with changes in temperature, at a fixed wavelength, the fraction of incident radiation in the primary coating that is reflected back into the cladding toward the core will vary periodically. This would account for the oscillations in the

solid curves in the Fig. 26 (*a*) and (*b*).

In Figure 26 (*a*) and (*b*), the discrepancy between the calculated TDLs and measured results could be caused by: 1) the approximations made in the calculation. The scalar approximation theory is built on a base of perturbation theory, and the interface of between the fiber cladding and infinite coating layer was treated as an infinite plane and the light field within the core is approximated by the unperturbed field of the straight fiber with an infinite cladding as mentioned in Section 4.1.2; 2) Temperature induced mechanical stress, for example asymmetric expansion between the primary and secondary coating layer as temperature changes. In table 4, one can see that the TEC values for the primary and secondary coatings are significantly different. This means that as temperature changes, varying stress forces will be induced between the coatings, increasing overall stress and perturbing the loss measurements. The theoretical and experimental work is ongoing on these issues.

4.1.4 Conclusion

In this paper, macrobending induced temperature dependent losses for a standard singlemode fiber (SMF28) have been investigated both theoretically and experimentally. The calculations of temperature dependent loss of bending SMF28 fiber are also presented based on perturbation theory and it shown that the developed model can be utilized to successfully predict the temperature dependence of an all-fiber bend loss edge filter, where the fiber has a dual coating.

4.1.5 Reference

[66]. R. Morgan, J. S. Barton, P. G. Harper and J. D. C. Jones, “Temperature

dependence of bending loss in monomode optical fibres," Electron. Lett. Vol. 26 No. 13, pp. 937-939 (1990).

[67]. F. M. Haran, J. S. Barton and J. D. C. Jones, "Bend loss in buffered over-moded optical fibre: LP_{11}mode and 'whispering gallery' mode interaction," Electron. Lett. Vol. 30 No. 17, pp. 1433-1434 (1994).

[68]. F. M. Haran, J. S. Barton, S. R. Kidd and J. D. C. Jones, "Optical fibre interferometric sensors using buffer guided light," Meas. Sci. Technol. Vol. 5, pp. 526-530 (1994).

[69]. Y.-G. Han, J. H. Lee and S. B. Lee, "Discrimination of bending and temperature sensitivities with phase-shifted long-period fiber gratings depending on initial coupling strength," Opt. Exp. Vol. 12 No. 14, pp. 3204-3208 (2004).

[70]. Q. Wang, G. Farrell, T. Freir, G. Rajan, and P. Wang, "Low-cost wavelength measurement based on a macrobending single-mode fiber," Opt. Lett., Vol. 31, No. 12, pp. 1785-1787 (2006).

[71]. Q. Wang, G. Farrell and T. Freir, "Study of transmission response of edge filters employed in wavelength measurements," Appl. Opt., Vol. 44, No.36, pp. 7789-7792 (2005).

[72]. P. Wang, G. Farrell, Q. Wang and G. Rajan, "An optimized macrobending-fiber-based edge filter", IEEE Photon. Technol. Lett., Vol. 19, No. 15, pp. 1136-1138 (2007).

[73]. C. Vassallo, "Perturbation of a LP mode of an optical fibre by a quasi-degenerate field: a simple formula," Opt. & Quantum Electron. Vol. 17, No. 3, pp. 201-205 (1985).

[74]. I. Valiente and C. Vassallo, "New formalism for bending losses in coated single-mode optical fibres," Electron. Lett., Vol. 25, No. 22, pp. 1544-1545 (1989).

[75]. H. Renner, "Bending losses of coated single-mode fibers: a simple approach," J. Lightwave Technol., Vol. 10, No. 5, pp. 544-551 (1992).

[76]. L. Faustini and G. Martini, "Bend loss in single-mode fibers," J. Lightwave Technol., Vol. 15, No.4, pp. 671-679 (1997).

[77]. Q. Wang, G. Farrell, and T. Freir, "Theoretical and experimental investigations of macro-bend losses for standard single mode fibers," Opt. Exp., Vol. 13, No. 12, pp. 4476-4484 (2005).

[78]. C.-C. Lai, W.-Y. Lee and W.-S. Wang, “Gamma radiation effect on the fiber Fabry–Pérot interference sensor,” IEEE Photon. Technol. Lett., Vol. 15, No. 8, 1132-1134 (2003).

[79]. S. H. Nam and S. Yin, “High-temperature sensing using whispering gallery mode resonance in bent optical fibers,” IEEE Photon. Technol. Lett., Vol. 17, No. 11, pp. 2391-2393 (2005).

[80]. Q. Wang, G. Rajan, P. Wang, and G. Farrell, “Polarization dependence of bend loss for a standard singlemode fiber,” Opt. Express, Vol. 15, No. 8, pp. 4909-4920 (2007).

4.2 Temperature dependence of a macrobending edge filter based on a high-bend loss fiber*

Abstract: The temperature dependence of a macrobending bare fiber based edge filter is investigated both theoretically and experimentally. The fiber used is a high bend loss fiber, type 1060XP. The experimental results show a good agreement with the proposed theoretical model over a temperature range from 0 to 80oC. It is shown that the strong temperature dependence of a high-bend loss fiber has a significant influence on the performance of a fiber edge filter used in a wavelength measurement application. However it is also concluded that such a temperature dependent performance can be beneficially utilized in a fiber temperature sensing application.

OCIS codes 060.2310, 120.2440, 120.6780

4.2.1 Introduction

A singlemode bent fiber can provide a range of useful characteristics which can be utilized, for example, in novel fiber components such as sensors and edge filters [81-83] or can be used to enhance the operation of fiber lasers. Such bent fiber based components have the advantages of ease of fabrication and simplicity of interconnection to other fibers.

Recently, in an application involving an edge filter for rapid wavelength measurement, the macrobending loss of multiple turns of SMF28 fiber has been investigated theoretically and experimentally [83] in order to optimize the

* P. Wang, G. Rajan, G. Farrell, Y. Semenova, "Temperature dependence of a macrobending edge filter based on a high-bend loss fiber," Optics Letters, Vol. 33, No. 21, pp. 2470-2472, 2008.

structure. Such a fiber based edge filter utilizes a splitter, a bending fiber based edge filter, a reference arm and two photodetectors. One splitter arm connects to the edge filter, while the other arm acts as a reference arm. Both arms are terminated in photodetectors to measure optical power levels. Given the wavelength dependence of bend loss, the ratio of the measured power levels at the two photodetectors is a strong function of wavelength. Therefore with a suitable calibration wavelength can be measured.

Two key parameters for an edge filter are baseline loss and discrimination range. A bend loss based edge filter operates over a wavelength range from λ_1 with a progressively larger attenuation as the wavelength increases from λ_1 to λ_2. The baseline loss is defined as the loss of the filter at λ_1, while the discrimination range is the difference between the attenuation at λ_1 and λ_2.

In our previously published investigations [84, 85], it was found that the fiber polymer coating layer, which provides mechanical protection for the fiber, has a significant influence on both fiber bending loss and polarization dependent loss. For the fiber bend loss edge filter application, such coating layer(s) can also induce random variations throughout the measured transmission spectrum [86].

Removal of the coating(s) is only feasible if a relatively short length of fiber is used in the filter. Therefore it is desirable to use a bend loss sensitive fiber where the normalized frequency V is lower. A shorter fiber length also reduces the length of fiber exposed to mechanical stress, reducing the chance of mechanical failure. For this reason, an optimized macrobending fiber edge filter based on a bend sensitive fiber with single turn structure has been developed and presented [86]. 1060XP fiber is chosen in [87] as an example of a high-bend loss fiber, originally developed for fiber laser applications. The fiber is stripped of its

coating layer to remove the influence of the fiber coatings and has an optical absorption layer applied to the cladding. By comparison with SMF28 fiber presented previously [83], both theoretical and experimental results have shown that the 1060XP fiber based edge filter can effectively remove the coating(s) induced influences mentioned above, and the bending loss of bare 1060XP fiber with an absorbing layer can achieve a marginally better polarization dependent loss behavior than an equivalent SMF28 based edge filter, with the added benefit of a more compact physical structure (1 turn instead of 22 turns for SMF28, for a similar bend radius). For a wavelength measurement system based on a 1060XP based edge filter [87], the measurement resolution was found to be 10 pm at 1550 nm.

In practice, in the experiments in [86] it was found that changes in temperature affected the measured bending loss. Upon investigation it was realized that because the bend loss of 1060XP is approximately two times more temperature sensitive than SMF28, so the spectral response of an edge filter based on 1060XP fiber would be more temperature dependent. Used in a wavelength measurement system, temperature changes could adversely affect the accuracy of the wavelength measurement system. There is a need therefore to properly quantify the temperature dependence of 1060XP fiber, to determine the extent of the effect on the spectral response of an edge filter so as to develop solutions such as active temperature control of the filter or ambient temperature feedback to adjust the calibration of the system as temperature changes. The temperature dependent properties of 1060XP bent fiber also suggest a possibility of designing and developing a novel temperature sensor based on a simple bending fiber structure, with the fiber bend loop optimized as an optical fiber

probe with small bending radii.

In this letter, the temperature dependent loss (TDL) behavior for the key edge filter parameters, baseline loss and discrimination range, for a 1060XP based edge filter are investigated and presented. The investigation involves both theoretical modeling of TDL and experimental verification. The theoretical numerical modeling shows a good agreement with the measured results for the TDL of bent 1060XP fiber with a correction factor (namely, the wavelength dependent effective bend radius, which is employed to achieve good agreement between the modeled results and the experimental results due to the fiber bending stress) of 1.298 at a wavelength of 1550 nm.

4.2.2 Theoretical modeling

In previously published work [87], for a fiber bend loss edge filter application, the bare cladding fiber was coated with an absorbing layer. Analytically this is approximately equivalent to a fiber structure with an infinite cladding and the expression for calculating the fiber bend loss coefficient with an infinite cladding has been expressed by Marcuse in Ref. [88]. The correction factor [89, 90] has been… utilized in the calculated model of bending loss to fit the experimental results.

For the silica material used in the fiber, the physical expansion or contraction of the material's volume in response to temperature changes is characterized by silica's thermal expansion coefficient (TEC).

The refractive index of an optical material depends on temperature and wavelength. For silica material when the ambient temperature changes the consequent refractive index variations, are characterised by the thermo-optic

coefficient (TOC). The bend loss of bare 1060XP fiber with a bend radius of 10.5 mm at a wavelength of 1550 nm is based in the first instance on the theoretical model by Marcuse presented in Ref. [88]. However the Marcuse model does not take account of temperature effects and so cannot be used to predict TDL. Therefore the model used here is that extended in [86] by using different TECs and TOCs for the fiber core and cladding, to allow prediction of temperature dependence.

For 1060XP singlemode fiber, the corresponding parameters are shown in Table 5:

Table 5. Parameters of the 1060XP fiber.

1060XP fiber	**Core**	**Cladding**
Diameter (μm)	5.3 ± 0.5	125 ± 0.5
TEC α (K^{-1})	~5.5×10^{-7}	—
TOC β (K^{-1})	~1.1×10^{-5}	~1×10^{-5}

Previously, the presented fiber bend loss edge filter [83] utilized for a measurable wavelength range from λ_1 to λ_2, provides a strong monotonically increasing discrimination range. The two parameters, baseline loss and discrimination range can be used to effectively evaluate the performance of a fiber edge filter.

To gain an insight into the influence of temperature on the baseline loss and discrimination range, the calculated baseline loss and discrimination range as a function of different bend radii at a temperature of 0 ^{o}C and 80^{o}C, is presented in Fig. 27.

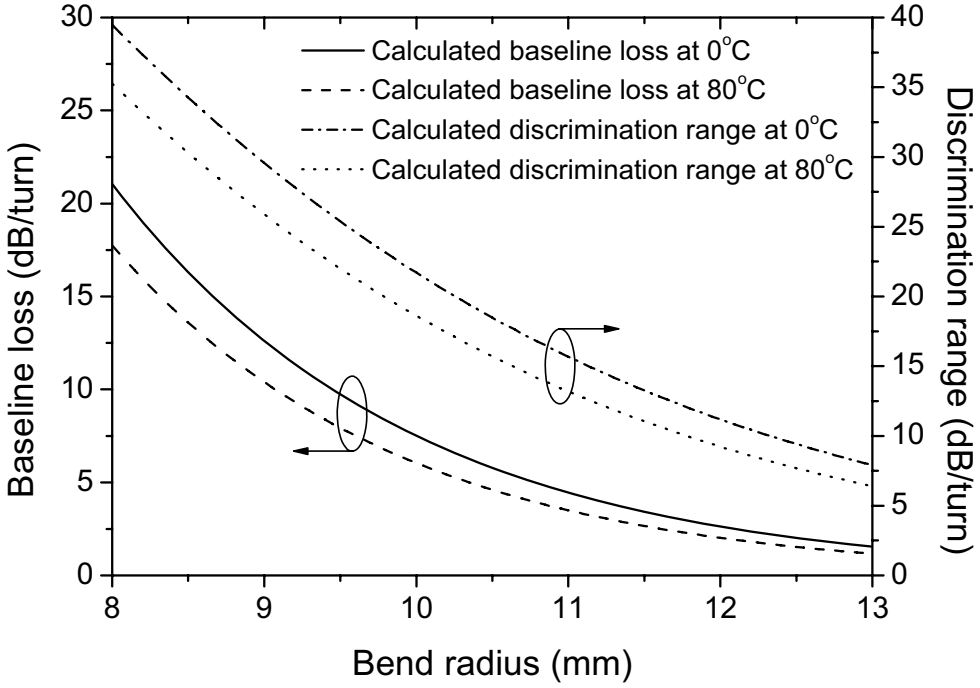

Figure 27. Calculated baseline loss and discrimination range at 0°C and 80°C, for a fiber length of one turn, with correction factors of 1.308 @1500 nm and 1.336@1600 nm.

Given the potential temperature sensing application mentioned above, this temperature range is chosen to match the available experimental range, even though it exceeds the temperature range one would expect in an ambient environment.

As shown in Fig. 27, if the temperature changes from 0°C to 80°C, significant changes occur in both baseline loss and discrimination range, with a consequent impact on the spectral response of a 1060XP based edge filter. For example, for a selected bend radius of 10.5 mm [87], the baseline loss changes from 5.785 dB to 4.604 dB, and the discrimination range changes from 18.48 dB to 15.698 dB when temperature changes from 0°C to 80°C.

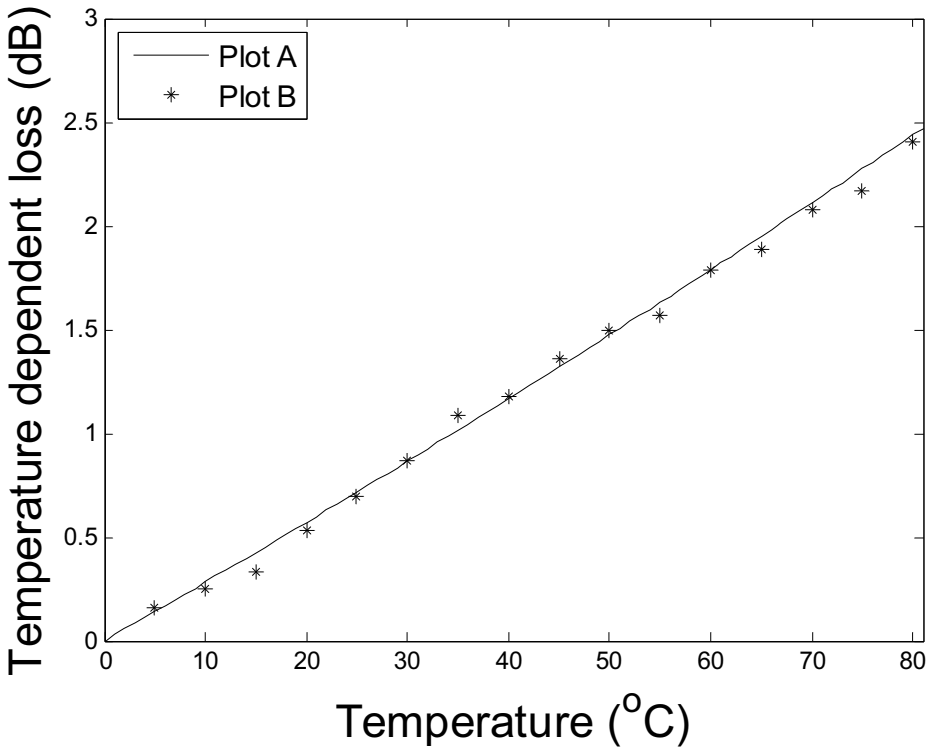

Figure 28. Calculated (Plot A) and measured (Plot B) TDL.

In this work, the TDL value is defined as the absolute value of the difference in bend loss between 0°C and a temperature of T^oC, where T can vary from 0°C to 80°C, thus:

$$TDL = \left| BL_{T^oC} - BL_{0^oC} \right| \tag{4.10}$$

The TDL of bending bare 1060XP fiber with a bend radius of 10.5 mm at a wavelength of 1550 nm is calculated. The model used is the same as that used for Figure 27. In Fig. 28, it is shown that the modeled TDL results (Plot A) demonstrate a strong monotonic increase from a start temperature (0°C) to an end temperature (80°C). For a SMF28 fiber base edge filter [86], it is found that the TDL displays several strong peaks in the bend loss response at different bend radii due to whispering gallery mode (WGM) effects guided at the cladding-coating interface, whereas for bare 1060XP fiber presented in Fig. 28, it is clear that the TDL changes monotonically over the measured temperature

range. This difference indicates that temperature induced variations in the bending loss response of coated fiber are strongly influenced by the fiber coatings and that a striped bare fiber with absorbing layer effectively reduces the impact of WGMs.

4.2.3 Experimental verification

In order to verify the theoretical model for TDL, an experimental setup for measuring TDL was developed and is shown in Fig. 29. The bending fiber was connected to a tunable laser and an optical spectrum analyzer. The bare 1060XP fiber section coated with an absorbing layer (acrylic based material) is bent to form a small 360^{o} bend, and is mounted on a thermoelectric Peltier cooler using a two-part epoxy to improve mechanical stability.

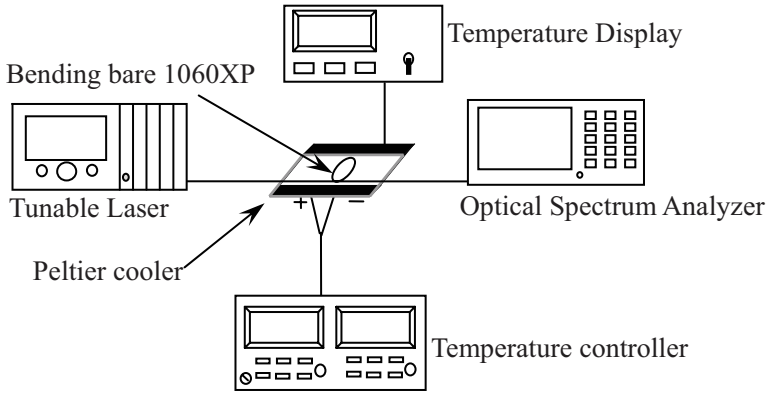

Figure 29. Experimental setup for measuring TDL.

The TDL of the 1060XP fiber was measured for a bending radius of 10.5 mm at a wavelength of 1550 nm. The experimental TDL results of 1060XP as a function of the temperature range from 0 to 80^{o}C are presented in Fig. 28 (Plot B).

In Fig. 28, one can also see that there is a good agreement between the calculated (Plot A) and experimental data (Plot B). The perceptible divergence

between the experimental and theoretical results may be caused by: 1) the limitations of the absorbing layer on the surface of the bare fiber where the absorbing layer does not absorb all the radiation lost at the bend at the fiber cladding-air interface, leading to WGMs effects. The limitations of the absorbing layer are twofold: firstly the absorption of the layer is limited and secondly it is known that there may be small gaps in the coverage of the layer on the glass as the layer is applied manually. Further investigation using different absorbing layer materials is ongoing; 2) minute discrepancies between the temperature of the fiber and the reference thermometer sensor probe, for example those resulting from ambient airflow.

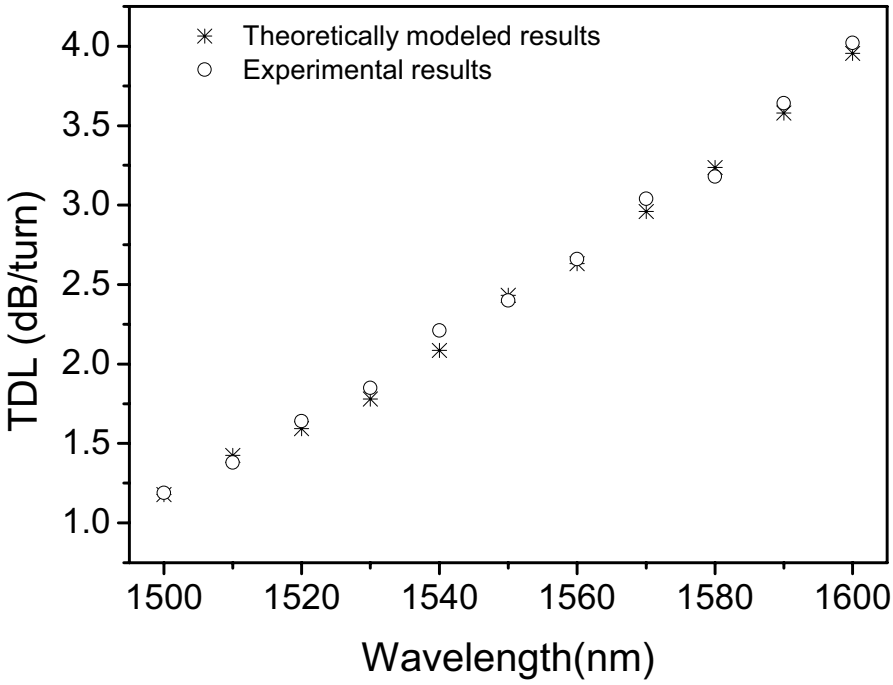

Figure 30. Calculated and measured TDL as a function of wavelength.

To better illustrate and evaluate the temperature influence of a macrobending-based 1060XP fiber edge filter as a wavelength measurement application over the whole wavelength range from 1500 to 1600 nm, the

theoretical and experimental macrobending loss differences between 0°C and 80°C over the wavelength range from 1500 to 1600 nm for a designed bend radius of 10.5 mm are presented in Fig. 30. The correction factors determined at 10 nm intervals over the wavelength range of interest between 1500 and 1600 nm are used in the TDL theoretical model. As shown in Fig. 30, one can see that there is very good match between the calculated and experimental data. The experimental TDL data shows a monotonically increasing characteristic which matches the proposed theoretical predictions well. The measured TDL is about 1.19 dB/turn at a wavelength of 1500 nm and is circa 4.02 dB/turn at a wavelength of 1600 nm.

4.2.4 Conclusion

In conclusion, we have studied and investigated the temperature dependence of bare macrobending 1060XP fiber theoretically and experimentally, for an all-fiber bending loss edge filter application. The experimental results show a good agreement with the proposed theoretical model. For a 1060XP fiber based edge filter, it is clear that temperature variations will significantly impact the accuracy of wavelength measurements. Our method can be used to evaluate the performance of a fiber macrobending based edge filter as a function of ambient temperature for a range of applications.

4.2.5 Reference

[81]. F. M. Haran, J. S. Barton, S. R. Kidd and J. D. C. Jones, "Optical fibre interferometric sensors using buffer guided light," Meas. Sci. Technol. 5(5), 526-530 (1994).

[82]. S. H. Nam, and S. Yin, "High-Temperature Sensing Using Whispering Gallery Mode Resonance in Bent Optical Fibers," IEEE Photon. Technol.

Lett., 17, 2391-2393 (2005).

[83]. Q. Wang, G. Farrell, T. Freir, G. Rajan, and P. Wang, “Low-cost wavelength measurement based on a macrobending single-mode fiber,” Opt. Lett., 31(12), 1785-1787 (2006).

[84]. Q. Wang, G. Farrell, and T. Freir, “Theoretical and experimental investigations of macro-bend losses for standard single mode fibers,” Opt. Express, 13(12), 4476-4484 (2005).

[85]. Q. Wang, G. Rajan, P. Wang, and G. Farrell, “Polarization dependence of bend loss for a standard singlemode fiber,” Opt. Express 15(8), 4909-4920 (2007).

[86]. P. Wang, Y. Semenova, and G. Farrell, “Temperature dependence of macrobending loss in all-fiber bend loss edge filter,” Opt. Commun., 281, 4312-4316 (2008).

[87]. P. Wang, G. Farrell, Q. Wang, G. Rajan, “An optimized macrobending-fiber-based edge filter,” IEEE Photon. Technol. Lett., 19(15), 1136-1138 (2007).

[88]. D. Marcuse, “Curvature loss formula for optical fibers,” J. Opt. Soc. Am. 66(3), 216-220 (1976).

[89]. H. Renner, “Bending losses of coated single-mode fibers: a simple approach,” J. Lightw. Technol., 10(5), 544-551, (1992).

[90]. L. Faustini and G. Martini, “Bend loss in single-mode fibers,” J. Lightw. Technol., 15(4), 671-679, (1997).

4.3 The temperature dependence of polarization dependent loss for a macrobending singlemode fiber based edge filter*

Keywords: Temperature dependence, polarization dependent loss, macrobending loss, singlemode fiber, edge filter

Abstract: The temperature dependence of polarization dependent loss (PDL) for a macrobending standard singlemode fiber (SMF28) is investigated both theoretically and experimentally. The experimental results show an overall agreement with the proposed theoretical model over a temperature range from 0 to 70^{o}C. An SMF28 based edge filter is used as an example regarding temperature dependent PDL performance. It is shown that the temperature variations have a significant influence on the polarization dependence of macrobending loss, and further impact on such a fiber bend loss edge filter used in a wavelength measurement application. It is also concluded that by using proposed models, such a temperature dependent birefringence can be beneficially predicted in bending fiber sensing applications.

4.3.1 Introduction

Fiber macrobending loss has been extensively investigated for applications in optical sensing and communication systems [91-94]. Recently an edge filter based on macrobending standard singlemode fiber (SMF28) using multiple turns has been demonstrated for application in a rapid ratiometric wavelength

* P. Wang, Y. Semenova, G. Rajan, T. Freir and G. Farrell, "The temperature dependence of polarization dependent loss for a macrobending singlemode fiber based edge filter," IEEE Photonics Technology Letters, accepted for publication, January 2009

measurement system [94, 95]. However, in the previously published investigations [96, 97], it was found that the fiber polymer coating layer(s), which provides a mechanical protection, has a significant influence on both the polarization and temperature dependence of macrobending loss as a result of the difference between the thermal expansion coefficients (TECs) and thermo-optic coefficients (TOCs) of the coating layer (CPC6 acrylate polymer) and the fused silica cladding layer. Both PDL and temperature dependent loss (TDL) can affect the accuracy of wavelength measurement [96, 97], therefore a low polarization and temperature dependence in the macrobending loss transmission spectrum is a requirement for such an edge filter.

It is well known that the refractive index of an optical material depends on temperature and wavelength. In practice, temperature variations will alter the spectral response of the fiber edge filter, in comparison to the response used at the point of calibration, leading to inaccuracy in the measurement of wavelength. Furthermore, the influence of temperature variations can also change the polarization states of the bending fiber. Several theoretical models have been developed and presented in Ref. [96, 97] for predicting the PDL/TDL influences on the spectral responses of bending singlemode fiber. To the best of our knowledge, a correlation between the temperature and polarization dependence of macrobending loss in a singlemode fiber has not been addressed yet and is important for the development and complete characterization of a macrobending fiber based edge filter.

In this letter, we study the temperature induced variations in PDL of standard singlemode fiber (SMF28) both theoretically and experimentally. The operating temperature in our experiments is controlled within the range from 0^{o}C to 70^{o}C.

The corresponding experimental results show a satisfactory agreement with the results of the theoretical modeling. The developed theoretical model offers a possibility of predicting the temperature induced PDL of a macrobending standard singlemode fiber employed as an edge filter, furthermore, it also suggests the possibility of utilizing the temperature induced birefringence in an interferometric fiber-optic gyro or a temperature sensor based on a bending fiber structure.

4.3.2 Theoretical modeling

In previously published work [96], the theoretical formulation of bend loss of the singlemode fiber was refined for the TE and TM modes separately based on a scalar approximation method, which takes account of the respective boundary conditions at the interface between the fiber cladding and coating layer. Following the theoretical approximations and formulations in that reference and extending them for any two adjacent layers of fiber structure, given the continuous boundary conditions of the field, the adjacent fields for the TE mode can be expressed as:

$$\begin{cases} D_q(\zeta)B_i[X_q(x_q,\zeta)] + H_q A_i[X_q(x_q,\zeta)] = D_{q+1}(\zeta)B_i[X_q(x_{q+1},\zeta)] + H_{q+1}A_i[X_q(x_{q+1},\zeta)] \\ \frac{1}{n_q^2}\left\{D_q(\zeta)B_i'[X_q(x_q,\zeta)] + H_q A_i'[X_q(x_q,\zeta)]\right\} = \frac{1}{n_{q+1}^2}\left\{D_{q+1}(\zeta)B_i'[X_q(x_{q+1},\zeta)] + H_{q+1}A_i'[X_q(x_{q+1},\zeta)]\right\} \end{cases} \tag{4.11}$$

And the adjacent fields for the TM mode can be expressed as:

$$\begin{cases} D_q(\zeta)B_i[X_q(x_q,\zeta)] + H_q A_i[X_q(x_q,\zeta)] = D_{q+1}(\zeta)B_i[X_q(x_{q+1},\zeta)] + H_{q+1}A_i[X_q(x_{q+1},\zeta)] \\ D_q(\zeta)B_i'[X_q(x_q,\zeta)] + H_q A_i'[X_q(x_q,\zeta)] = D_{q+1}(\zeta)B_i'[X_q(x_{q+1},\zeta)] + H_{q+1}A_i'[X_q(x_{q+1},\zeta)] \end{cases} \tag{4.12}$$

Applying these boundary conditions the bend loss coefficients, α_{TE} and α_{TM}, and the bend loss values, BL_{TE} and BL_{TM}, of the TE and TM modes can be

calculated. To characterize the polarization sensitivity of the bend loss, a PDL value can be calculated using the relationship $PDL = BL_{TE} - BL_{TM}$.

Corning standard singlemode fiber SMF28 consists of a fiber core, a cladding, primary coating and secondary coating layers. In our previous work [97], it is clear that the single coating layer model, while it may be accurate for the theoretical prediction of bending loss at a fixed temperature of 20^{o}C, is not adequate for predicting the variation of bending loss with temperature. Therefore, the TDL models with a dual coating layer have been employed, which are in reasonable overall agreement with the experimental results. In the model, a bending singlemode SMF28 fiber with dual coating layers and an absorbing layer should be treated as a core-cladding-primary coating-infinite coating structure. In this letter the scalar approximation method is utilized for the theoretical modeling of PDL for such a double coating structure.

In Figure 31, for a bending radius from 8 to 13 mm with a bending length of 10 turns, the calculated PDLs at a wavelength of 1550 nm are shown for two different temperatures 0^{o}C and 70^{o}C. The theoretical prediction was implemented by taking in account the corresponding TEC and TOC parameters of SMF28 fiber in the theoretical model described in Ref. [97]. From Figure 31, one can see that for either of the operating temperatures, as the bend radius decreases the PDL value does not increase monotonically but rather displays a number of peaks, e.g., PDL for bending radius of 9 mm is much higher (about two times) than that at 8 and 8.5 mm, so that in places the PDL actually decreases when the bend radius decreases. This effect is a result of a coherent coupling between the fundamental propagation mode and the so-called whispering-gallery modes (WGMs) which evolve at the cladding-coating and inner coating-outer coating

interfaces. These WGMs have a significant effect not only on the bend loss but also on the PDL characteristics. Overall the theoretical modeling results support the conclusion that the PDL at each temperature is not a monotonic function of the bend radius, and the temperature dependence of the PDL at different bent radii displays significant variations in value and also changes sign.

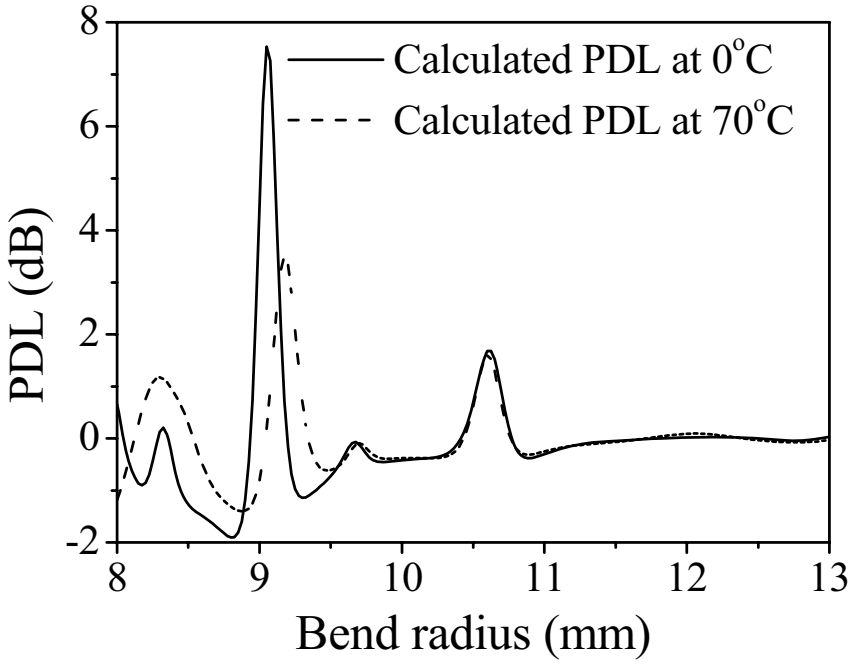

Figure 31. Calculated PDLs for SMF28 fiber at the temperature of 0°C and 70°C, respectively.

The primary concern in this letter is to investigate the impact of temperature induced variations in PDL for a standard singlemode fiber used in an edge filter for a rapid wavelength measurement application. Using the theoretical model above, it is possible to predict the impact of temperature variations on the PDL of an all-fiber based edge filter sample. Using SMF28 as an example two cases are considered: Case 1) a bending length of 10 turns (circa 667.59 mm) with a bending radius of 10.625 mm and case 2) a bending length of 20 turns (circa 1272.35 mm) with a bending radius of 10.125 mm.

Both samples (case 1 and case 2) have spectral responses suitable for

application as edge filters in a ratiometric wavelength measurement system. The polarization dependent performances as a function of ambient temperature for these two cases are plotted in Fig. 32. From the figure, both plots exhibit wave-like oscillations within the temperature range from 0 to 70°C, consistent with the temperature dependence of macrobending loss presented in Ref. [97]. From Fig. 32 it also can be seen that the calculated PDL for case 1 is larger than that of case 2. One possible reason is that as shown in Fig. 31, the calculated PDL is very sensitive to bend radius at certain bending radii; given the same bending length in Fig. 31 of 10 turns, the PDL at the bending radius of 10.625 mm is much larger than the PDL at the bending radius of 10.125 mm.

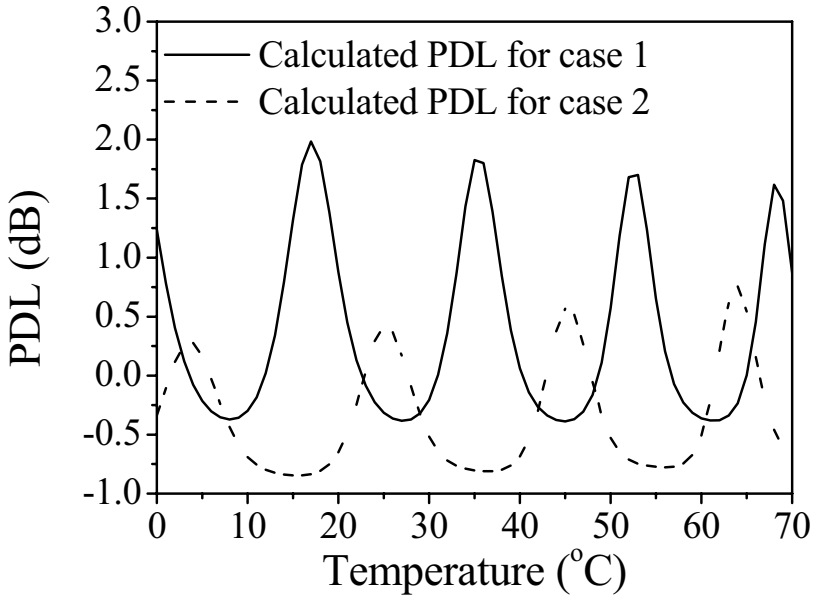

Figure 32. Calculated PDLs versus different temperature for two fiber bend loss edge filters.

4.3.3 Experimental verification and discussion

To verify the results calculated above, an experimental setup was used as shown in Fig. 33. The SMF28 fiber is wrapped over a series of precisely dimensioned metal mandrels, with each mandrel providing a different usable diameter. The beginning and end of the bending fiber section is fixed by a two-part epoxy to

ensure mechanical stability. A tunable laser (TL) and an optical spectrum analyzer (OSA) are employed as a source of light and detector and a polarization controller (PC) is added between the TL and bending fiber to change the polarization states of input signals. The bending loss value for the TE and TM modes can be estimated from the OSA while tuning the PC. Both the bending fiber with an outer absorbing layer and mandrel were bonded to a semiconductor thermo-electric Peltier cooler (STPC) and a heat sink by a silica-based thermally conductive adhesive. The STPC is controlled by a digital temperature controller, while a digital resistance thermometer sensor probe is attached to the mandrel to accurately measure the temperature.

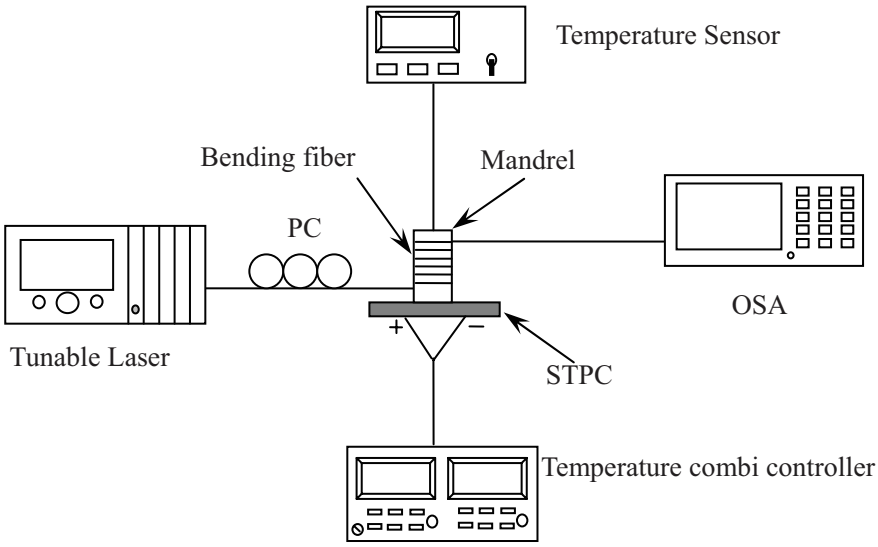

Figure 33. Experimental setup for measuring temperature dependence of PDL.

The experiment is carried out by measuring the PDL of the two edge filter samples, Case 1 and Case 2, over the range of temperatures from 0^{o}C to 70^{o}C with $5\,^{o}$C increments. Both calculated and measured results are plotted in Figure 34 (a) and (b). As a comparison, the calculated temperature dependent PDL with single coating is also presented in Figure 34 (a) and (b). It is clear also that the single coating layer model, while it may be accurate at predicting PDL at a fixed

temperature of 20°C, is not adequate for predicting the variation of PDL with temperature. From both of Figures, one can see that the calculated PDLs using a dual coating layer model are in reasonable agreement with the experimental results. Wave-like variations exist in both the modeled and measured temperature dependent PDL results which can be explained as follows: In the theoretical model, the primary coating has a finite thickness and the secondary coating is assumed to be infinitely thick. Hence radiation entering the primary coating from the cladding is partially reflected at the first interface between the cladding and the primary coating layer and again at the interface between the primary and secondary coating layers. The finite thickness of the primary coating layer combined with the refractive index differences on either side comprises a simple Fabry-Perot (F-P) interferometer. Hence as the index/thickness of the primary coating varies with temperature the fraction of the incident radiation from the cladding that is transmitted into the primary coating will vary periodically, which further results in the periodicity of the PDL spectral response and the oscillations in the PDL curves in Fig. 34 for both the modeled and experimental results. In the theoretical model with a single-coating layer, the fiber coating is assumed to be infinitely thick and hence the radiation entering the coating layer from the cladding propagates away from the fiber without any subsequent reflection. The monotonic behaviour of the single coating layer results in Fig. 34 (a) and (b) is a confirmation that no F-P cavity is formed in this case.

The discrepancies between the calculated temperature dependent PDLs and measured results could be caused in the first instance by the scalar approximations made in the calculation. The scalar approximation theory is based on perturbation theory, which was developed for predicting the bending

loss of singlemode fiber [98-101], and the calculation of polarization dependence for a singlemode fiber includes some approximations. For example, to consider the polarization dependence of bend loss caused by the coating layers, the boundary conditions at the interface between the cladding and coating layers in the calculation of the bend loss need to be treated separately for the TE and TM mode and using the conventional definition, the PDL can be calculated by the difference between the simulated TE and TM modes, thus the calculated PDL results inherit the approximations of the scalar approximation theory; Secondly, in the model the interface between the cladding and coating layers is approximated as a plane. The limited dimensional accuracy of each bend radius, set by the accuracy of the mandrel diameter is also a source of error, which is compounded by the fact that, as was shown in earlier and in Fig. 31, the calculated PDL is very sensitive to temperature at certain bending radii. Finally, the temperature step of 5 degrees was utilized in the experiments in order to ensure reasonable experimental durations. Using of a smaller temperature step could improve the agreement between calculated and measured results.

From this experimental verification, for an SMF28 fiber based edge filter, it is clear that temperature variations will significantly impact the PDL, and will further influence the accuracy of wavelength measurements. Our theoretical method can be used to evaluate the PDL performance of a fiber macrobending based edge filter as a function of ambient temperature. Moreover, PDL and its temperature dependence can significantly influence light transmission properties for any simple bending fiber structure such as, for example, bending fiber loops utilised for sensing applications as polarisation interferometers or fiber gyroscopes. The general agreement between calculated and measured results

suggests that this model could be used for analysis and evaluation of performance of such devices, improving their temperature stability and facilitating the development of new types of fiber sensors.

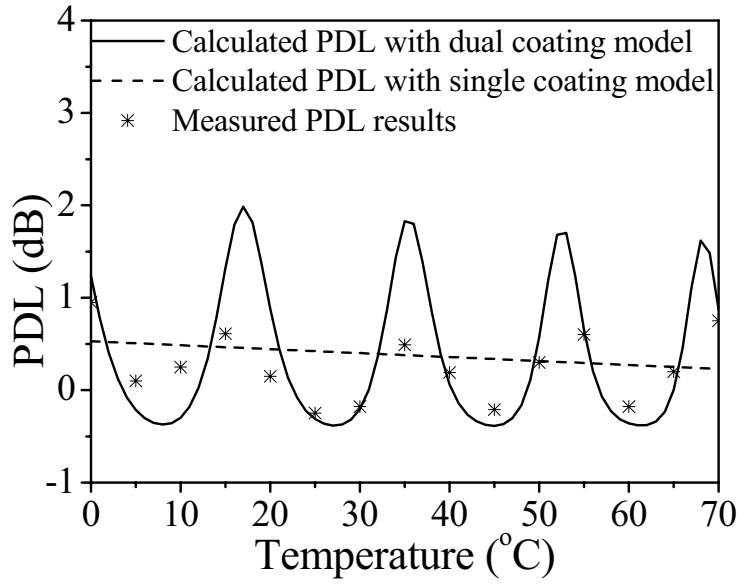

(a)

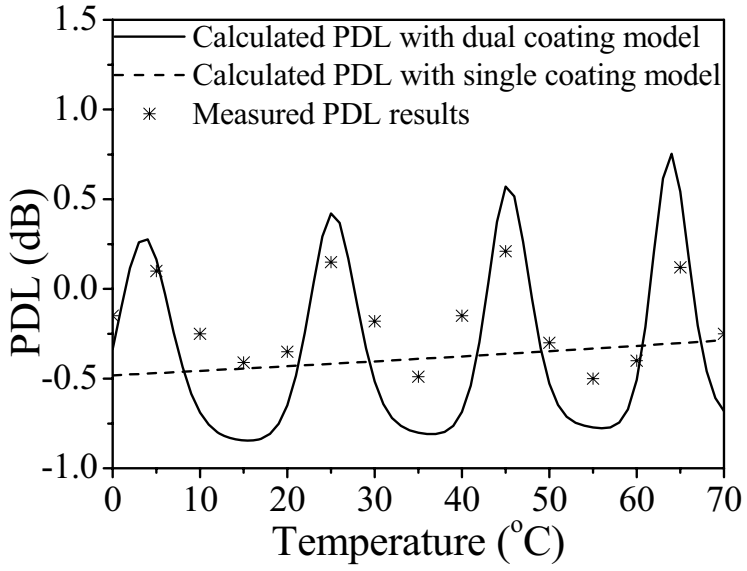

(b)

Figure 34. Calculated and measured macrobending loss results for temperature ranging from 0 to 70°C at the wavelength of 1550 nm, the bending radius is (a) 10.5+0.125 mm with a bending length of 10 turns; (b) 10+0.125 mm with a bending length of 20 turns.

4.3.4 Conclusion

In this letter the temperature dependent PDL characteristics of a macrobending standard singlemode fiber-SMF28 have been studied theoretically and experimentally. A theoretical model based on a scalar approximation method has been presented. Corresponding experimental verifications have been carried out and the acceptable agreement between the simulated and measured results indicate that the developed model can be utilized for predicting the temperature induced variations of PDL for a singlemode fiber with a dual coating.

4.3.5 Reference

[91]. R. Morgan, J. S. Barton, P. G. Harper and J. D. C. Jones, "Temperature dependence of bending loss in monomode optical fibres," Electron. Lett., Vol. 26, No. 13, pp. 937-939, 1990.

[92]. F. M. Haran, J. S. Barton, S. R. Kidd and J. D. C. Jones, "Optical fibre interferometric sensors using buffer guided light," Meas. Sci. Technol. Vol. 5 No. 5, pp. 526-530, 1994.

[93]. S. H. Nam, and S. Yin, "High-Temperature Sensing Using Whispering Gallery Mode Resonance in Bent Optical Fibers," IEEE Photon. Technol. Lett., Vol. 17, No. 11, pp. 2391-2393, 2005.

[94]. Q. Wang, G. Farrell and T. Freir, "Study of transmission response of edge filters employed in wavelength measurements," Appl. Opt., Vol. 44, 36, pp. 7789-7792, 2005.

[95]. Q. Wang, G. Farrell, T. Freir, G. Rajan, and P. Wang, "Low-cost wavelength measurement based on a macrobending single-mode fiber," Opt. Lett., Vol. 31, No. 12, pp. 1785-1787, 2006.

[96]. Q. Wang, G. Rajan, P. Wang, and G. Farrell, "Polarization dependence of bend loss for a standard singlemode fiber," Opt. Express Vol. 15, No. 8, pp. 4909-4920, 2007.

[97]. P. Wang, Y. Semenova, and G. Farrell, "Temperature dependence of macrobending loss in all-fiber bend loss edge filter," Opt. Commun., Vol.

281, pp. 4312-4316, 2008.

[98]. D. Marcuse, “Curvature loss formula for optical fibers,” J. Opt. Soc. Am. Vol. 66, No. 3, pp. 216-220, 1976.

[99]. H. Renner, “Bending losses of coated single-mode fibers: a simple approach,” J. Lightw. Technol., Vol. 10, No. 5, pp. 544-551, 1992.

[100]. L. Faustini and G. Martini, “Bend loss in single-mode fibers,” J. Lightw. Technol., Vol. 15, No. 4, pp.671-679, 1997.

[101]. Q. Wang, G. Farrell, and T. Freir, “Theoretical and experimental investigations of macro-bend losses for standard single mode fibers,” Opt. Express, Vol. 13, No. 12, pp. 4476-4484, 2005.

❖ Comments by the author on Chapter 4

I. This chapter contributes to achieving the overall aim of the thesis by demonstrating that the models developed can be expanded to include the effect of temperature and also are comprehensive and robust enough to deal with the effect of temperature on a variety of fiber types. And this chapter contains a range of experimental data results as well. In most cases the measurements were repeated multiple times to improve the accuracy of the measured data. It is therefore possible to illustrate and quantify the estimated experimental error existing in the published papers and by way of an example Figure 30 is reproduced here with the addition of error bars.

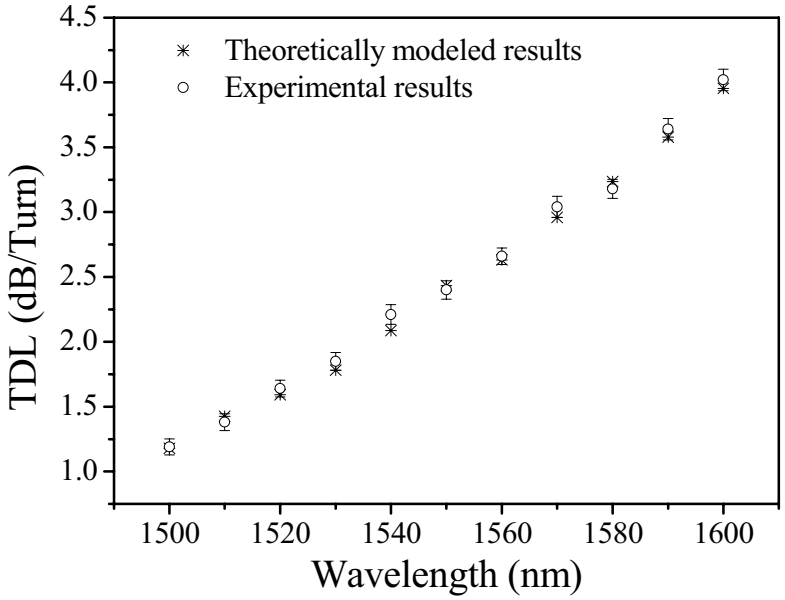

Figure 30. Calculated and measured TDL as a function of wavelength.

Chapter 5

Influence of fiber manufacturing tolerances on the parameters of fiber bend loss edge filters

A primary aim of this research is to develop an effective modeling platform for singlemode fiber bend loss which can deal with a variety of fiber and to utilize this modeling platform to investigate various important aspects of a novel fiber bending loss edge filter.

Manufacturing tolerance limitations are inherent in the process of fiber manufacturing, and such limitations affect both the size of each fiber layer and the refractive index profile and result in significant influences on the performance of fiber edge filter for wavelength measurement application. This chapter contributes to achieve this aim by presenting the theoretical predictions on the performance of fiber edge filter involving in the given manufacturing tolerance range and an effective solution is given in the filter fabrication stage.

Fiber manufacturing tolerance plays a vital role in the performance of a fiber bend loss edge filter. Fiber parameters such as core radius will always have a finite manufacturing tolerance and while specialist fibers may be sourced with improved tolerances, such fibers are more difficult to source and more expensive. To investigate this problem for standard fibers and based on the tolerance data available from manufacturers, a theoretical model for evaluating the influence of tolerance is developed.

The theoretical model, based on a scalar approximation method and

validated by experimental results, is used to determine the changes in key spectral parameters for an edge filter, resulting from changes within their manufacturing tolerance range, for both the core radius and NA. Finally, it is shown that an effective solution is the use of bending-radius tuning during fabrication of such edge filters as a means of mitigating the effect of manufacturing variations.

Influence of Fiber Manufacturing Tolerances for All-Fiber Bend Loss Edge Filter*

Keywords: Singlemode fiber, manufacturing tolerance, bend loss, edge filter

Abstract: It is shown that manufacturing tolerances of the fiber parameters bend radius and NA significantly influence the fiber bend loss performance and spectral response of a fiber-based edge filter. A theoretical model, validated by experimental results, is used to determine the changes in key spectral parameters for an edge filter, resulting from changes within their manufacturing tolerance range, for both the bend radius and NA. Finally is shown that bend-radius tuning during fabrication of such filters is a means of mitigating the effect of manufacturing variations.

5.1 Introduction

Fiber bend loss has been previously investigated for application in areas such as fiber-optic sensing and communications [102-104]. Recently, it was shown that

* P. Wang, G. Farrell, Y. Semenova, G. Rajan, "Influence of fiber manufacturing tolerances on the spectral response of a bend loss based all-fiber edge filter," Applied Optics, Vol. 47, No. 16, pp. 2921-2925, 2008.

fiber bend loss could be used as the basis of an edge filter for an all-fiber ratiometric wavelength measurement system [105-108]. Based on the previously published work for fiber bend loss [109-111], both theoretical and experimental results have shown that both the bend radius and fiber length have a significant influence on the fiber bend loss [107, 108].

In addition, in practice, the fiber bend loss will be sensitive to the fiber's own parameters, such as fiber core radius, refractive index and so on. Given the manufacturing tolerances for singlemode fiber, small variations in fiber parameters are unavoidable. All of these parameter tolerances resulting from the manufacturing process may significantly affect the resulting ratio response of a fiber based ratiometric wavelength measurement system. Therefore, it is highly desirable to investigate the influence of these fiber parameter variations on the response of fiber bend loss based edge filters.

In past work, both fiber bend loss theoretical modeling and experiments were carried out on SMF28 fiber with a multi-turn structure and 1060XP fiber with a compact single-turn structure, e.g., bend radius of 11 mm with 22 turns in Ref. [107], and bend radius in 10.5 mm with single turn in Ref. [108]. In order to evaluate the fiber bend loss performance of a fiber edge filter employed in a wavelength measurement system, two important parameters, baseline loss and discrimination range have been also defined [107, 108].

In this paper, the dependences of fiber bend loss on parameter tolerances are presented for the fiber core radius and the numerical aperture (NA) value. Through examination of the dependence of bend loss behavior on the parameters of bend loss sensitive singlemode fiber-1060XP, it is found that these small variations in these parameters have a significant impact on the spectral response

of the fiber bend loss edge filter. We also show that bend-radius tuning during fabrication of such filters is a means of mitigating the effect of manufacturing variations.

5.2 Design of a 1060XP based fiber edge filter

Fig. 35 (a) shows a fiber edge filter used within a ratiometric wavelength measurement system. The input signal is split into two equal signals. One passes through the fiber bend loss edge filter (upper arm) and the other passes through a reference arm (lower arm). Photodiodes are placed at the ends of both arms. By measuring the ratio of the electrical outputs of the two photodiodes, we can determine the wavelength of the input signal assuming a suitable calibration has taken place. The fiber bend loss edge filter, for a measurable wavelength range from λ_1 to λ_2, provides a strong monotonically increasing wavelength dependent attenuation (discrimination range), from a given lower start wavelength (baseline loss, λ_1) to an end wavelength λ_2 [see Fig. 35(b)].

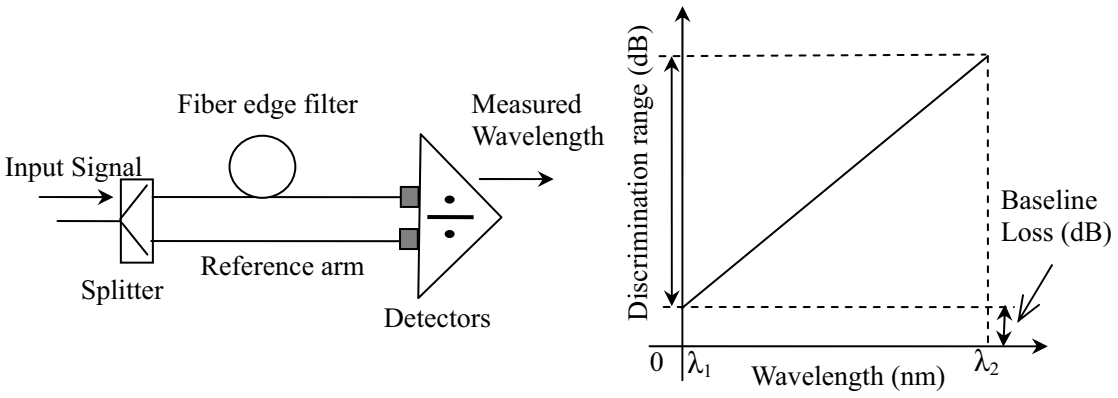

Figure 35. (a) Schematic configuration of the ratiometric wavelength measurement system with the fiber edge filter; (b) desired spectral response of the fiber edge filter.

In our previously published work on wavelength ratiometric measurements

[105, 106], it was found that with higher slope values for the transmission response of the edge filters for a given measurable wavelength range, the output ratio *R*, which was measured by a dual channel power meter, diverged from the actual transmission response of the edge filters at the upper end of the wavelength range due to the limited Signal-to-Noise Ratio (SNR) of real optical sources. To take account of this fact the slope of the transmission response of edge filters must be limited, effectively placing an upper limit on the useable discrimination. In regard to baseline loss, there are inevitable transmission losses, splicing losses, and insertion losses in such a system and these losses increase the baseline loss as well, reducing the overall signal power available for Optical-to-Electrical (OE) conversion and thus degrading accuracy due to noise. Ideally, the baseline loss should be lower than 5 dB and the discrimination range should be lower than 20 dB and larger than 15 dB for wavelength measurement.

For the 1060XP fiber, the essential parameters are shown in Table 6:

Table 6. Parameters of the 1060XP singlemode fiber; (the refractive index values are defined at a wavelength of 1550 nm).

Parameter of fiber	**1060XP**
Refractive index difference (between fiber core and cladding)	0.0067 ± 10%
Diameter of fiber core	5.3 ± 0.5 μm
Diameter of fiber cladding	125 ± 0.5 μm
Nominal core NA (Numerical Aperture)	0.1393

Fig. 36 shows that the calculated baseline loss (solid line), discrimination range (dashed line), measured baseline loss (hollow circles), discrimination range (solid squares) as a function of bend radius for the bend loss sensitive

singlemode fiber-1060XP, with an applied absorbing layer and a fiber bend of 1 turn. A so-called effective bend radius (correction factor, 1.308@1500nm; 1.336@1600nm) is also employed in the theoretical modeling, as presented in Ref. [108]. In the experiments, a tunable laser is employed as a power source, which has an output power of 0 dBm with a wavelength tuning range from 1500 to 1600 nm. To experimentally determine the baseline loss and discrimination range, the bend losses of bare 1060XP fiber with an absorbing layer (to remove the reflection occurring at the interface between the cladding layer and air) were measured at 1500 nm and at 1600 nm. The measurements were taken at 0.5 mm intervals over a bending radius range from 8.5 to 14 mm.

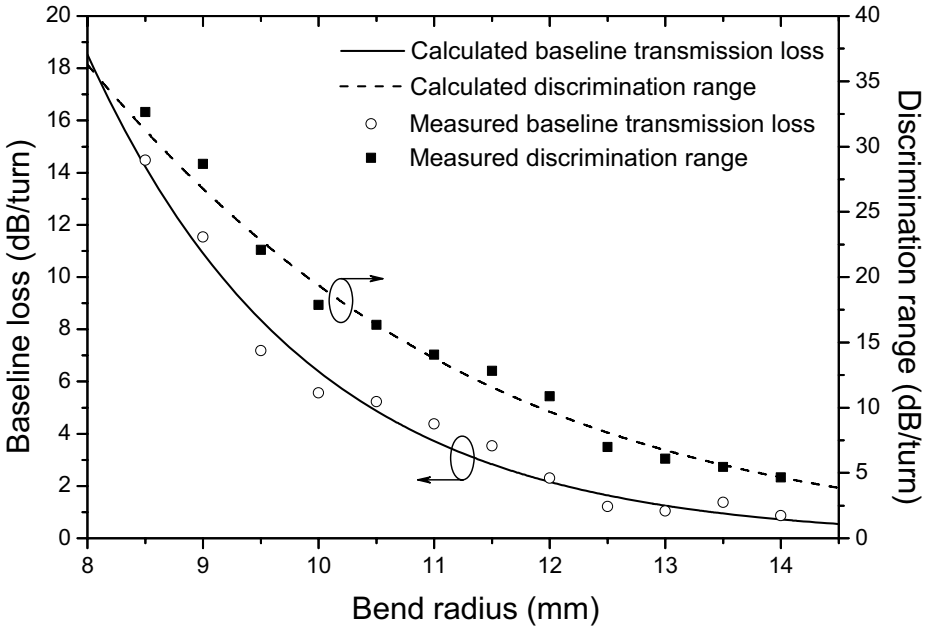

Figure 36. Calculated and measured baseline transmission loss and discrimination range as a function of bend radius for 1060XP fiber with an absorbing layer, the fiber length is 1 turn.

In Fig. 36, the theoretical modeling shows a reasonable agreement with the experimental results overall, and the divergence between the experimental and theoretical results is most likely caused by: 1) measurement error of the bending

loss and errors due to temperature induced fluctuations of the bend loss; 2) the experimental inaccuracy of the bend radius (both baseline loss and discrimination range are sensitive to the bend radius as shown in Fig. 36; 3) the limitations of the absorbing layer material coated on the bare fiber cladding surface leading to partial reflections from the fiber cladding-air boundary so that radiation launched from fiber core will re-couple with the fundamental propagation mode in the fiber core, resulting in a perceptible quasi-periodic behaviour for the measured results in Fig. 36. Finally the calculation of the bend loss itself has some minor limitations: 1) the approximations made in the calculation from D. Marcuse [109] and 2) the calculation of bend loss is based on a scalar approximation to enable reasonable processing times with limited processing power and memory.

From Fig. 36, one can also see that both the baseline loss and discrimination range are highly sensitive to the bend radius. When the bend radius is less than 8 mm, as in our previous experiments [112], it is found that when the bare fiber is bent, it is more susceptible to breakage. Furthermore, to reduce the fiber bend induced mechanical stress and improve the reliability of the fiber filter, it is suggested that a bend radius is larger than 8 mm is employed for fiber edge filter applications. Thus in this paper a bend radius of 10.5 mm is chosen to characterize the influence of bend loss due to the manufacturing tolerance of fiber parameters.

5.3 Influence of the manufacturing tolerance of key fiber parameters on the performance of a fiber-based edge filter

For a 1060XP fiber based edge filter, the influence of manufacturing variations in

key fiber parameters needs to be considered in the design process. In the first instance the influence of variations in the fiber core radius (nominal value 2.65 μm) was modeled for a range of core radii from 2.35 to 2.95 μm. The results are shown in Fig. 37 in which the calculated baseline loss (solid square line) is shown along with the discrimination range (hollow square line) as a function of fiber core radius for 1060XP fiber with an absorbing layer. The fiber bend radius is 10.5 mm, and bend length is 1 turn.

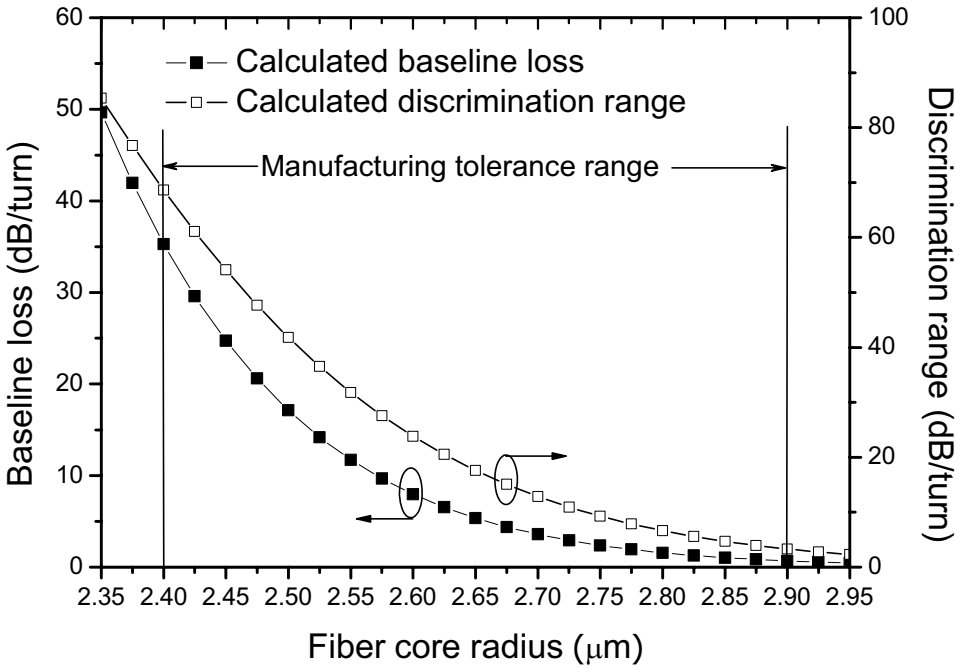

Figure 37. Calculated baseline transmission loss and discrimination range as a function of variable fiber core radius for 1060XP fiber with an absorbing layer, the fiber bend radius is 10.5 mm, and length is 1 turn.

It is clear that both the baseline loss and discrimination range, decrease rapidly with an increase in fiber core radius. In practice the manufacturing tolerance for the fiber core radius is ± 0.25 μm, so from Fig. 37, one can see that a large variation in the baseline loss and discrimination range will occur within this manufacturing tolerance range. The worst case variation for either the

baseline loss value or the discrimination range value is the difference between the highest value, calculated for the lowest possible core radius (2.4 μm) and the lowest value calculated for the highest possible core radius (2.9 μm). For the baseline loss the worst case variation is 34.6 dB, and for the discrimination range it is 65.3 dB.

Next, the influence of manufacturing tolerance for fiber NA value was modeled. During the fiber manufacturing process, the tolerance of refractive index difference between fiber core and cladding can be controlled below ± 10%, and the corresponding calculated core NA tolerance (nominal value 0.1393) of the 1060XP fiber is thus within the range from 0.1321 to 0.1461. The results of the modeling are shown in Fig. 38, for a range of NA value from 0.1275 to 0.1515.

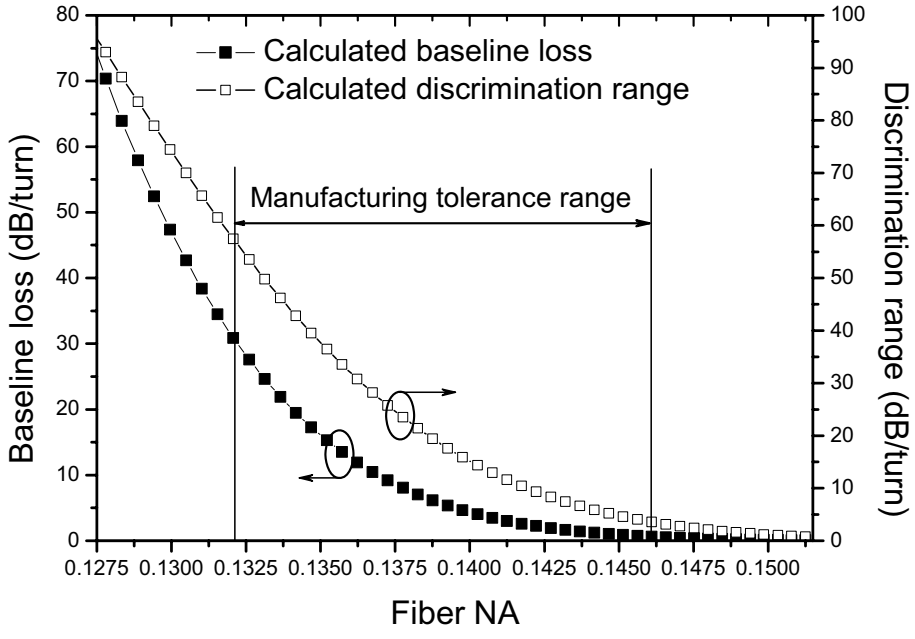

Figure 38. Calculated baseline transmission loss and discrimination range as a function of fiber core NA for 1060XP fiber with an absorbing layer, the fiber bend radius is 10.5 mm, and length is 1 turn.

The baseline loss and discrimination range vary with the fiber NA, and for a fiber with lower NA value the result is a larger baseline loss and discrimination range. Within the manufacturing tolerance range for the NA, the worst case variation for the baseline loss is 27.6 dB, and for the discrimination range is 52.3 dB.

5.4 Discussion

Even allowing for worst case nature of manufacturing tolerances, for the fiber parameters *core radius* and *NA* it is clear from Figures 37 and 38 that such variations have a profound effect on the discrimination range and baseline loss of a fiber bend loss edge filter. In manufacturing such filters in significant quantities such variations in discrimination range and baseline loss would result in unacceptably low production yields. However in practice there are mitigating issues which can reduce or even eliminate the impact of manufacturing tolerances.

The first issue is the statistical nature of manufacturing tolerances. It is known for example that the core radius variations of a fiber normally conform to a Gaussian statistical distribution, which has been demonstrated in the Ref. [113]. To determine the standard deviation it can be assumed that the worst case variations about the nominal value of the core radius correspond to approximately ± 3 standard deviations about the nominal value. Based on Gaussian statistics one could assume the while the worst case variation is indeed ± 0.25 μm, in practice in 95% of cases the actual fiber tolerance will be within ± 2 standard deviations or ± 0.166 μm. The corresponding variation of the discrimination range is reduced from 65.32 dB worst case to 39.55 dB for ± two

standard deviations, reducing the impact of manufacturing variations.

The second mitigating issue is that fiber bending loss filters can be fabricated to allow the discrimination range and baseline loss to be set and fixed at the point of manufacture. This means that a preset mandrel around which the fiber is fixed cannot be used but instead a freespace fiber bend loop is fabricated and the radius of the loop is "tuned" manually to give the correct discrimination at a given wavelength. The fiber loop is then fixed using an epoxy droplet at the crossover point of the fibers. To verify if this is possible the model described earlier is used to determine the fiber bend radius that would need to be set to ensure that the discrimination range is equal to the design example value of 16.32 dB (achieved with a nominal core radius (2.65 μm) for a bend radius of 10.5 mm) where the actual core radius can vary by ± 0.166 μm (± 2 standard deviations). The results are presented in Table 7. As expected for low values of core radius, a larger bend radius is needed, up to 14.55 mm. For high values of core radius a smaller bend radius is needed, down to 8 mm, which is acceptable in terms of the minimum radius needed to avoid fiber failure.

Table 7. Fiber bend radius range needed to compensate for two-standard deviation variations in the fiber core radius

Fiber core radius R (μm)	ΔR (μm)	Bend radius needed (mm)
2.483 (lowest)	-0.166	14.55
2.65 (nominal)	0	10.50
2.817 (highest)	+0.166	8.02

Variations in the fiber NA from nominal can be also be dealt with using bend radius tuning during fabrication. The nominal NA is 0.1393. Again assuming Gaussian statistics, the worst case value of NA variation is equal to

approximately three standard deviations. For 95% of fibers the variation will be within ± two standard deviations or ± 0.004887. If bend radius tuning is employed to ensure that even with NA variations the discrimination range is still 16.32 dB, then the bend radius range needed to compensate NA variations is shown in Table 8.

Table 8. Fiber bend radius range needed to compensate for two-standard deviation variations in the fiber NA

Fiber NA	ΔNA	Bend radius needed (mm)
0.1321 (lowest)	-0.0072	16.24
0.1393 (nominal)	0	10.50
0.1461 (highest)	+0.0068	7.25

The bend radius needed to compensate for NA variations has a minimum value of 7.25 μm, which is acceptable in terms of fiber reliability. Bend radius "tuning" during fabrication of the fiber filter is thus a feasible approach to reducing the effect of manufacturing tolerances. To confirm this, for a design bend radius of 10.5 mm, we calculated the tuned bend radius required to meet the edge filter specifications over the range of possible fiber core radii and NA values. The results are shown in Fig. 39 which shows in a graphical form that is possible to compensate for manufacturing variations in the fiber core size and fiber NA changes, by tuning the actual bend radius used.

In practice the need to "tune" the bend radius to meet a given discrimination range should not be an onerous task. The fiber to be used for a batch of fiber bend loss filters will most likely come from the same drawn length of fiber, so similar "tuned" bend radii can be expected for a given batch of filters. Finally it is also true that for many applications of such fiber bend loss filters (such as

wavelength measurement as discussed earlier), there is no need to achieve a precise discrimination through radius tuning as in any event the overall system calibration will take account of variations in the discrimination range.

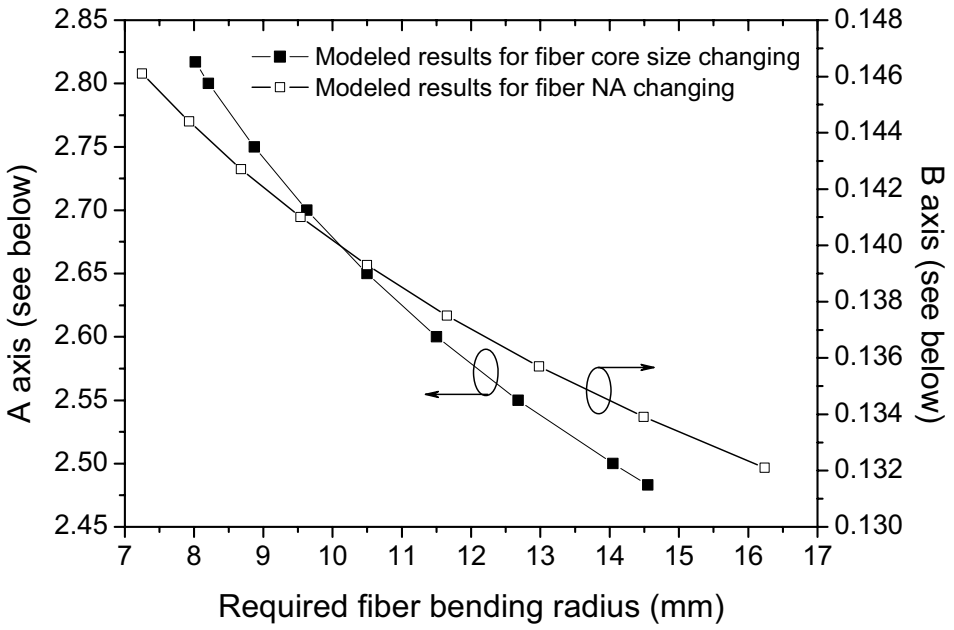

Figure 39. Calculated results for the changes in the fiber core and NA as a function of the required fiber bending radius. A axis: "Range of possible fiber core radius values based on manufacturing tolerance (μm)"; B axis: "Range of possible NA values based on manufacturing tolerance"

Finally it is recognized that parameter variations during manufacture will not occur in just one parameter at a time, but rather variations in several parameters will occur. We have not considered such combined variations in this paper. However we have shown that in the fabrication of bend-loss based fiber edge filters, bend radius tuning can be employed to mitigate the effects of parameter variations. Where the fiber used displays variations from a nominal value for several parameters, bend radius tuning will still offer a means of achieving the correct filter response, albeit with a lower yield, depending on the magnitude of the parameter variations.

5.5 Conclusions

The design of a 1060XP singlemode fiber based edge filter has been examined in the context of variations in fiber parameters. We have shown that two such parameters, core radius and NA, influence the fiber bend loss spectral response performance significantly, and two analytical models have been presented for calculating the influence of the manufacturing tolerance of the fiber parameters on fiber bend loss. Finally we have shown that bend-radius tuning during the fabrication of such filters is a viable way to mitigate the effect of manufacturing variations.

5.6 References

[102]. M. T. Wlodarczyk, "Wavelength referencing in single-mode microbend sensors," Opt. Lett., 12, 741-743 (1987)

[103]. S. H. Nam, and S. Yin, "High-temperature sensing using whispering gallery mode resonance in bent optical fibers," IEEE Photon. Technol. Lett., 17, 2391-2393 (2005).

[104]. M. D. Nielsen, N. A. Mortensen, M. Albertsen, J. R. Folkenberg, A. Bjarklev, and D. Bonacinni, "Predicting macrobending loss for large-mode area photonic crystal fibers," Opt. Express, 12, 1775-1779 (2004).

[105]. Q. Wang, G. Farrell and T. Freir, "Study of transmission response of edge filters employed in wavelength measurements," Appl. Opt., 44, 7789-7792 (2005).

[106]. Q. Wang, G. Rajan, P. Wang and G. Farrell, "Resolution investigation of ratiometric wavelength measurement system," Appl. Opt., 46, 6362-6367 (2007).

[107]. Q. Wang, G. Farrell, T. Freir, G. Rajan and P. Wang, "Low-cost wavelength measurement based on a macrobending single-mode fiber," Opt. Lett., 31, 1785-1787 (2006).

[108]. P. Wang, G. Farrell, Q. Wang and G. Rajan, "An optimized

macrobending-fiber-based edge filter," IEEE Photon. Technol. Lett., 19, 1136-1138 (2007).

[109]. D. Marcuse, "Curvature loss formula for optical fibers," J. Opt. Soc. Am., 66, 216-220, (1976).

[110]. H. Renner, "Bending losses of coated single-mode fibers: a simple approach," J. Lightwave Technol., 10, 544-551 (1992).

[111]. L. Faustini and G. Martini, "Bend loss in single-mode fibers," J. Lightwave Technol., 15, 671-679 (1997).

[112]. P. Wang, Q. Wang, G. Farrell, G. Rajan, T. Freir and J. Cassidy, "Investigation of macrobending losses of standard single mode fiber with small bend radii," Microw. Opt. Techn. Lett. , 49, 2133-2138 (2007).

[113]. P. H. Krawarik and L. S. Watkins, "Fiber geometry specifications and its relation to measured fiber statistics," Appl. Opt., 17, 3984-3989 (1978).

❖ Comments by the author on Chapter 5

I. This chapter contains experimental data results presented in Fig. 36. We repeated the experiments, using a different attenuation layer ("absorbing layer" named in the previous publications) material. The new acrylic based layer has more effectively attenuated the radiation from the guided mode in the fiber core and reduced considerably the effect of any residual whispering-gallery modes. However, the new acrylic layer still does not attenuate all radiation at the interface between fiber cladding and air (99% attenuation as reported in G. Rajan, et al., "All fibre temperature sensor based on macro-bend singlemode fibre loop," Electronics Letters, Vol. 44, No. 19, pp. 1123-1124, 2008). The limitation of the layer is evident from the quasi-periodic behaviour of the measured results.

Chapter 6

Generalized design for a fiber bend loss edge filter

A primary aim of this research is to develop an effective modeling platform for singlemode fiber bend loss which can deal with a variety of fiber and to utilize this modeling platform to investigate a novel fiber bending loss edge filter.

To investigate the generalized design approach to a bending fiber based edge filter, and for desirable features of a fiber for a bend loss edge filter, a number of issues need to be considered, which involves: 1) to meet the fiber filter specifications: baseline loss $\leq$ 5 dB; 15 dB $\leq$ discrimination range $\leq$ 20 dB; 2) the filter fiber should have similar core size with common fiber used in the rest of system-low splicing loss is desired; 3) ideally the fiber should have a jacket which can act as an absorbing layer, hence applying absorbing layer is not necessary for the edge filter; 4) if possible, minimize number of turns to improved mechanical reliability. This chapter contributes to achieve this aim by presenting the theoretical predictions on the selection of singlemode fiber which can satisfy the requirements of fiber edge filter and investigating the performance evaluations based on selected fiber both theoretically and experimentally.

This Chapter outlines a generalized, systematic design methodology for a fiber bend loss edge filter in a wavelength measurement application. It is based on a previously developed theoretical model for predicting the macrobending loss of singlemode fiber, which has been verified by experiments. The models developed in previous chapters underpin the design methodology for a fiber bend

loss edge filter. The factors influencing the choice of fiber are examined in detail and an approach is described to determining the effectiveness of a candidate fiber's coating or buffer as an absorber layer. Retaining the coating or buffer as an absorber layer is useful as it results in easier fabrication and improved reliability for the bent fiber filter.

As an example, SMF28e fiber is selected to evaluate the proposed design methodology.

A generalized design process for fiber bend loss based edge filters for a wavelength measurement system*

Keywords: Singlemode fiber, bend loss, edge filter, SMF28e, polarization dependence

Abstract: A generalized methodology for the design of a fiber bend loss based edge filter is investigated and presented, starting with the task of evaluating and selecting suitable fibers and then considering the design of fiber bending loss edge filter. As an example to illustrate the methodology, a Corning SMF28e fiber with a 900 μm jacket is selected and two sample edge filters are designed for experimental verification. The designed edge filters are compact, easy to fabricate, meet target spectral specifications and show low PDL, confirming the effectiveness of the proposed methodology for fiber bend loss based edge filter design.

* P. Wang, G. Farrell, Y. Semenova, "A generalized design process for fiber bend loss based edge filters for a wavelength measurement system," Submitted to Applied Optics. Manuscript ID: 106080

6.1 Introduction

It is well known that macrobending loss occurs when an optical fiber is bent, and such fiber macrobending losses have been widely investigated as an important issue in optical fiber communications and sensing applications in recent decades [114-117]. The wavelength dependence of macrobend loss can be employed in an all-fiber based edge filter systems for rapid wavelength measurement in Dense Wavelength Division Multiplexing optical communication systems and in optical sensing applications [118-123]. In this regard a fiber bend loss filter based on low bend loss fiber (such as SMF28) has recently been investigated theoretically and experimentally for application in a ratiometric wavelength measurement system. The filter had a bending radius around 10 mm and multiple turns with a length circa 1~2 meters [118-120]. For such a filter both calculated and measured results showed that the fiber coating layers have a significant influence on polarization dependent loss (PDL) [121], which could reduce the precision of wavelength measurement. In order to ensure accuracy in wavelength measurement, low polarization dependence for the bend loss is required. As reducing the length of the fiber will reduce polarization dependence, using a bend sensitive fiber is one possibility to improve accuracy. Such a fiber bend loss filter based on bend loss sensitive fiber (1060XP fiber was used as an example) has been presented, demonstrating reduced PDL, using a bending radius of 10.5 mm and single turn structure [122], compared to 22 turns for an SMF28 based filter. In this case the fiber was stripped of its coating and an absorbing layer was applied to eliminate the development of whispering gallery modes (WGMs) at the glass-air interface. This is necessary as WGMs can result in a bend loss

spectral response for the filter that is not monotonically increasing and is unusable in a wavelength measurement application.

However there are disadvantages to using a bare bend-sensitive fiber. Firstly a single loop structure is not mechanically reliable without the protection of polymer coating(s). Secondly discrepancies in fiber core size and NA between conventional fibers and 1060XP fiber will induce excess splicing losses in the system. Finally residual whispering gallery modes (WGMs) still occur due to imperfections in the necessary absorbing layer [122], negatively affecting the bend loss spectrum over the range of measured wavelengths. Taken together these three disadvantages will have a detrimental effect on the performance and reliability of such a fiber bend loss edge filter.

In this paper the requirements for a fiber for a bend loss fiber based edge filter are described in detail. A generalized process of evaluation and selection for a suitable fiber, along with a design process for a bend loss fiber based edge filter is described. An SMF28e fiber is evaluated and selected as a sample fiber to illustrate the process. Our investigation includes: 1) a methodology for the design of a fiber bend loss based edge filter; 2) an example of fiber evaluation; 3) determination of fiber bending radius and length for the sample fiber; 4) experimental verification for the sample fiber. The good agreement between theoretical modeling and measured results for the sample fiber confirms that the generic process proposed for fiber evaluation, selection and filter design is effective, resulting in improved baseline loss, discrimination range and PDL performance and ease of fabrication for the filter.

6.2 The process of bend loss based edge filter design

The design process for an edge filter involves a number of critical steps. Firstly the required spectral parameters of the edge filter must be decided; in particular the baseline loss and the discrimination range over the wavelength range of interest. Two key parameters for an edge filter are baseline loss and discrimination range. A bend-loss-based edge filter operates over a wavelength range from λ_1 to λ_2 with a progressively larger attenuation as the wavelength increases from λ_1 to λ_2. The baseline loss is defined as the loss of the filter at λ_1, while the discrimination range is the difference between the attenuation at λ_1 and λ_2.

A second step is the evaluation of different fibers as to their suitability for use in the edge filter and a decision needs to be taken as to whether the fiber coating(s) need to be stripped or not, prior to fabrication. Finally once a fiber is selected, the exact value of bend radius and fiber length required must be determined.

Modeling of fiber bend loss is a very important part of this process. Theoretical modeling for fiber bend loss has been investigated for over 30 years [124-127]. D. Marcuse first developed a bend loss model for an optical fiber with a core-infinite cladding cylindrical structure [124]. Since then, a series of theoretical models and corresponding experimental investigations on macrobending loss have been presented, which considered the impact of WGMs caused by the reflection of the radiated field at the interface between the fiber cladding and coating layer. Examples include those presented in [125, 126], but these models are specific to a fiber with a single coating layer. In selecting a fiber

for an edge filter application, fibers with multiple-coatings will need to be evaluated, so a model that can deal with multiple coatings is needed. A theoretical model based on a weak perturbance of fundamental mode propagation constants which considered single and multi-coating layers has been presented [127], which demonstrates a high level of agreement between calculated and experimental results. Therefore the theoretical formulation presented in Ref. [127] is employed in this paper to analyze the macrobending loss of singlemode fiber in this paper.

With regard to the required spectral response parameters of the edge filter, in our previous publication on ratiometric wavelength measurements [118], it was shown that for higher slope values for the transmission response of the edge filters for a given measurable wavelength range, the output ratio *R*, diverged from the actual transmission response of the edge filters at the upper end of the wavelength range due to the limited Signal-to-Noise Ratio (SNR) of real optical sources, e.g. a tunable laser. In regard to the spectral parameter baseline loss, as well as the fiber bend loss there are inevitable transmission losses, splicing losses, and insertion losses in such a system and these losses increase the baseline loss as well, reducing the overall signal power available for Optical-to-Electrical (OE) conversion and thus degrading accuracy due to noise. Consequently, for a fiber bend loss based edge filter used in a wavelength measurement application, the desired baseline loss should be lower than 5 dB and the desired discrimination range should lie in the range 15-20 dB [118-120].

Evaluating different fiber candidates as to their suitability for use in an edge filter involves a number of issues. In the first instance in order to minimize the excess splicing loss in the system, the physical parameters of a proposed fiber,

such as the fiber core size, should be close to those of standard singlemode fiber typically used for interconnection between optical units in optical fiber systems. The bend loss sensitivity of the fiber is also important as it is desirable to minimize the physical length of the fiber used in the edge filter for three reasons: firstly to reduce the physical space occupied by the filter and most importantly to improve long term reliability by reducing the total length of the fiber subjected to mechanical stress; secondly reducing the physical length of fiber will also reduce polarization dependent loss and finally if the fiber coating has to be stripped off to be replaced by an absorbing layer then a shorter fiber length makes this processing step considerably easier. As a benchmark for fiber length if possible the fiber bending length should be significantly shorter than the circa 1.5 m length (22 turns) reported earlier for a SMF28 fiber (a low bend loss sensitivity fiber) based edge filter in Ref. [120].

Selecting a fiber for use in filter is an iterative process but one starting point to determine a range of useable NA values as a guide to initial selection. One approach to this is to select a reasonable target radius and maximum number of turns, hence setting a maximum length and then use the model to plot the baseline loss and discrimination range for different NA values. Based on previous results a bend radius circa 10.5 mm is a good starting point and based on the need for a reasonable bend length, as outlined above an upper a bend length of 5 turns is selected. The corresponding modeled baseline loss (solid line) and discrimination range (dashed dot line) as a function of NA is presented in Fig. 40. The desired fiber diameter is defined as 8.3 μm, and discrimination range is defined within the common optical communication and sensing widows, from 1500 nm to 1600 nm.

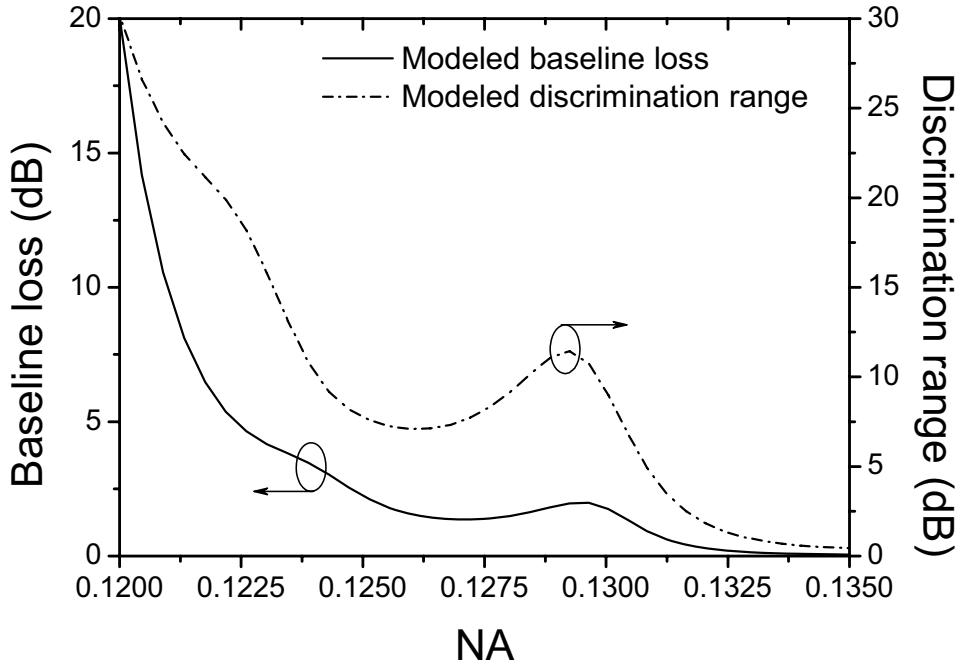

Figure 40. Calculated baseline loss and discrimination range as a function of different fiber NA with a fiber length of 5 turns when the bend radius is 10.5 mm.

As an example consider SMF28 fiber, which has an NA of 0.1285. Using Fig. 40, one can see that given the low bend loss sensitivity of the fiber, the baseline loss is acceptably low < 2 dB but the discrimination range is circa 10 dB, outside the desirable range of 15-20 dB discussed earlier [118-120]. The only solution, verified in practice, for a SMF28 fiber would be to use longer bend lengths. As will become evident in the next section and as shown in Fig. 40, selecting a fiber with lower NA value will increase the discrimination range, for example for an NA value of 0.1226, the calculated baseline loss is 4.64 dB, and the modeled discrimination range is 18.206 dB.

Finally in selecting a fiber, it is also necessary to consider the coating(s) used on the fiber. In general, to suppress the generation of WGMs, coatings are stripped off the fiber used in a bend-loss based edge filter and replaced with an

absorbing layer. However removal of the coating adds to the fabrication complexity and also makes the fiber filter more fragile. Thus in selecting a fiber, an ideal coating would be one which showed a strong absorption over the wavelength range of interest, removing the need to strip the fiber coating in the first place. The decision here is complicated by the fact that manufacturers rarely release sufficiently detailed data on the absorption characteristics and chemical composition of the fiber coatings used in their products. This means that is difficult to determine from fiber specifications alone whether or not a coating can be left in place or not. One reliable approach is to measure the bend loss versus bend radius characteristic for a sample of the fiber. This will reveal a characteristic signature that is strongly influenced by coating absorption. By comparing the characteristic of the bent fiber with the characteristic predicted by the model [127] for the same fiber with an infinite coating assumed, one can determine whether or not the coating is an efficient absorber and thus if it can be retained or not. An example of this approach is provided in the next section.

Finally it should be noted that in the design of a fiber edge filter, there are mechanical limits on the usable bend radius. In previous experiments, it was found that a bare fiber filter was too fragile and easily broken when the bend radius was less than 10 mm for a bare fiber. Thus to ensure the reliability and longevity of the fiber bend loss filter, the fiber bend radius used should be ≥ 10 mm. If it is possible to retain the coating, a lower bend radius down to 8 mm is possible.

6.3 An example of fiber evaluation: SMF28e fiber

In Section 6.2 a process for evaluating and selecting candidate fibers for use in

an edge filter was outlined. In this section an example of the use of this process is described.

Corning SMF28e is fiber type which offers several advantages over traditional SMF28 fiber, such as lower attenuation at the so-called “water-peak” wavelength, but offering splice compatibility with SMF28. The desirability of compatibility with standard fiber has been discussed in Section 6.2 and is an important advantage of SMF28e.

For standard Corning SMF28e fiber, both the manufacturing tolerances and NA changes induced by bending stress have been investigated and discussed in Ref. [128]. The composition of the fiber cladding for SMF28e is pure silica glass and refractive index (RI) is 1.4440 at 1550nm, confirmed by Corning. Therefore this value of cladding RI is chosen for the theoretical bend loss modeling. Based on the quoted MFD (10.4 μm@1550nm) of SMF28e in the Corning official specifications, the RI of the fiber core is chosen as 1.4490 in this paper.

For commercial Corning SMF28e fiber, there is a 900 μm diameter jacket adhering to the outer coating layer. In our previous experiments [118-123, 127], all the fiber bend loss edge filters were coated with an absorbing layer, which eliminated wave-like WGM induced variations in the bend loss spectrum. Such wave-like variations are largely caused by WGMs formed at the interface between the outer coating layer and air (such as SMF28 [127]), or the interface of between the cladding and air where the coatings are stripped (such as 1060XP [122]). Ideally, if the jacket could completely absorb radiation, the bending SMF28e fiber could be treated as a fiber with core-cladding-infinite coating structure and practically there would be no need to strip the fiber jacket and apply an absorption layer, considerably simplifying the fabrication process.

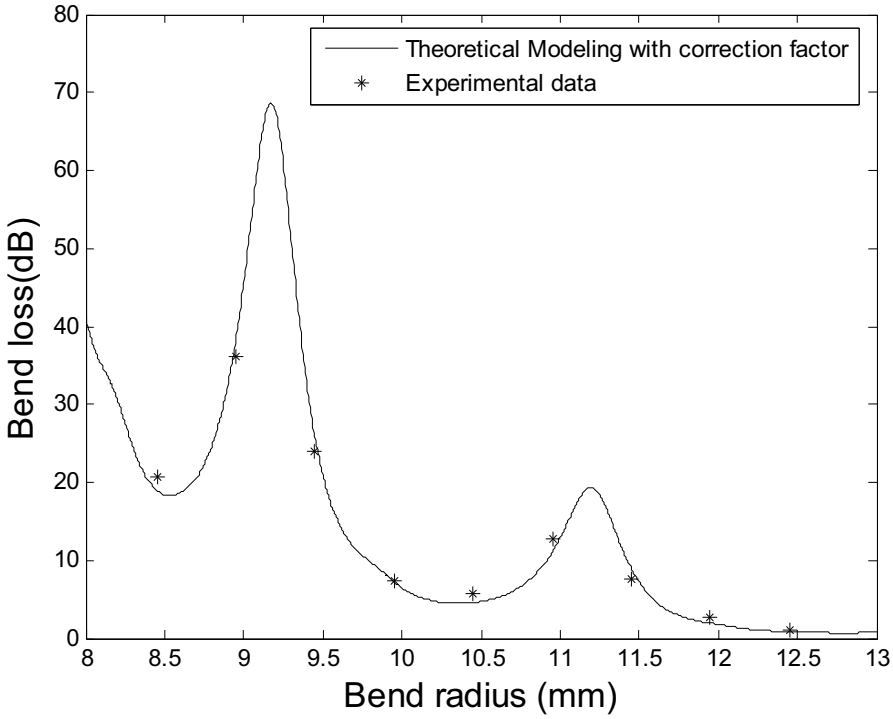

Figure 41. Theoretical modeling with correction factor and experimental bend loss results for SMF28e fiber for different bending radii at a wavelength of 1550 nm and 10 turns of fiber.

As mentioned in Section 6.2, the manufacturer of SMF28e does not release detailed data about the jacket that would allow one to determine if the jacket absorbs radiation and suppresses the formation of strong WGMs at the coating-air interface. Thus to determine whether the jacket needs to be stripped or not, the bend loss of SMF28e fiber with a jacket was measured for bending radii over a range from 8 to 12 mm at the operating wavelength of 1550 nm. The measured results are compared to the results from a model, based on the theoretical formulas presented in Ref. [127] and also shown in the Fig. 41, which assumes an infinite coating, effectively a 100% efficient absorber. Based on the good agreement between the modeled and the experimental results, one can conclude that the jacket for SMF28e is acting as an efficient absorbing layer. Note that all bend radii take into account the radius of fiber jacket (450 μm).

The theoretical modeling (solid line in Fig. 41), utilizes a correction factor of 1.338 at 1550 nm, higher than a common conventional singlemode correction factor of 1.27 at a wavelength of 1300 or 1150 nm [125, 129]. The good agreement between measured and modeled values indicates that the so-called correction factor (effective bending radius) is required in modeling SMF28e fiber. As the correction factor varies slightly with wavelength in principle the correction factor needs to be determined for all wavelengths. However in practice it is acceptable to determine the correction factor at 10 nm intervals over the wavelength range of interest between 1500 and 1600 nm. For completeness the correction factors as a function of wavelength are shown in Fig. 42.

In summary the evaluation of SMF28e fiber so far shows that it is a potential candidate for use in an edge filter as it has a low splicing loss to conventional fibers and most importantly the fiber jacket is an efficient absorber, so that stripping of the jacket will not be needed in fabricating an edge filter.

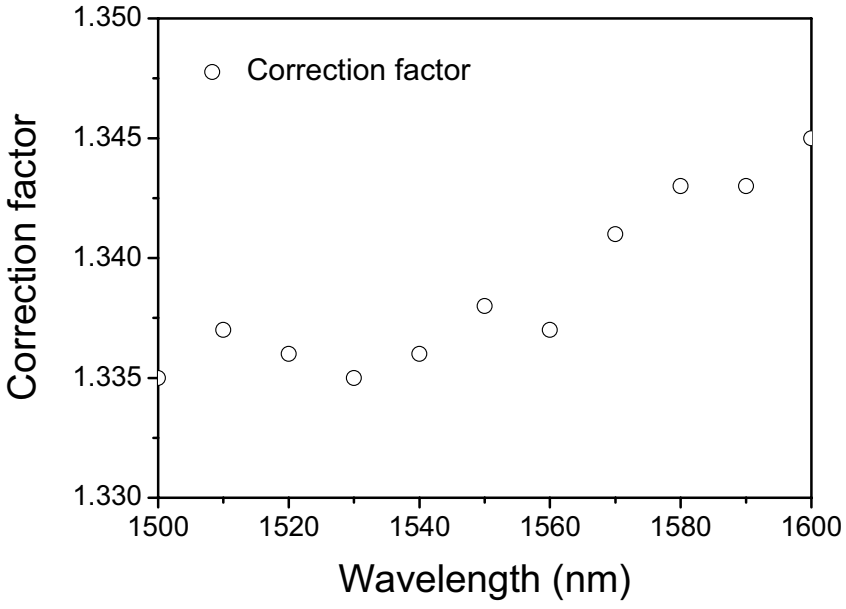

Figure 42. Correction factor as a function of wavelength for SMF28e fiber.

6.4 Determination of fiber bending radius and length for an SMF28e based edge filter

The design of the macrobending fiber filter based on SMF28e involves determining the bending radius and bending length to provide a desired baseline loss and discrimination range for the filter. In this section we present the design of an SMF28e fiber based edge filter, including consideration of the polarization sensitivity of the bend loss over the range of measured wavelengths.

Fig. 43 shows the calculated baseline loss per turn at a wavelength of 1500 nm and discrimination range per turn as a function of different bending radii, where the fiber bending length is one turn. From the Fig. 6.4, one can see that as the bend radius increases, the non-monotonic decrease of both the baseline loss and discrimination range as a function of bend radius confirms the presence of a residual WGM effect at the interface between the cladding and the coating layers.

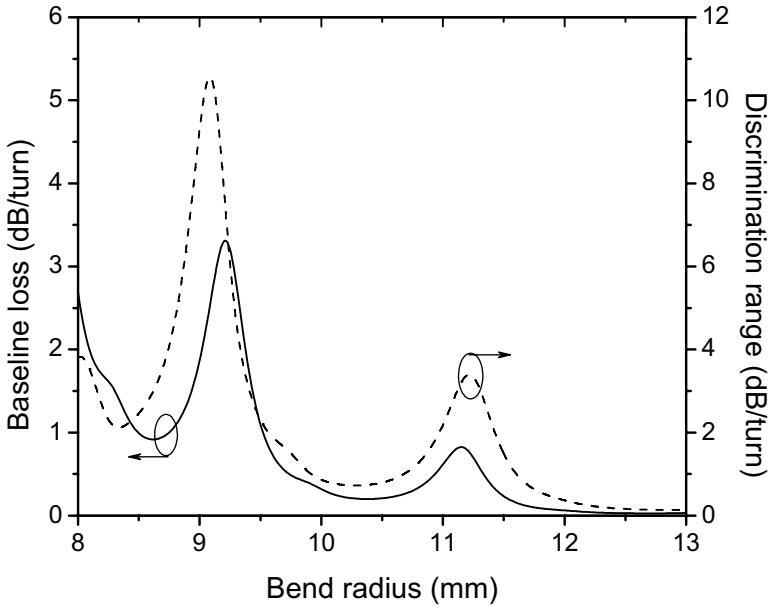

Figure 43. Calculated baseline loss (bend loss at the wavelength of 1500 nm with the correction factor of 1.335) and discrimination range versus different bending radii; the fiber length is one turn.

In the first instance from Fig 43 and Table 9 it is clear that there are multiple solutions of bending radius and bending length for the fiber edge filter. For a given bend radius a useful approach is to divide the minimum discrimination range target of 15 dB by the discrimination range value in dB/turn from Fig. 43. If the number of turns is acceptable, typically a single digit value, then one can proceed to check the baseline loss by multiplying the number of turns by the baseline loss value in dB/turn. If this is less than 5 dB then such a filter is feasible. Using this approach and to help interpret Fig 40, some baseline loss and discrimination values for selected bend radii are shown in Table 9, along with the minimum number of turns needed to reach a target discrimination range of 15 dB and the resultant baseline loss.

Table 9. Calculated parameters versus bending radii for selected bend radii

Bend radius (mm)	**Baseline loss (dB/turn)**	**Discrimination range (dB/turn)**	**Min number of turns**	**Total Baseline loss (dB)**
8.45	1.0772	2.3135	6.5	6.98
8.95	1.5793	7.9776	1.9	2.97
9.45	1.3907	2.642	5.7	7.90
10.95	0.52424	1.8852	8.0	4.17
11.45	0.29061	1.8273	8.2	2.39
12.45	0.02991	0.1693	88.6	2.65
12.95	0.03	0.13593	110.4	3.31

It can be seen from Table 9 that filters with bend radii of 8.45 and 9.45 mm would need 6.5 and 5.7 turns of fiber respectively to reach the minimum discrimination range of 15 dB but that such filters would breach the 5 dB limit for baseline loss. A bend radius of 12.95 mm is not usable for a different reason,

the low discrimination range value in dB/turn would mean that to achieve 15 dB of discrimination would require about 110 turns of fiber, a very long length of fiber that is likely to result in a very high PDL value. It is also clear from Table 9 that using bend radii of 8.95, 10.95 and 11.45 mm would all produce a filter with an acceptable number of turns and a baseline loss less than 5 dB.

These three candidate designs are chosen with bend radii of 8.95, 10.95 and 11.45 mm and a multiple turn structure. The number of turns in each case is adjusted upwards from the value in Table 9 to round off the number of turns to an integer value for ease of fabrication and also to provide discrimination ranges that are distributed over the range of 15-20 dB. Along with the bend radius and number of turns, the calculated baseline loss and discrimination range are summarized in Table 10 for each of the three filters.

Table 10. Calculated baseline loss and discrimination range versus selected bending radii with different fiber length

Selected Bend radius (mm)	**Fiber bending length(turns)**	**Baseline loss (dB)**	**Discrimination range (dB)**
8.95	2	3.1586	15.9552
10.95	9	4.71816	16.9668
11.45	10	2.9061	18.2730

In Ref. [121], it is shown that the fiber polymer coating layer has a significant influence on the bending induced PDL, and that higher PDL values will reduce the accuracy of wavelength measurement. The corresponding PDLs for the three candidate designs in Table 10 are calculated based on scalar approximation method by using the technique presented in [121]. The theoretical polarization dependent losses for the three different bending radii and

bending lengths are shown in Fig. 44. The calculated PDL results were determined with correction factors applied at 10 nm intervals, over the wavelength range of interest between 1500 and 1600 nm. From Fig. 44, one can see that the maximum PDL value (0.475 dB at 1600 nm) occurs with a bending radius of 11.45 mm, clearly larger than the maximum PDLs for bending radii of 8.95 (solid line) and 10.45 mm (dashed dot line). Therefore for experimental verification of the candidate designs, two of the designs in Table 10 were chosen, that has bending radii of 8.95 and 10.95 mm. This selection process underscores the need to include an estimate of likely PDL in the design of an edge filter.

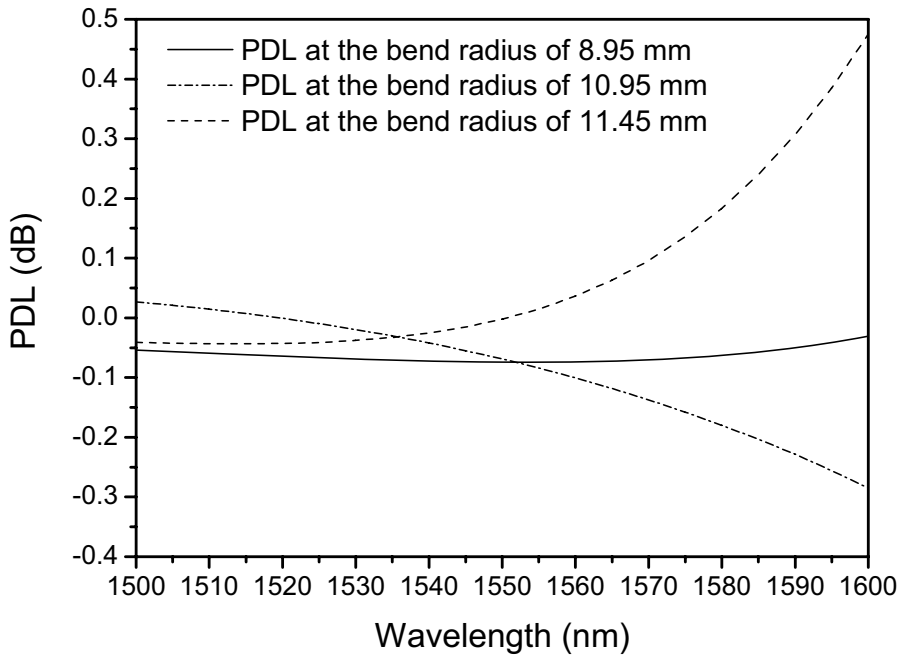

Figure 44. Calculated polarization dependent losses of SMF28e fiber with the bending radius of 8.95 (solid line), 10.95 (dashed dot line) and 11.45 mm (dashed line), and with the lengths of 2 turns, 9 turns and 10 turns, respectively.

6.5 Experimental verification and discussion

Using a tunable laser and an optical spectrum analyzer, the bend loss was

measured as a function of wavelength between 1500 and 1600 nm for the two SMF28e fiber based edge filters selected in the last section. The theoretical and experimental macrobending losses over the wavelength range from 1500 to 1600 nm for edge filters with a bend radius of 8.95 (bend length of 2 turns) and 10.95 mm (bend length of 9 turns) are presented in Fig. 45. From Fig. 45, one can see that there is reasonable overall agreement between the calculated modeling and experimental data. For example for a bend radius of 10.95 mm the measured baseline transmission loss is about 5.096 dB at the wavelength of 1500 nm (calculated value is 4.82 dB) and the measured discrimination range is circa 17.418 dB from 1500 to 1600 nm (calculated value is 16.97 dB) . The discrepancies between the calculated and measured results are most likely a result of: 1) the approximations made in the calculation, e.g., the curved interface between the coating and cladding is treated as an infinite plane and the light field within the core is approximated by the unperturbed field of the straight fiber with infinite cladding as explained in Ref. [125-127]; 2) the application of a correction factor at only a limited number of wavelength points (10 nm intervals) in the calculation of bend loss and 3) the experimental accuracy of the bend radius (both baseline loss and discrimination range are sensitive to the bend radius as presented in Fig. 43.

One final reason for the deviations between calculated and measured results in Fig. 45, are the residual wave-like variations in the transmission spectrum over the wavelength range from 1580 to 1600 nm, in particular for a bending radius of 8.95 mm. The main source of such variations is the formation of WGMs at the interface of the cladding and coating. In practice, from Fig. 43, one can see that the wave-like variations were more evident when the fiber bending radius was

smaller than 9.45 mm in the SMF28e fiber bend loss measurements, as a result of stronger WGMs at lower bend radii.

Finally, we experimentally investigated the PDL performances of bending SMF28e fiber over the range from 1500 to 1600 nm at the bend radius of 8.95 (bend length of 2 turns) and 10.95 mm (bend length of 9 turns). The measured average PDL results are 0.0312 dB for the case of bend radius of 8.95 dB, and 0.0871 dB for the case of bend radius of 10.95 mm, significantly better than 0.1072dB of SMF28 fiber and 0.0922dB of 1060XP fiber presented in Ref. [122].

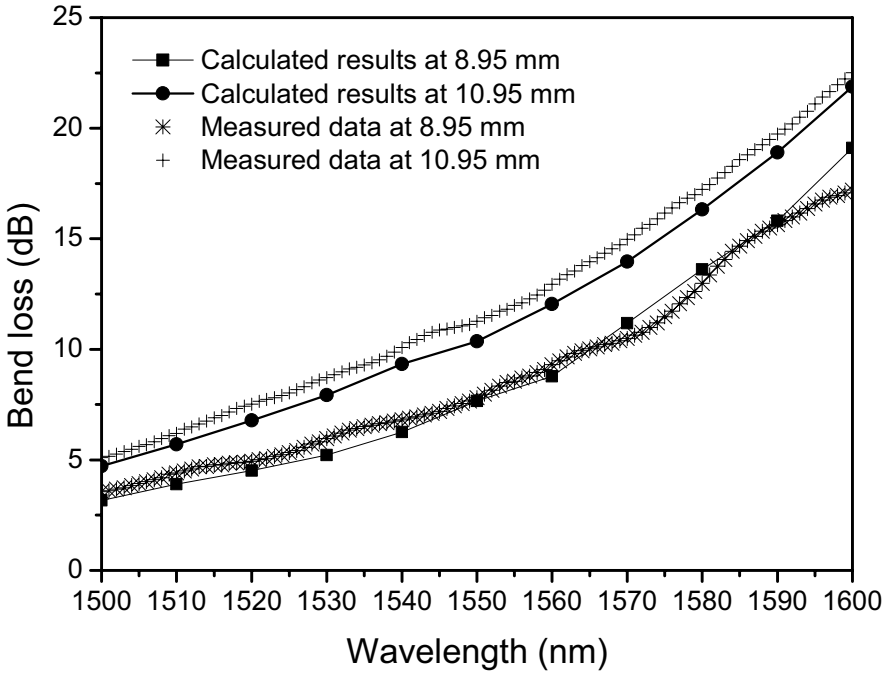

Figure 45. Calculated (solid symbols connected with solid lines) and measured (* and + symbols) macrobending results for bend SMF28e fiber at the bend radius of 8.95 and 10.95mm, respectively.

6.6 Conclusion

In this paper, a generalized methodology for the design of a fiber bend loss based edge filter has been investigated and presented, starting with the task of selecting suitable fibers and then considering the design of the fiber bending loss edge filter. As an example, a Corning SMF28e fiber with a 900 μm jacket is selected to illustrate the fiber evaluation and selection process. Sample filters using this fiber are designed and two are selected for experimental verification. There is good agreement between theoretical modeling and measured results for the sample fiber. The edge filters deigned meet target specifications for baseline loss and discrimination range and show a lower average PDL than previous reports. The filters are also compact and are easy to fabricate. The buffer jacket can be retained on the fiber, reducing fiber stress and thus improving long term reliability. Overall these results confirm the effectiveness of the generic process discussed and proposed in this paper for fiber evaluation, selection and edge filter design.

6.7 References

[114]. M. T. Wlodarczyk, "Wavelength referencing in single-mode microbend sensors," Opt. Lett., Vol. 12, No. 9, pp. 741-743, 1987.

[115]. R. C. Gauthier and C. Ross, “Theoretical and experimental considerations for a single-mode fiber-optic bend-type sensor,” Appl. Opt., Vol. 36, No. 25, pp. 6264-6273, 1997.

[116]. S. H. Nam, and S. Yin, “High-Temperature Sensing Using Whispering Gallery Mode Resonance in Bent Optical Fibers,” IEEE Photon. Technol. Lett., Vol. 17, No. 11, pp. 2391-2393, 2005.

[117]. M. D. Nielsen, N. A. Mortensen, M. Albertsen, J. R. Folkenberg, A. Bjarklev, and D. Bonacinni, “Predicting macrobending loss for large-mode

area photonic crystal fibers," Opt. Exp., Vol. 12, No. 8, pp. 1775-1779, 2004.

[118]. Q. Wang, G. Farrell and T. Freir, "Study of transmission response of edge filters employed in wavelength measurements," Appl. Opt., Vol. 44, No.36, pp. 7789-7792, 2005.

[119]. Q. Wang, G. Rajan, G. Farrell, P. Wang, Y. Semenova and T. Freir, "Macrobending fiber loss filter, ratiometric wavelength measurement and application," Meas. Sci. Technol., Vol. 18, pp. 2082-3088, 2007.

[120]. Q. Wang, G. Farrell, T. Freir, G. Rajan and P. Wang, "Low-cost Wavelength Measurement based on a Macrobending Singlemode Fiber," Opt. Lett., Vol. 31, No. 12, pp. 1785-1787, 2006.

[121]. Q. Wang, G. Rajan, P. Wang, and G. Farrell, "Polarization Dependence of Bend Loss for a Standard Singlemode Fiber," Opt. Express, Vol. 15, No. 8, pp. 4909-4920, 2007.

[122]. P. Wang, G. Farrell, Q. Wang and G. Rajan, "An optimized macrobending fiber based edge filter," IEEE Photon. Technol. Lett., Vol. 19, No. 15, pp. 1136-1138, 2007.

[123]. Q. Wang, G. Rajan, P. Wang and G. Farrell, "Resolution investigation of ratiometric wavelength measurement system," Appl. Opt., Vol. 46, No. 25, pp. 6362-6367, 2007.

[124]. D. Marcuse, "Curvature loss formula for optical fibers," J. Opt. Soc. Am. Vol. 66, No. 3, pp. 216-220, 1976.

[125]. H. Renner, "Bending losses of coated single-mode fibers: a simple approach," J. Lightw. Technol., Vol. 10, No. 5, pp. 544-551, 1992.

[126]. L. Faustini and G. Martini, "Bend loss in single-mode fibers," J. Lightw. Technol., Vol. 15, No. 4, pp. 671-679, 1997.

[127]. Q. Wang, G. Farrell and T. Freir, "Theoretical and experimental investigations of macro-bend Losses for standard single mode fibers," Opt. Express, Vol.13, No.12, pp. 4476-4484, 2005.

[128]. R. T. Schermer and J. H. Cole, "Improved bend loss formula verified for optical fiber by simulation and experiment", IEEE J. Quantum Elect., Vol. 43, No. 10, pp. 899-909, 2007.

[129]. Y. Murakami and H. Tsuchiya, "Bending losses of coated single-mode optical fibers," IEEE J. Quantum Elect., Vol. QE-14, No. 7, pp. 495-501, 1978.

Chapter 7

Conclusions and future work

In this chapter, achievement of aims and conclusions from across the thesis are reviewed and the contributions to current technology and knowledge from the whole thesis are discussed. Future research as an extension of this PhD thesis is also discussed.

7.1. Achievement of aims

The aim of this research thesis, stated in Chapter1, is to develop an effective modeling platform for singlemode fiber bend loss which can deal with a variety of fiber types and to utilize this modeling platform to investigate the design of a novel fiber bending loss edge filter, taking account of the effect of temperature, polarization and fiber tolerance. This aim has been achieved, as evidenced by:

I. The theoretical modeling platform for predicting the bend loss of singlemode fiber has been developed and practically investigated through purpose built real world experiments. The improved model can be utilized to predict the bend loss of fibers with single or multiple cladding/coating layers with the added advantage of effectively reducing the computation time. The development of the model has also resulted in the dissemination of a deeper understanding of the performance characteristics of singlemode fiber bend loss. The model developed also provides a foundation for further modeling research on polarization dependent loss and temperature dependent loss and the improvement of such models using both the scalar approximation and beam propagation

method.

II. The developed theoretical model using the scalar approximation method has been proven to be a fast and effective technique without significantly affecting the accuracy of calculated results compared with the conventional beam propagation method.

III. The developed theoretical modeling platform has been shown to be adaptable to deal with a variety of issues, for example a successful adaptation of the model has been demonstrated which allows the model to take account of thermal expansion and thermo-optic effects to allow for the prediction of the temperature dependent loss of the fiber. This and other adaptations of the developed theoretical model have been verified experimentally and are shown to be a fast and effective technique, compared with the conventional bend geometry considerations published previously.

IV. Given the existence of a significant whispering gallery modes* associated with the bend loss peaks from both modeling and experimental investigations, a more robust and efficient theoretical model was developed which has considerably less computation time. The improved model is capable of providing acceptable computational accuracy and can be adapted and utilized to predict not only the bend loss, but also polarization dependent loss and temperature dependent loss of fibers with single or multiple cladding/coating layers.

V. Based on the outcomes of the research the research methodology outlined in Chapter 1, it is proposed as an effective and reliable

* The corresponding explanation for "Whispering-gallery mode" can be found in the footnote of Page 8.

approach to research on fiber bend loss and its applications.

7.2. Conclusions from the research

I. **Conclusions regarding the theoretical modeling of fiber bend loss**

In this thesis, theoretical models based on the scalar approximation method are developed for predicting the macrobending loss of singlemode fiber with single or multiple cladding/coating layers. The models can be utilized to predict both polarization dependent loss and temperature dependent loss of a bent singlemode fiber. The conclusions are:

- The developed models based on the scalar approximation method have been shown to be a fast and effective alternative to the previous beam propagation method for predicting the macrobending loss of singlemode fiber with single or multiple coating layers. Given the same personal computer with an Intel Pentium 4 processor with a clock speed of 3.0 GHz, 1 GB RAM and 80 GB hard disk storage, the speed of computation time of the scalar approximation based model is hundreds times of beam propagation method base model.
- It is necessary to take into account the impact of whispering gallery modes in the developed models for predicting the bend loss of a singlemode fiber. The whispering gallery modes have an effect on the spectral responses of bend loss, so that the coherent coupling between the fundamental propagation field and the reflected radiated field by the coating layer needs to be taken

account of in the modeling.

- The absorbing layer can be utilized for mitigating the effect of whispering gallery modes in the bend loss spectral response and also to allow experimental verification for the theoretical models, which are based on a singlemode fiber with an infinite cladding or coating layer.

II. Conclusions in regard to polarization dependent loss

A theoretical model based on the scalar approximation method is built for calculating the polarization dependence of macrobending loss for a singlemode fiber with core-cladding-infinite coating structure. The agreement between the theoretical models and experimental results shows that the fiber coating has a significant influence on the polarization dependence of bend loss. However, bare fiber with a stripped coating can effectively mitigate such an influence on the polarization dependent loss, a result that is also experimentally verified. The conclusions are:

- The developed theoretical model for predicting polarization dependent loss has been proven to be a fast and effective technique without significantly affecting the accuracy of calculated results, compared with the conventional beam propagation method. Given the same personal computer with an Intel Pentium 4 processor with a clock speed of 3.0 GHz, 1 GB RAM and 80 GB hard disk storage, the speed of computation time of the scalar approximation based model is hundreds times of beam propagation method base model.

- It is shown that the so-called whispering gallery modes impact not only on the spectral response of bend loss, but also on the polarization dependent loss and it is necessary to take account of the influence of whispering gallery modes in the developed models for predicting polarization dependent loss.
- A correction factor, namely, the effective bending radius, is needed to allow the experimental results to be compared with those from the developed models. It is shown that the polarization dependent loss can be calculated as the difference between the simulated bend loss of the TE and TM modes, thus the developed models for predicting the polarization dependent loss inherit the correction used in the bend loss models.

III. Conclusions regarding temperature dependent loss

A theoretical model based on the scalar approximation method is developed for predicting the temperature dependence of low bend loss fiber with a core-cladding-inner coating-infinite outer coating layer structure. Another model is developed for predicting the temperature dependence of high bend loss fiber with a core-infinite cladding structure. The effect of temperature on polarization dependent loss is also studied theoretically and experimentally. Both the theoretical models and experimental results show that ambient temperature variations have a significant influence not only on the polarization dependence, but also on the bend loss. The conclusions are:

- The developed theoretical model for predicting the temperature dependent loss is shown to be an accurate and effective simulation

method, compared with the model based on conventional bend geometry considerations published previously.

- It is necessary to take into account of the influence of whispering gallery modes occurring between the two coating layers. If the influence of whispering gallery modes is not taken into account in the theoretical models, the models will not agree with the measured wave-like variation of bend loss with temperature.
- It is shown that the single coating layer model, while it may be accurate for the theoretical prediction of bending loss at a fixed room temperature of 20^{o}C, is not adequate for predicting the variation of both bend loss and polarization dependent loss with temperature, especially for a fiber with a dual coating.
- It is shown that the developed theoretical models can be used to evaluate the performance of a fiber macrobending based edge filter as a function of ambient temperature not only for high-speed wavelength measurements but also for fiber-based temperature sensing applications.

IV. Conclusions regarding the manufacturing tolerance

The impact of manufacturing tolerances for an all-fiber based bend loss edge filter is investigated. It is shown that the manufacturing tolerances of the fiber parameters, such as fiber core radius and NA, significantly influence the fiber bend loss performance and spectral response of a fiber-based edge filter. The conclusions are:

- It is necessary to take account of the influence of manufacturing tolerances of the fiber parameters on the performance prediction of

designed fiber edge filter.

- It is shown that bend-radius tuning during fabrication of such filters is a means of mitigating the effect of manufacturing variations. For example for a fiber core radius variation of ± 6.26%, bend radius tuning circa 38% can be successfully employed to mitigate the influence of manufacturing tolerance on the spectral response of edge filter.

V. Conclusions in regard to a generalized design methodology

A generalized methodology for the design of a fiber bend loss based edge filter is investigated. SMF28e fiber is used as an example to illustrate the design process. The conclusions are:

- The agreement between modeled and measured results confirms the effectiveness of the generic process discussed and proposed for fiber evaluation, selection and edge filter design.
- In the absence of manufacturer's data regarding the absorption characteristics of the fiber jacket, an effective approach to assessing the absorption characteristics of the jacket is to compare the measured bend loss versus bend radius characteristic to that modeled assuming an infinite coating, effectively a 100% efficient absorber.

7.3. Future work

This thesis has described the study, applications and limitations of a fiber bend loss based edge filter from a number of perspectives. The theoretical study has also shown promise for the development of fiber bend loss edge filters that may

be tailored to specific applications, most importantly a fast wavelength measurement system but also potentially sensors with a high sensitivity to wavelength, strain, temperature or refractive index.

There remain a number of unanswered research questions and challenges. For example, work is needed in future to investigate the discrepancy between theory and experiment for the correction factor, namely, the effective bending radius. This could take the form of a theoretical study as well as an experimental investigation. One possible investigation could be undertaken to develop a finite element method (FEM) model for the predicting macrobending loss that will verify and support the predictions that have been made for the spectral responses of bend loss to wavelength, strain and temperature. The realization of such a model could facilitate the accurate prediction of the correction factor, which is vital if modeling is to be useful, for example, for the development of new bend-loss based sensors. The success of this FEM model, verified by experimental results, could provide an opportunity to take into account the influence of the mechanical strain caused by both macrobending and microbending on the bend loss. Such a model could be used to investigate the probability of stress related failure in fiber bend loops and will also serve as a further validation of the theoretical predictions of the performance of a bent fiber put forward in this thesis.

In this thesis, in order to achieve reasonable processing times with limited processing power and memory, the calculation of macrobending loss and polarization dependent losses have been based on a scalar approximation method, so that the models contain some approximations. However such approximations result in a discrepancy between the calculated results and the measured results.

Thus it is necessary to develop another more accurate numerical model for prediction. The beam propagation method (BPM) is a very powerful numerical technique for investigating lightwave propagating phenomenon along integrated waveguide based optical devices. However it is very demanding on processing power and has not been commonly used for modeling bend loss as a result. Essentially, the BPM is a numerical method for approximating the exact wave equations for monochromatic waves and solving the wave equations numerically. To date, a number of variations of BPM have been developed, such as the Fast Fourier Transform (FFT) [130-132], Finite-Difference (FD) [133-139], Finite element (FE) [140-144] and Time Domain (TD) [145-150] methods. In Appendix B, to provide a comparison with calculated results based on the scalar approximation method, a 3-dimensional full-vectorial (FV) finite difference-beam propagation method (FD-BPM) is developed using an alternating direction implicit (ADI) method with a perfectly matched layers (PML) numerical boundary condition for investigating wave propagation in macrobending singlemode optical fibers.

Existing fiber based sensors have many advantages, but such advantages are offset in many cases by the complexity of such systems. One strand of future research* can address this shortfall by developing macrobending fiber based displacement, strain and refractometer sensors that offer the performance and advantages of existing fiber sensors but which require a significantly less complex interrogation system. In Appendix C, as an example of preliminary research on this topic, simulation results for a proposed refractometer based on macrobending singlemode fiber are presented.

* Funding for the research project entitled "Displacement, strain and refractometer sensor based on macrobending singlemode fiber," has been awarded from the Irish Research Council for Science, Engineering and Technology (IRCSET).

7.3 References

[130]. M. D. Feit and J. A. Freck, Jr., “Light propagation in graded-index optical fibers,” Appl. Opt., 17, pp. 3990-3998, (1978).

[131]. L. Thylen, “The beam propagation method: An analysis of its applicability,” Opt. Quantum Electron, 15, pp. 433-439, (1983).

[132]. J. Yamauchi, J. Shibayama, and H. Nakano, “Beam propagation method using Pad approximant operators,” Trans. IEICE Jpn., J77-C-I, pp. 490-494, (1994).

[133]. Y. Chung and N. Dagli, “Assessment of finite difference beam propagation,” IEEE J. Quantum Electron., 26, pp. 1335-1339, (1990).

[134]. G. R. Hadley, “Wide-angle beam propagation using Pad approximant operators,” Opt. Lett., 17, pp. 1426-1428, (1992).

[135]. G. R. Hadley, “A multistep method for wide angle beam propagation,” Integrated Photon. Res., ITu 15-1, pp. 387-391, (1993).

[136]. J. Yamauchi, J. Shibayama, and H. Nakano, “Modified finite-difference beam propagation method on the generalized Douglas scheme for variable coefficients,” IEEE Photon. Technol. Lett., 7, pp. 661-663, (1995).

[137]. J. Yamauchi, T. Ando, and H. Nakano, “Beam-propagation analysis of optical fibres by alternating direction implicit method,” Electron. Lett., 27, pp. 1663-1665, (1991).

[138]. P. L. Liu and B. J. Li, “Study of form birefringence in waveguide devices using the semivectorial beam propagation method,” IEEE Photon. Technol. Lett., 3, pp. 913-915, (1991).

[139]. W. P. Huang and C. L. Xu, “Simulation of three-dimensional optical waveguides by a full-vector beam propagation method,” IEEE J. Quantum Electron., 29, pp. 2639-2649, (1993).

[140]. M. Koshiba and Y. Tsuji, "A wide-angle finite element beam propagation method," IEEE Photon. Technol. Lett., 8, pp. 1208-1210, (1996).

[141]. Y. Tsuji and M. Koshiba, “Guided-mode and leaky-mode analysis by imaginary distance beam propagation method based on finite element scheme,” J. Lightwave Technol., 18, pp. 618-623, (2000).

[142]. K. Saitoh and M. Koshiba, “Full-vectorial finite element beam

propagation method with perfectly matched layers for anisotropic optical waveguides," J. Lightwave Technol., 19, pp. 405-413, (2001).

[143]. K. Saitoh and M. Koshiba, "Approximate scalar finite-element beam-propagation method with perfectly matched layers for anisotropic optical waveguides," J. Lightwave Technol., 19, pp. 786-792, (2001).

[144]. S. S. A. Obayya, B. M. Azizur Rahman, Kenneth T. V. Grattan, and H. A. El-Mikati, "Full vectorial finite-element-based imaginary distance beam propagation solution of complex modes in optical waveguides," J. Lightwave Technol., 20, pp. 1054-1060, (2002).

[145]. G. H. Jin, J. Harari, J. P. Vilcot, and D. Decoster, "An improved time-domain beam propagation method for integrated optics components," IEEE Photon. Technol. Lett., 9, pp. 348-350, (1997).

[146]. H. M. Masoudi, M. A. AlSunaidi, and J. M. Arnold, "Time-domain finite-difference beam propagation method," J. Lightwave Technol., 11, pp. 1274-1276, (1999).

[147]. J. Shibayama, T. Takahashi, J. Yamauchi, and H. Nakano, "Time-domain finite-difference BPM with padé approximants in time axis for analysis of circularly symmetric fields," Electron. Lett., 36, pp. 319-321, (2000).

[148]. J. Shibayama,.T. Takahashi, J. Yamauchi, and H. Nakano, "Efficient time-domain finite-difference beam propagation methods for the analysis of slab and circularly symmetric waveguides," J. Lightwave Technol., 18, pp. 437-442, (2000).

[149]. J. Shibayama, T. Takahashi, J. Yamauchi, and H. Nakano, "Comparative study of absorbing boundary conditions for the time-domain beam propagation method," IEEE Photon. Technol. Lett., 13, pp. 314-316, (2001).

[150]. J. Shibayama, A. Yamahira, T. Mugita, J. Yamauchi, and H. Nakano, "A finite-difference time-domain beam-propagation method for TE- and TM-wave analyses," J. Lightwave Technol., 21, pp. 1709-1715, (2003).

Appendix A

Statement of Contribution

For the publications presented within this thesis, the co-authors listed below certify that:

1. Pengfei Wang is the first author for all the publications.

2. As first author, Pengfei Wang undertook all aspects of the research described in each publication, including preparation and submission of the publication and the preparation of any revisions requested by referees, with the support and advice of the co-authors.

3. The co-authors agree to the use of the publications in this thesis.

Dr. Gerald Farrell

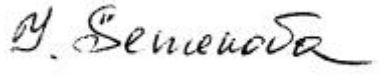

Dr. Yuliya Semenova

Dr. Qian Wang

Mr. Ginu Rajan

Mr. Thomas Freir

Dr. John Cassidy

Mr. Agus Muhamad Hatta

Appendix B

Accurate Theoretical Prediction for Singlemode Fiber Macrobending Loss and Bending Induced Polarization Dependent Loss*

Keywords: Macrobending, polarization dependent loss, full vectorial finite difference beam propagation method

Abstract: For an all-fiber edge filter used in a rapid wavelength measurement system for optical sensing, a low polarization dependent loss (PDL) is required to ensure high measurement accuracy. The calculation of the bend loss for the TE and TM modes based on scalar approximations results in a discrepancy between the calculated PDLs and measured results. Here a full vectorial finite difference beam propagation method (FV FD-BPM) is used to compute the complex propagation constant and the field distributions of the TE and TM modes in the bending fiber, allowing the accurate calculation of the PDL of bending fiber.

Introduction

It is well known that a radiation loss occurs when a singlemode fiber is bent. Macrobending induced polarization dependent loss (PDL) has been investigated

* P. Wang, G. Farrell, Y. Semenova, Q. Wang, A. M. Hatta and G. Rajan, "Accurate theoretical prediction for singlemode fiber macrobending loss and bending induced polarization dependent loss," Optical Sensors 2008, Proceedings of SPIE, Vol. 7003, pp. 7003Y1-7003Y13, 2008.

as an important issue in many fiber-optic communication applications [151-154]. Recently, fiber bend loss induced polarization dependence for standard Corning SMF28 singlemode fiber was investigated theoretically and experimentally for an all-fiber edge filter for rapid wavelength measurement in optical sensing [155]. To ensure high measurement accuracy a low polarization dependence for the bend loss is required.

In a previous publication by the authors the calculation of the bend loss of a singlemode fiber for the TE and TM mode based on scalar approximation has been presented [156], considering the respective boundary conditions at the interface between the cladding and coating layer. With the proposed normalized polarization dependent loss, the polarization sensitivity for different bending radii was also characterized. For reasonable processing times with limited processing power and memory, the calculation of polarization dependent losses has previously been based on a scalar approximation method, so that the model contains some approximations. However such approximations result in a discrepancy between the calculated polarization dependent losses by the scalar approximation and the measured results.

To date, the scalar, semi-vectorial and full-vectorial finite difference beam propagation method (FV FD-BPM) have been developed for the analysis of optical waveguides and is being widely utilized due to its unique combination of properties. Here a 3-dimentional (3-D) FV FD-BPM is used to compute the complex propagation constant and the field distributions of the quasi-TE and quasi-TM modes in a macrobending singlemode fiber with a perfectly matched layer boundary condition, allowing for the accurate calculation of the polarization dependent loss of bending fiber.

As shown previously [155, 156] where a bending fiber is used as an edge filter, it is important to suppress whispering-gallery modes to ensure a smooth wavelength response. This can be achieved by coating the fiber with an absorbing layer, or alternatively utilizing a fiber with an outer protective 900 μm diameter jacket which can function as an absorbing layer. In this paper a standard Corning singlemode fiber-SMF28e with a 900 μm protective jacket is employed for the theoretical calculations and for experimental verification in this paper. The 3-D FV FD-BPM theoretical modeling agrees well with the measured results for the bend loss of SMF28e fiber with a correction factor of 1.27 at a wavelength of 1550 nm. Through the experimental examination of both the bend loss and PDL behavior of SMF28e fiber, it is found that the FV FD-BPM based theoretical model can achieve a significantly better agreement with experimental results than the well known scalar approximation method.

Theoretical analysis

The full-vectorial BPM is widely employed instead of the semi-vectorial and scalar BPM method because it provides superior precision for calculating different polarization states. As is well known, the vectorial wave equation for the electric fields can be defined as [157]:

$$\nabla^2 \times \vec{E} - k^2 n^2 \vec{E} = 0 \qquad \text{(A.1)}$$

where $k = \omega\sqrt{\varepsilon_0 \mu_0}$ is the wave number in free space and $n = n(x, y, z)$ is the refractive index of the isotropic medium. Transverse components in equation (A.1) can be expressed as follows with an approximation $\partial n^2 / \partial z \approx 0$:

$$\nabla^2 \vec{E}_t + k^2 n^2 \vec{E}_t = \nabla_t \left[\nabla_t \cdot \vec{E}_t - \frac{1}{n^2} \nabla_t \cdot \left(n^2 \vec{E}_t \right) \right] \tag{A.2}$$

By defining $\vec{E}_t = \hat{E}_t e(-jn_0 kz)$ (the slowly varying envelope approximation), both the x and y components of the 3-D vectorial wave equations for the electrical field can be presented as:

$$2jkn_0 \frac{\partial E_x}{\partial z} = \frac{\partial}{\partial x}\left(\frac{1}{n^2} \frac{\partial}{\partial x}\left(n^2 E_x \right) \right) + \frac{\partial^2 E_x}{\partial y^2} + k^2 \left(n^2 - n_0^2 \right) E_x - \frac{\partial}{\partial x}\left[\frac{\partial E_y}{\partial y} - \frac{1}{n^2} \frac{\partial}{\partial y}\left(n^2 E_y \right) \right] \tag{A.3a}$$

$$2jkn_0 \frac{\partial E_y}{\partial z} = \frac{\partial^2 E_y}{\partial x^2} + \frac{\partial}{\partial y}\left(\frac{1}{n^2} \frac{\partial}{\partial y}\left(n^2 E_y \right) \right) + k^2 \left(n^2 - n_0^2 \right) E_y - \frac{\partial}{\partial y}\left[\frac{\partial E_x}{\partial x} - \frac{1}{n^2} \frac{\partial}{\partial x}\left(n^2 E_x \right) \right] \tag{A.3b}$$

finally, the full-vectorial wave equation for the electric fields can be expressed by:

$$2jkn_0 \frac{\partial}{\partial z}\left(\begin{bmatrix} E_x \\ E_y \end{bmatrix} \right) = \begin{bmatrix} P_{xx} & P_{xy} \\ P_{yx} & P_{yy} \end{bmatrix} \begin{bmatrix} E_x \\ E_y \end{bmatrix} \tag{A.4}$$

where the corresponding operators are given by:

$$P_{xx} E_x = \frac{\partial^2 E_x}{\partial y^2} + \frac{\partial}{\partial x}\left[\frac{1}{n^2} \frac{\partial}{\partial x}\left(n^2 E_x \right) \right] + k^2 \left[\left(n^2 - n_0^2 \right) E_x \right] \tag{A.5a}$$

$$P_{xy} E_y = \frac{\partial}{\partial x}\left[-\frac{\partial E_y}{\partial y} + \frac{1}{n^2} \frac{\partial}{\partial y}\left(n^2 E_y \right) \right] \tag{A.5b}$$

$$P_{yx} E_x = \frac{\partial}{\partial y}\left[-\frac{\partial E_x}{\partial x} + \frac{1}{n^2} \frac{\partial}{\partial x}\left(n^2 E_x \right) \right] \tag{A.5c}$$

$$P_{yy}E_y = \frac{\partial^2 E_y}{\partial x^2} + \frac{\partial}{\partial y}\left[\frac{1}{n^2}\frac{\partial}{\partial y}\left(n^2 E_y\right)\right] + k^2\left[\left(n^2 - n_0^2\right)E_y\right] \tag{A.5d}$$

and the full-vectorial wave equation for magnetic fields can also be expressed by:

$$2jkn_0\frac{\partial}{\partial z}\left(\begin{bmatrix} H_x \\ H_y \end{bmatrix}\right) = \begin{bmatrix} Q_{xx} & Q_{xy} \\ Q_{yx} & Q_{yy} \end{bmatrix}\begin{bmatrix} H_x \\ H_y \end{bmatrix} \tag{A.6}$$

where the corresponding operators given by

$$Q_{xx}H_x = \frac{\partial^2 H_x}{\partial x^2} + n^2\frac{\partial}{\partial y}\left(\frac{1}{n^2}\frac{\partial H_x}{\partial y}\right) + k^2\left[\left(n^2 - n_0^2\right)H_x\right] \tag{A.7a}$$

$$Q_{xy}H_y = \frac{\partial^2 H_x}{\partial x \partial y} - n^2\frac{\partial}{\partial y}\left(\frac{1}{n^2}\frac{\partial H_y}{\partial x}\right) \tag{A.7b}$$

$$Q_{yx}H_x = \frac{\partial^2 H_x}{\partial y \partial x} - n^2\frac{\partial}{\partial x}\left(\frac{1}{n^2}\frac{\partial H_x}{\partial y}\right) \tag{A.7c}$$

$$Q_{yy}H_y = \frac{\partial^2 H_y}{\partial y^2} + n^2\frac{\partial}{\partial x}\left(\frac{1}{n^2}\frac{\partial H_y}{\partial x}\right) + k^2\left[\left(n^2 - n_0^2\right)H_y\right] \tag{A.7d}$$

Equation (A.4) can be efficiently derived utilizing the well-known alternating direction implicit (ADI) method [158, 159] as following:

$$2jkn_0\frac{\partial}{\partial z}\left(\begin{bmatrix} E_x \\ E_y \end{bmatrix}\right) = \begin{bmatrix} A_x + A_y & P_{xy} \\ P_{yx} & B_x + B_y \end{bmatrix}\begin{bmatrix} E_x \\ E_y \end{bmatrix} \tag{A.8}$$

where A_x and A_y are the dependent parts of the x- and y-direction for P_{xx}, while. B_x and B_y are the dependent parts of the x- and y-direction for P_{yy}. Following the discretization of the Crank-Nicholson scheme, the equation can also be expressed as:

$$2jkn_0\frac{1}{\Delta z}\left(\begin{bmatrix}E_x\\E_y\end{bmatrix}^{n+1}-\begin{bmatrix}E_x\\E_y\end{bmatrix}^{n}\right)=\frac{1}{2}\left(\begin{bmatrix}A_x & P_{xy}\\0 & B_x\end{bmatrix}+\begin{bmatrix}A_y & 0\\P_{yx} & B_y\end{bmatrix}\right)\left(\begin{bmatrix}E_x\\E_y\end{bmatrix}^{n+1}+\begin{bmatrix}E_x\\E_y\end{bmatrix}^{n}\right) \tag{A.9}$$

the formula (A.9) can also be solved as two substeps. For the first substep, we have:

$$E_x^{n+\frac{1}{2}}+\frac{j\Delta z}{4kn_0}\left(A_xE_x^{n+\frac{1}{2}}+P_{xy}E_y^{n+\frac{1}{2}}\right)=E_x^n-\frac{j\Delta z}{4kn_0}A_yE_y^n \tag{A.10a}$$

$$E_y^{n+\frac{1}{2}}+\frac{j\Delta z}{4kn_0}B_xE_y^{n+\frac{1}{2}}=E_y^n-\frac{j\Delta z}{4kn_0}\left(B_yE_y^n+P_{yx}E_x^n\right) \tag{A.10b}$$

for the second substep, we have

$$E_x^{n+1}+\frac{j\Delta z}{4kn_0}A_yE_y^{n+1}=E_x^{n+\frac{1}{2}}-\frac{j\Delta z}{4kn_0}\left(A_xE_x^{n+\frac{1}{2}}+P_{xy}E_y^{n+\frac{1}{2}}\right) \tag{A.11a}$$

$$E_y^{n+1}+\frac{j\Delta z}{4kn_0}\left(B_yE_y^{n+1}+P_{yx}E_x^{n+1}\right)=E_y^{n+\frac{1}{2}}-\frac{j\Delta z}{4kn_0}B_xE_y^{n+\frac{1}{2}} \tag{A.11b}$$

Solving the formulations of (A.10) and (A.11) by using finite difference expressions, the quasi-transverse electric (TE) component is obtained. By following a similar procedure, equation (A.6) can be solved for the quasi-transverse magnetic (TM) component. Therefore the bend loss coefficient, namely, the imaginary part of the complex propagation constant β, is defined for the bending fiber as shown in equation (A.12):

$$\alpha = -10 \times \log_{10} \left(\left| \int E^* E_0 dxdy \right|^2 \Big/ \left[\int |E_0|^2 dxdy \right]^2 \right) \qquad \text{(A.12)}$$

where E^* is the propagation field at the different component, E_0 is the incident field of the fundamental mode. Based on the equation (A.12), the bend loss can be calculated.

Fig. 1 presents the schematic structure of a typical bending singlemode fiber, which consists of the fiber core, cladding, primary coating and secondary coating layer. In our previous experimental investigations [160], it was found that in a bending singlemode fiber, the radiation radiated from fiber core was mostly absorbed in the primary coating layer. Furthermore, an attached absorbing layer was also applied on the surface of the secondary coating layer to absorb the radiation that penetrated through the coating layer as presented in Ref. [160]. In effect in our previous investigations the structure of a bending fiber was treated as a core-cladding-infinite coating structure.

For a bending fiber structure without an absorbing layer, the reflection of the radiated field occurring at the interface of between the coating and air has a significant effect on the bend loss, when the bend radius is relatively small, because the reflection occurring is much stronger due to the significant refractive index difference between the coating and air. Some types of fiber are available with a protective jacket outside of the conventional 250 μm diameter coating. One example of this is the Corning SMF28e fiber employed in this paper, which has a 900 μm diameter jacket attached to the secondary coating layer. As it is found that the 900 μm diameter jacket absorbs radiated energy from the core and thus functions as the absorbing layer used in our previous investigations, so a bending SMF28e fiber can be also treated as a core-cladding-infinite coating

structure. One caveat is that all bend radii need to be increased because of the addition of the radius of the fiber jacket (450 μm).

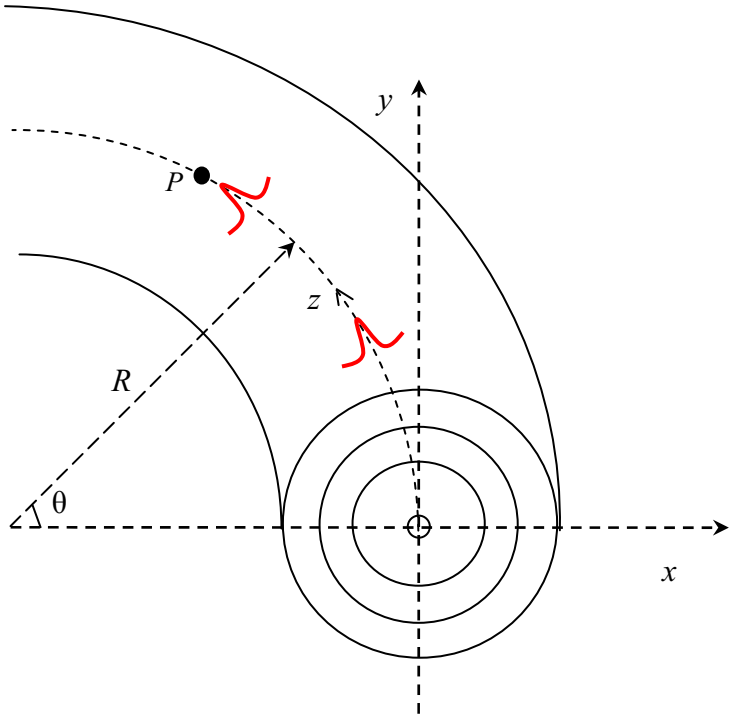

Figure 1. Schematic structure of a typical bending singlemode fiber consisting of core, cladding and dual coating.

As a sample, the calculated 2-D mode field distributions of the quasi-TE and quasi-TM modes (E_x dominant component) in the macrobending SMF28e fiber are presented in Figure 2 (a) and (b) respectively, and the 3-D mode field distributions are presented in Figure 2 (c) and (d) as well. The bend radius in all cases is 9.45 mm, and the wavelength is 1550 nm. From the figures, firstly, one can see that the changes in the mode field for different polarization states are most distinct at the core-cladding layer (x = 4.1μm). The quasi-TE mode pattern is continuous at the interfaces of the fiber layers, along the direction of propagation (z). However, conversely, the quasi-TM mode pattern is discontinuous at the interfaces between the fiber core-cladding and cladding-coating layers. Secondly, it is shown that the leaky modes radiated from

the fundamental mode and the wave-like deformations occur toward the outer side of the bend. Finally the deformation of the field of the quasi-TM mode is found to be larger than that for the quasi-TE mode through the comparison of 3-D mode patterns, which is the mechanism that results in PDL for the bending fiber.

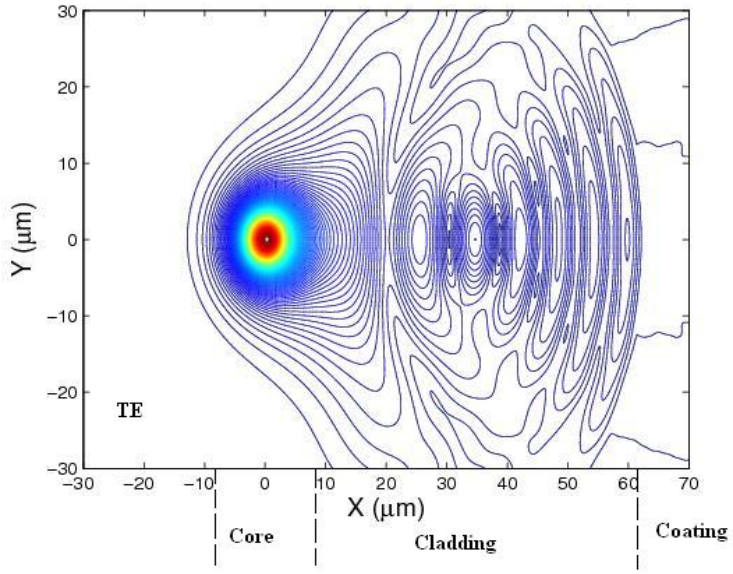

(a)

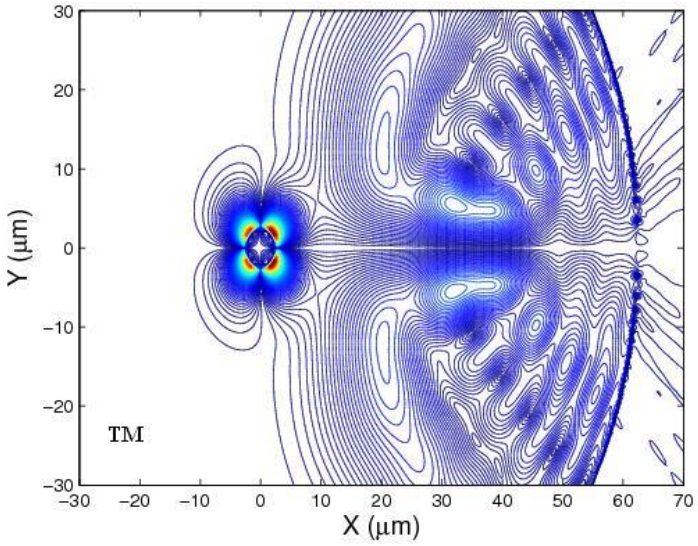

(b)

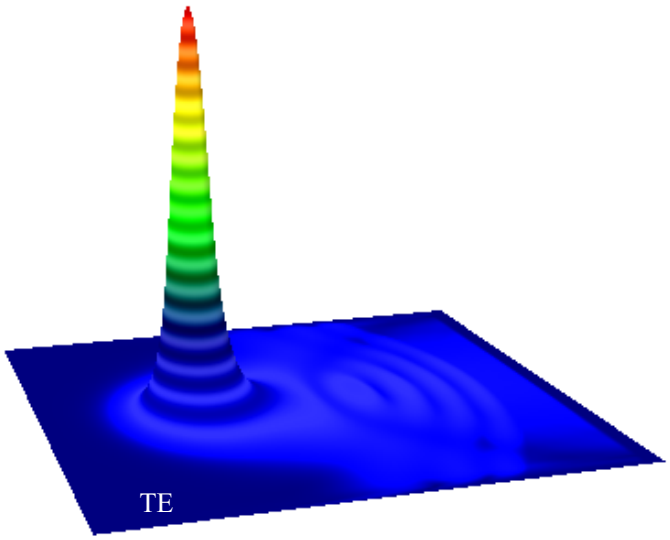

(c)

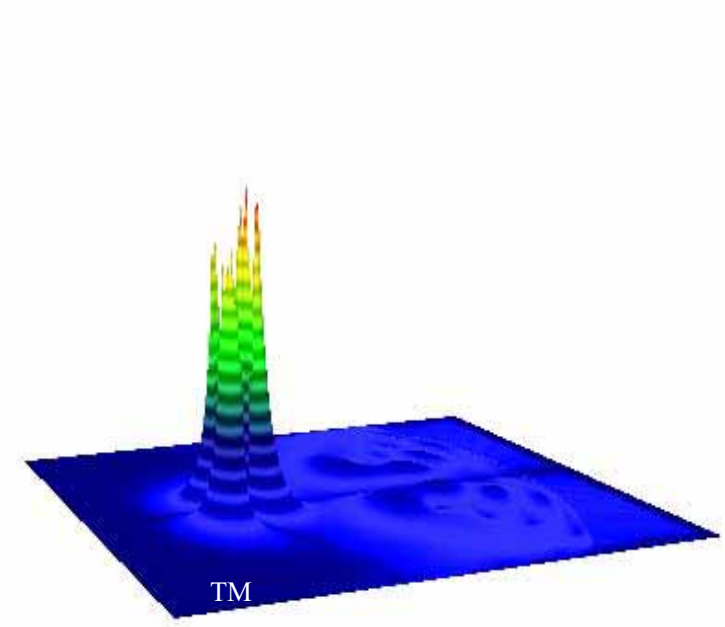

(d)

Figure 2. Mode patterns of the bending fiber with fiber core-cladding-infinite coating structure for a radius of curvature *R* of 9.45 mm: a) 2-D contour plot of quasi-TE mode field; b) 2-D contour plot of quasi-TM mode field; a) 3-D plot of quasi-TE mode field; b) 3-D plot of quasi-TM mode field Only E_x (dominant component) evolution is shown here.

The conditions for the calculation of bend loss using the BPM, are that the wavelength is λ = 1550 nm, the bend radius is from 8 to 12 mm, and the bending

length is 20 turns. the computational window dimensions are given by 60×100 μm^2, the transverse mesh size is $\Delta x = \Delta y = 0.2$ μm and the propagation step size is $\Delta z = 2$ μm, In order to minimize unwanted reflection, the perfectly matched layers (PML) [161] are chosen as the numerical simulation boundary conditions and a vertical PML layer of thickness of $d = 25$ μm is constructed parallel to the right vertical boundary in the direction in which the mode radiates. The corresponding calculated bend loss of quasi-TE and quasi-TM results of bending SMF28e fiber are shown in Table 1:

Table 1. Calculated PDL results of a bending SMF28e singlemode fiber based on 3-D FV FD-BPM at the wavelength of 1550 nm, where the fiber bending length is 20 turns.

Bend radius (mm)	**Bend loss of quasi-TM mode (dB)**	**Bend loss of quasi-TE mode (dB)**	**PDL (dB)**
8+0.45	40.9874	42.6333	-1.6459
8.5+0.45	89.3461	88.4685	0.8776
9+0.45	57.5683	57.2050	0.3633
9.5+0.45	14.7824	15.2464	-0.4640
10+0.45	10.8136	11.1994	-0.3858
10.5+0.45	27.5763	27.1666	0.4097
11+0.45	17.3891	17.1943	0.1948
11.5+0.45	4.9388	5.0686	-0.1298
12+0.45	1.3823	1.5872	-0.2049

Experimental results and discussion

Fig. 3 shows the experimental setup used for the measurement of fiber bending loss. In the experiment, the singlemode fiber was wrapped on a mandrel consisting of multiple sections, each providing a different usable diameter. The bending fiber was connected to a tunable laser and an optical spectrum analyser. The tunable laser has an output power range from +7 dBm to -7 dBm, and the

tuning range of the wavelength is from 1500 to 1600 nm. The bend losses of SMF28e fiber with a 900 μm jacket layer (which prevents the reflection occurring at the interface between the coating layer and air) were measured for the bending radii range from 8 to 13 mm when the wavelength is 1550 nm and bending length is 20 turns. Both measured results (star points) and the calculated bend losses of the quasi-TE mode utilizing FV FD-BPM (circle points) are presented in Fig. 4 The calculated results using the scalar approximation method (triangle points) is also included in Fig. 4 for the sake of comparison. A correction factor of 1.27, which has been used as an effective bend radius for pure fused silica fiber presented in Ref. [162], is applied by convention in both of theoretical models to fit the experimental results.

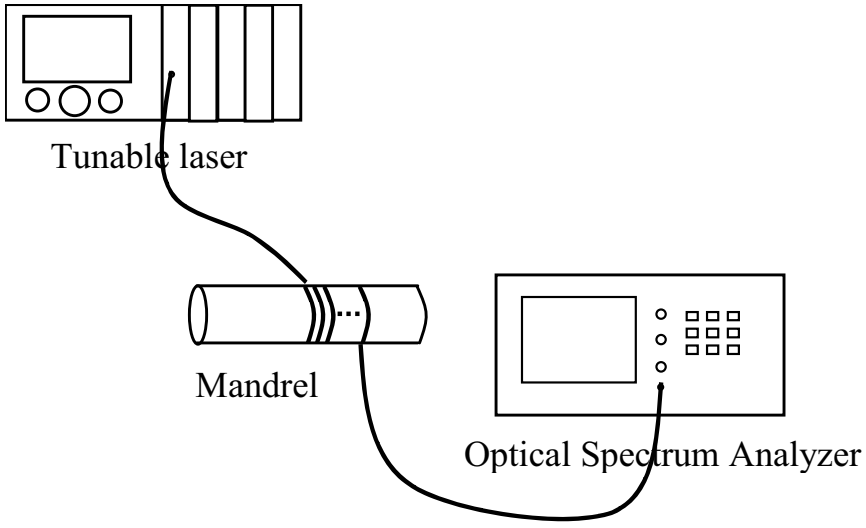

Figure 3. Experiment setup for measuring fiber bending loss.

It can be seen from Fig. 4 that the numerical calculation results using 3-D FV FD-BPM agree better with the measured bend losses than those obtained using scalar approximation method. However, in the above calculations the agreement between the 3-D FV FD-BPM based theoretical model and measured results for SMF28e suggests that the elastooptical correction factor (1.27@1550 nm) is required in both the models.

Where discrepancies do exist between the measured bend losses and 3-D FV FD-BPM theoretical model they can be explained as follow: 1) For calculating single mode fiber bend loss, there are some approximations, e.g., the curved interface between the coating and cladding is treated as an infinite plane and the light field within the core is approximated by the unperturbed field of the straight fiber with an infinite cladding. However as mentioned in Ref. [163], such an approximation can limit accuracy. However, bend loss has been widely investigated with BPM simulation in previously published work [164, 165], and the accuracy of calculated results output from BPM has yet to be firmly established; 2) experimental errors, for example environmental effects in the measurements and the accuracy of the bend radii.

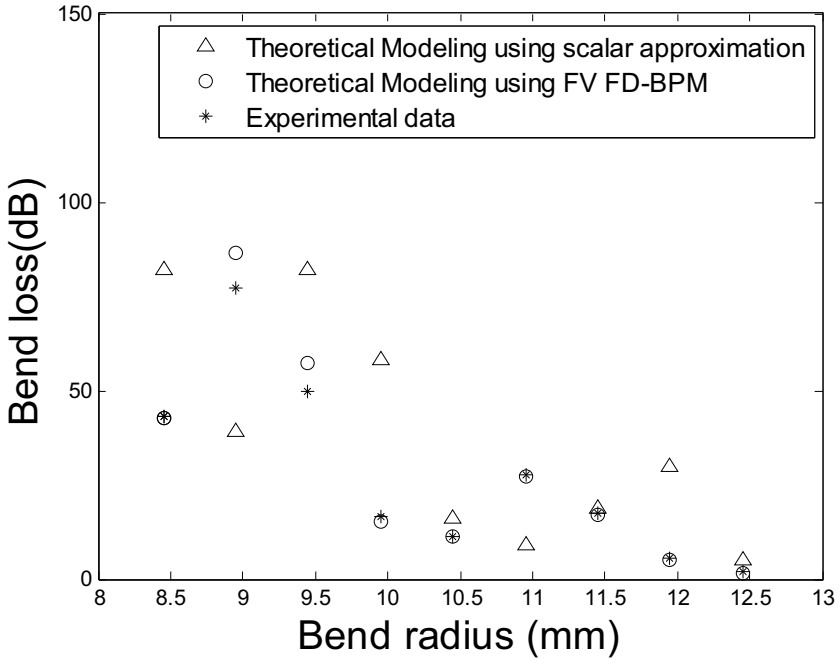

Figure 4. Calculated bend loss results on TE mode and measured bend loss for the bending radii range from 8 to 13 mm at the wavelength of 1550 nm, and the bending length is 20 turns.

Experimental PDL measurements were carried out based on the apparatus

shown in Fig. 3. A polarization controller is placed between the tunable laser and the bending fiber, thus the input signal from the tunable laser is polarization-controlled by the polarization controller, and the TE and TM responses were measured using an optical spectrum analyser and associated data-collection software. The experimental results and calculated PDL using FV FD-BPM (with a correction factor 1.27) shown in Table 11 are presented in Fig. 5, along with the calculated PDL results utilizing a scalar approximation method (with a correction factor 1.27). From Fig. 5, one can see that the measured PDL results show a good agreement with the calculated PDL results using FV FD-BPM, significantly better than the theoretical prediction from the scalar approximation method Where divergence between the experimental and theoretical BPM results occurs it is most likely caused by the changes of measuring environment and the experimental accuracy of the bend radius.

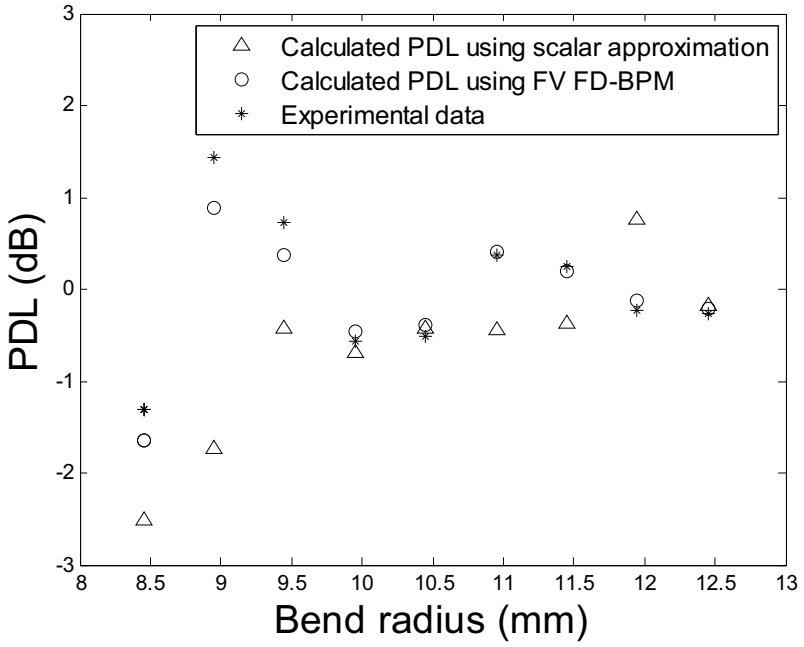

Figure 5. Calculated PDL results on TE mode and measured bend loss for the bending radii range from 8 to 13 mm at the wavelength of 1550 nm, and the bending length is 20 turns.

Conclusion

In conclusion, a 3-D FV FD-BPM based theoretical model for predicting the bend loss and PDL of a bending singlemode fiber has been presented. The good agreement between the theoretical BPM models and experimental results shows that the 3-D FV FD-BPM can be utilized to accurately predict both the bend loss and PDL of singlemode fiber, with a superior accuracy to a scalar approximation.

References

[151]. Mecozzi, A. and Shtaif, M., "The Statistics of Polarization-Dependent Loss in Optical Communication Systems," IEEE Photon. Technol. Lett. 14(3), 313-315 (2002).

[152]. Craig, R. M., "Accurate Spectral Characterization of Polarization-Dependent Loss," J. Lightwave. Technol. 21(2), 432-437 (2003).

[153]. Chen, L., Zhang, Z. and Bao, X., "Polarization dependent loss vector measurement in a system with polarization mode dispersion," Opt. Fiber Technol. 12, 251–254 (2006).

[154]. Zhou, J. Q., Dong, H., Aditya, S., Gong,Y. D., Shum, P., Guo X. and Ma, L., "Two-states method for polarization dependent loss measurement," Opt. Fiber Technol. 13, 139–142 (2007).

[155]. Wang, Q., Farrell, G., Freir, T., Rajan, G. and Wang, P., "Low-cost Wavelength Measurement based on a Macrobending Singlemode Fiber," Opt. Lett. 31(12), 1785-1787 (2006).

[156]. Wang, Q., Rajan, G., Wang P. and Farrell, G., "Polarization Dependence of Bend Loss for a Standard Singlemode Fiber," Opt. Express 15(8), 4909-4920 (2007).

[157]. Huang, W. P. and Xu, C. L., "Simulation of Three-Dimensional Optical Waveguides by a Full-Vector Beam Propagation Method," IEEE J. Quantum Electron., 29(10), 2639-2649 (1993).

[158]. Press, W. H., Teukolsky, S. A., Vetterling, W. T. and Flannery, B. P.,

"Numerical Recipes in C—The Art of Scientific Computing," 2nd ed. New York: Cambridge University Press, (1992).

[159]. Yamauchi, J., Ando, T. and Nakano, H., "Beam-propagation analysis of optical fibers by alternating direction implicit method," Electron. Lett. 27(18), 1663–1665 (1991).

[160]. Wang, Q., Farrell G. and Freir, T., "Theoretical and experimental investigations of macro-bend Losses for standard single mode fibers," Opt. Express 13(12), 4476-4484 (2005).

[161]. Huang, W. P., Xu, C. L., Lui, W. and Yokoyama, K., "The perfectly matched layer (PML) boundary condition for the beam propagation method," IEEE Photon. Technol. Lett. 8(5), 649–651 (1996).

[162]. Murakami, Y., and Tsuchiya, H., "Bending losses of coated single-mode optical fibers," IEEE J. Quantum Electron. QE-14(7), 495-501 (1978).

[163]. Renner, H., "Bending losses of coated single-mode fibers: a simple approach," J. Lightwave Technol. 10(5), 544-551 (1992).

[164]. Yamauchi, J., Kikuchi, S., Hirooka, T. and Nakano, H., "Beam propagation analysis of bent step-index slab waveguides," Electron. Lett. 26(12), 822–824 (1990).

[165]. Yamauchi, J., Ikegaya, M. and Nakano, H., "Analysis of bent asymmetric slab waveguides by the beam propagation method," Opt. Commun. 79(5), 291–294 (1990).

Appendix C

A Macrobending Singlemode Fiber Based Refractometer: Proposal and Design*

Keywords: Macrobending loss, singlemode fiber, SMF28, refractometer sensor, ratiometric

Abstract: A novel macrobending based all-fiber refractometer sensor with a simple optical configuration is proposed and modeled theoretically. The proposed fiber refractometer sensor consists of a half-loop structure of bare macrobending standard singlemode fiber (SMF28) with an optimally selected bending radius and reduced cladding radius. The well-known scalar approximation theory, which uses the perturbation method, is employed to design the proposed fiber refractometer sensor. An approach to improve the resolution of the refractometer is presented which shows that the refractometer should have an estimated resolution of 6.08×10^{-5} for a measurable refractive index range from 1.46 to 1.56. A possible system implementation for the proposed fiber refractometer using a ratiometric power measurement scheme is also presented.

Introduction

To date, a series of optical refractometers, such as Abbe and Rayleigh

* P. Wang, Y. Semenova, G. Farrell, "A Macrobending Singlemode Fiber Based Refractometer: Proposal and Design," Oral Presentation at the IOP Photon 08 Conference, Edinburgh, 26-28th August 2008.

refractometers have been developed and utilized for measuring the refractive indices and concentrations of liquids in biotechnology applications, such as the sugar content, blood protein concentration and salinity of urine in the area of experimental medicine. Optical refractometers are also widely employed in chemical applications for measuring fluid concentrations for commercial liquids such as petrochemicals, antifreeze, cutting fluid and industrial fluids.

Recent research has shown that optical fiber based sensors offer distinct advantages over conventional electronic sensors in a number of ways, such as immunity to electromagnetic interference, ease of fabrication and installation, safety in hazardous or explosive environments, high sensitivity and a long-distance remote measurement capability. So far, a number of fiber refractometers have been presented, such as fiber gap based Fabry-Perot structure [166], a refractometer based an abrupt taper Michelson interferometer based refractometer [167], multimode-singlemode-multimode fiber core diameter mismatch [168] and a refractometer based on a singlemode-multimode-singlemode fiber structure [169]. Fiber based refractometers offer the advantages of cost savings and the avoidance of possible contamination of the liquid by the refractometer. Here, as an alternative to these previously presented fiber optic refractometers, we propose and design a novel macrobending based bare fiber refractometer sensor with a simple bending half loop structure.

In this paper, a thorough theoretical investigation of the proposed bare fiber bending refractometer is presented, which includes: 1) theoretical modeling for the bending fiber refractometer; 2) an approach to improving the sensitivity of the refractometer, using a reduced cladding radius; and 3) a possible

measurement system implementation based on ratiometric power measurement. The proposed fiber refractometer offers a much simpler configuration by comparison with existing waveguide/fiber-based optical refractometer sensors with the advantage of ease of fabrication.

Theoretical modeling for a bending fiber refractometer

In 1978, H. Murakami et al [170] investigated the bending loss of a bent singlemode fiber, from which the coating had been stripped, when the fibre was immersed in a liquid. They found that the bend loss varied with the refractive indices of the liquid. Furthermore, G. J. Veldhuis et al [171, 172] reported a simple macrobending integrated optical waveguide based refractometer sensor, which was fabricated by a chemical vapor deposition photolithography technique and chemical etching process.

In this paper, the proposed fiber refractometer sensor consists of a half-loop structure of coating stripped macrobending fiber with a selected bending radius (see Fig. 6). It utilizes the characteristics of fiber macrobending loss in the bare fiber section. If the bare bending fiber section is immersed in a liquid after the coating is removed, the bending loss becomes a function of the liquid refractive index. By measuring the changes in macrobending loss, the refractive index of the surrounding liquid can be determined, assuming a suitable calibration has taken place.

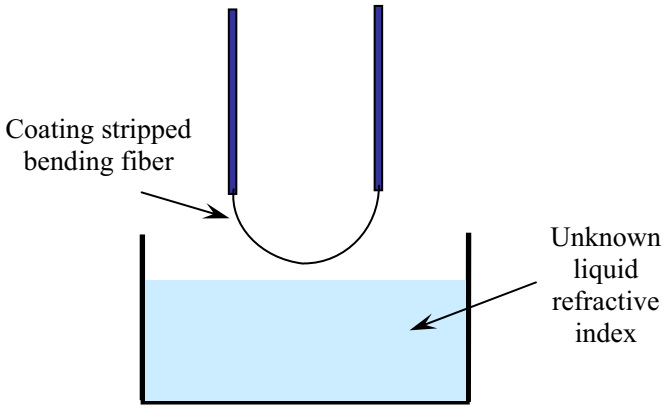

Figure 6. Schematic of macrobending singlemode fiber based refractometer sensor.

Theoretical models for predicting the macrobending loss in singlemode fibers can be categorized into two types: 1) the models originally developed by D. Marcuse [173] which treated the bending fiber as a fiber core-infinite cladding structure; 2) models for a bending fiber with a fiber core-cladding-infinite coating structure, encompassing a number of theoretical models and corresponding experimental investigations presented in Refs. [174-177]. These models considered the impact of the whispering-gallery mode (WGM) caused by the reinjected field arising at the cladding-coating interface. In this paper, the liquid under test is treated as an infinite coating for the bare bending fiber section; therefore, a simulation method utilizing a scalar approximation method (for a fiber core-cladding-infinite coating structure) presented in Ref. [177], is employed to simulate and optimize the proposed fiber refractometer sensor.

As a design example, Corning standard singlemode fiber (SMF28) is chosen, and the parameters of the fiber are the same as those presented in Ref. [177]. Given that the refractive index of the fiber core is 1.4504 at a wavelength of 1550 nm, the measurable minimum liquid refractive index is limited by the refractive index of the fiber core and thus must be greater than 1.4504. Furthermore it is

well known that the refractive indices of most petrochemicals lie in the range of 1.46~1.56, such as glycerol (1.47), turpentine (1.475), lubricating oils for automobiles (1.50) and clove oil (1.53). For the purpose of this study therefore the desired refractive index range of the proposed bent fiber refractometer is defined as 1.46 to 1.56. The calculated bending losses versus bending radii and refractive index of SMF28 singlemode fiber refractometer sample are presented in Fig. 7, where the proposed operating wavelength is 1550 nm.

In Figure 7, the simulated bending losses are calculated using the scalar approximation method, which can predict the light propagating through the whole bending fiber structure. The eigenmodes within the fiber bending section are determined by the refractive index of the liquid under test and fiber bending radius, thus the bending loss is affected correspondingly. Fig. 7 shows the relationship between bending loss and refractive index. For some bending radii the bending loss is relatively insensitive to refractive index changes, for example for a bending radius circa 10 mm. Such bend radii are clearly unsuitable for use in a refractometer. However bending radii in the vicinity of 6.6, 7.5 and 9 mm demonstrate a strong quasi-linear relationship between bend loss and refractive index and thus these bending radii are suitable for use in refractive index sensing. In particular for a bending radius circa 6.6 mm, one can see that the discrimination range (the difference in bend loss between an refractive index of 1.46 and 1.56) of the bending loss characteristic around this bending radius is the largest over the whole realizable bending radius range from 6 to 11 mm. Beyond 11 mm the refractometer sensitivity is too low, while below 6 mm, the risk of fiber breakage by excessive stress is too high.

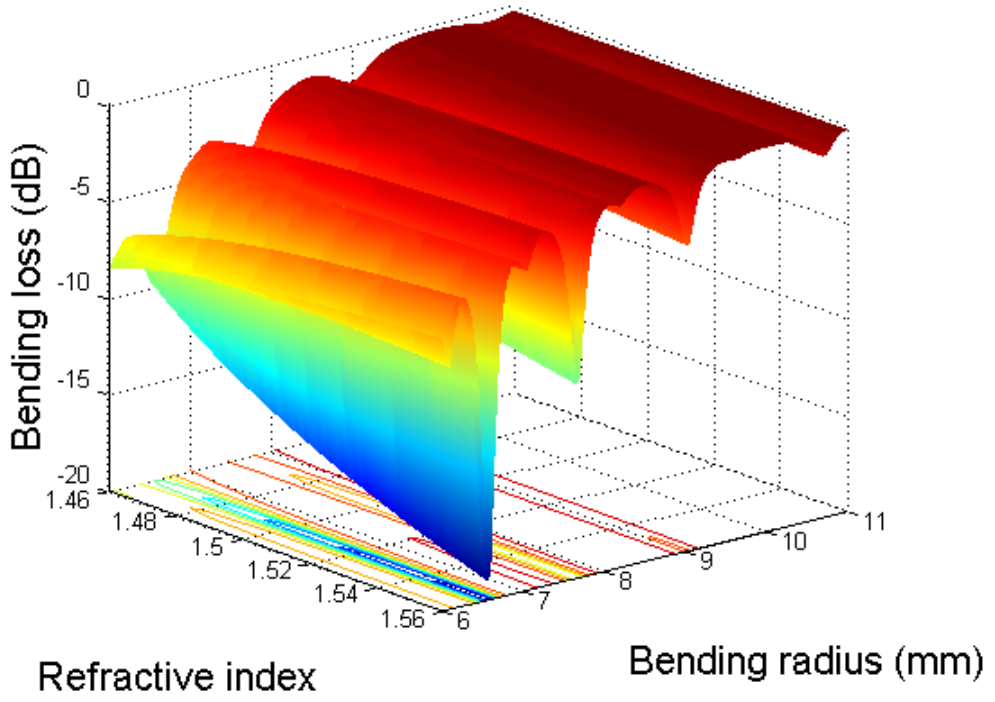

Figure 7. Calculated bend losses versus bend radius and refractive index for SMF28 singlemode fiber based refractometer, where the operating wavelength is 1550 nm.

To obtain the greatest sensitivity to changes in refractive index, one can see that the desired bending radius should lie in the vicinity of 6.6 mm. Therefore, bending losses as a function of measurable refractive index range around the bending radii of 6.6 mm are scanned in Fig. 8. From Fig. 8, it is clear that there is a one-to-one relationship between the bending losses and measureable refractive index when the bending radius varies around 6.6 mm. The bending loss curve at a bending radius of 6.6 mm shows the largest discrimination range from −9.67 to −18.784 dB, which is quasi-linear over the desired refractive index range.

It is well known that the typical precision of a commercial optical powermeter is about 0.01 dB, and the resolution of a fiber refractometer can be estimated as:

$$\text{Resolution} = \frac{\text{Measureable RI range}}{\text{Discrimination range}} \times \text{Typical precision of detector} \qquad \text{(A.13)}$$

Therefore a bending fiber refractometer sensor with a bend radius of 6.6 mm has an estimated resolution of 1.1×10^{-4}.

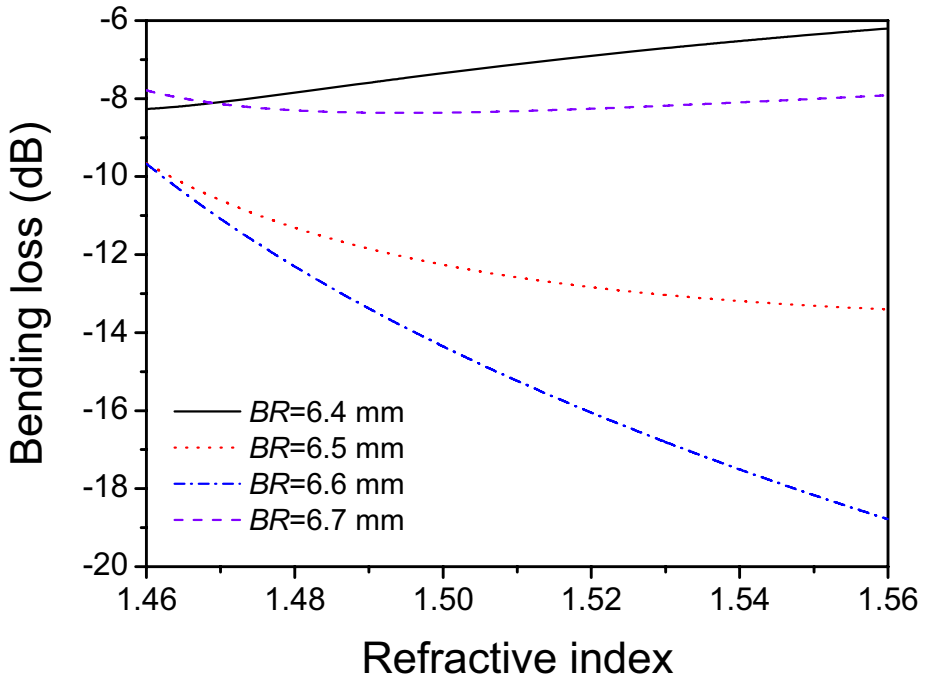

Figure 8. Calculated bending losses as a function of refractive index for bending radii in the vicinity of 6.6 mm, where the wavelength is 1550 nm.

Achieving improved resolution for the fiber refractometer sensor

In order to achieve high sensitivity for the measurement of the refractive index we choose a bending radius of 6.6 mm. From the developed models based on the scalar approximation method for predicting macrobending losses of singlemode fibers [174-177], it was known that the bending losses depend not only on specific bending radii, but also the fiber cladding radii. In addition, decreasing the cladding radius will also have the beneficial effect of reducing the bending induced mechanical stress on the fiber. It should be noted that in practice a

possible experimental approach to achieving a reduced fiber cladding radius is chemical etching of the fiber using HF acid.

Assuming a bending radius at 6.6 mm, we wish to find an appropriate fiber cladding radius with an improved sensitivity using a simulation model. In Fig. 9, the calculated bending losses versus cladding radii and refractive index for a SMF28 singlemode fiber based refractometer are presented, where the bending radius is defined at 6.6 mm, and the wavelength is 1550 nm. From Fig. 9, one can see that the bending loss is a strong function of refractive index and shows a quasi-linear relationship between the bending loss and the liquid refractive index when the cladding radii are close to 31, 38, 44 and 48 μm, etc.

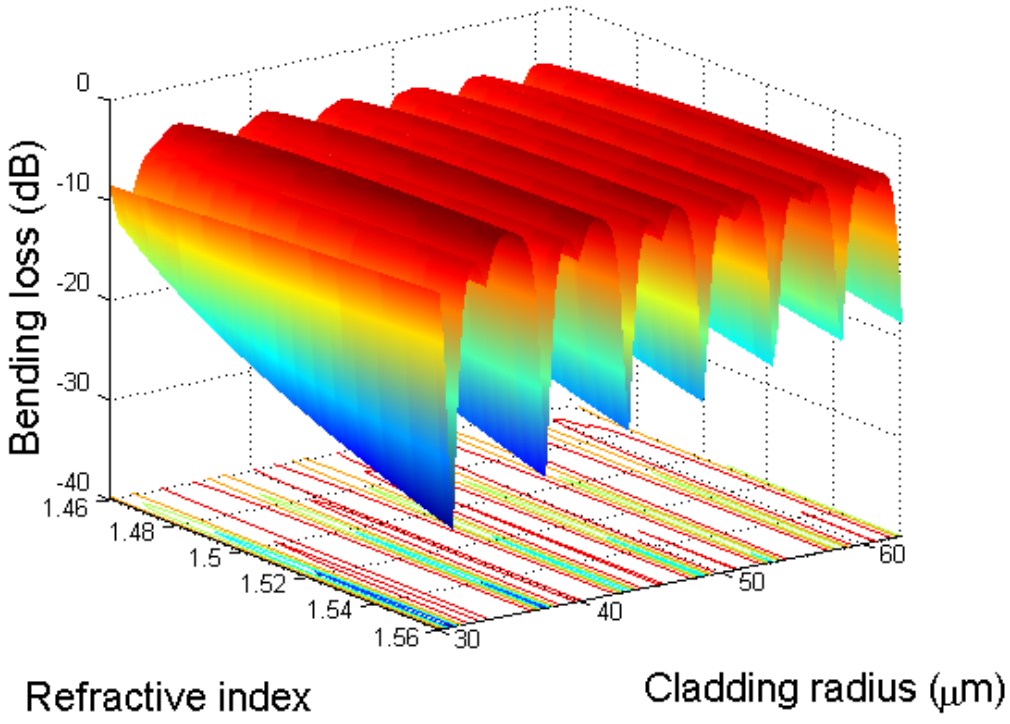

Figure 9. Calculated bending loss versus cladding radii and refractive index for SMF28 singlemode fiber based refractometer, the bending radius is 6.6 mm, and the wavelength is 1550 nm.

In Fig. 9, one can also see that the discrimination range of the bending loss at a cladding radius of 31 μm is the largest by comparison with the other cladding

radii. To better illustrate this, four cladding radii for the bent fiber refractometer sensor are chosen. The calculated bending losses of these fiber refractometer sensors with these four cladding radii are shown in Fig. 10. One can see that the discrimination range with a cladding radius of 31 μm is significantly better than that of the initial designed structure shown in Fig. 8. The discrimination range of a bending fiber refractometer sensor with a cladding radius of 31 μm is 16.46 dB, which ranges from -13.257 dB to -29.717 dB, significantly better than the other cladding radii. Using the formula (A.13) presented above, for the improved refractometer the estimated resolution is 6.08×10^{-5}, significantly better than the resolution of 1.1×10^{-4} presented in Section C.2, for a fiber with a conventional 62.5 μm cladding radius.

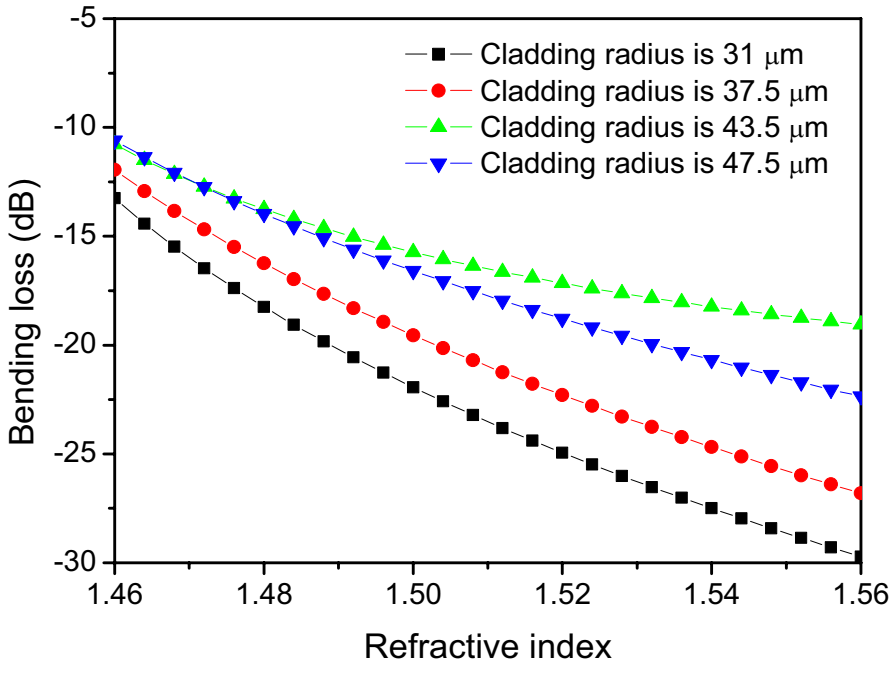

Figure 10. Calculated bending losses as a function of refractive index at a bending radius of 6.6 mm, where the wavelength is 1550 nm and the cladding radius is 31, 37.5, 43.5 and 47.5 μm.

Possible measurement system implementation

In previously published work [178, 179], the principle of a macrobending fiber based edge filter for a rapid wavelength measurement application was investigated and presented theoretically and experimentally. This system used a ratiometric power measurement technique, which is again utilized here. Compared to a conventional measurement system, a ratiometric measurement system has several advantages including simple configuration, lower fabrication cost and independence from input power variations.

Figure 11 shows the schematic configuration of a ratiometric refractive index measurement system, which involves a splitter, a bare bending fiber refractometer sensor probe, a reference arm and two photodetectors. One splitter arm connects to the bending fiber refractometer sensor, while the other arm acts as a reference arm. Both arms are terminated in photodetectors to measure optical power levels. Given the refractive index dependence of fiber bending loss, the ratio of the measured power levels at the two photodetectors is a strong function of measured refractive index. Therefore with a suitable calibration refractive index can be measured.

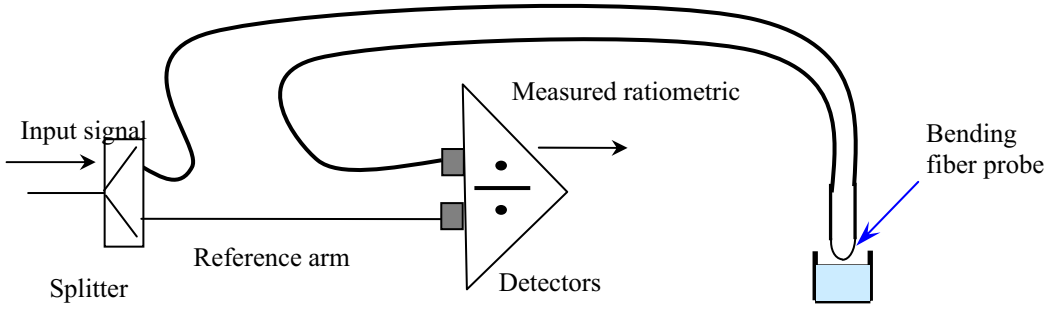

Figure 11. Schematic of bending fiber refractometer in a ratiometric measurement system.

To estimate the detectable resolution of the ratiometric measurement system, while taking into account the noise added by opto-electronic conversion, a

simulation is carried out using the approach described in [178, 179]. It is assumed that the input signal from the tunable laser source has a wavelength at 1550 nm (and the source signal-to-noise ratio is 60 dB), the input power is 0 dBm and the corresponding fluctuations due to the opto-electronic conversion noise are 0.01 dB.

The result of the simulation is presented in Fig. 12, in which the output ratio is calculated over a series of 1000 measurements assuming the liquid refractive index increments in value by an amount equal to the estimated refractive index resolution, calculated earlier. For the ratiometric measurement system to reliably detect this minimum refractive index change, the change in the output ratio should be greater than the ratio fluctuation caused by opto-electronic conversion noise. From the calculated results presented in Fig. 12, it can be seen that that the fluctuation of the ratio is less than 0.01 dB and that a refractive index change of 6.08×10^{-5} can be detected clearly in the system output ratio at a measured refractive index of 1.50.

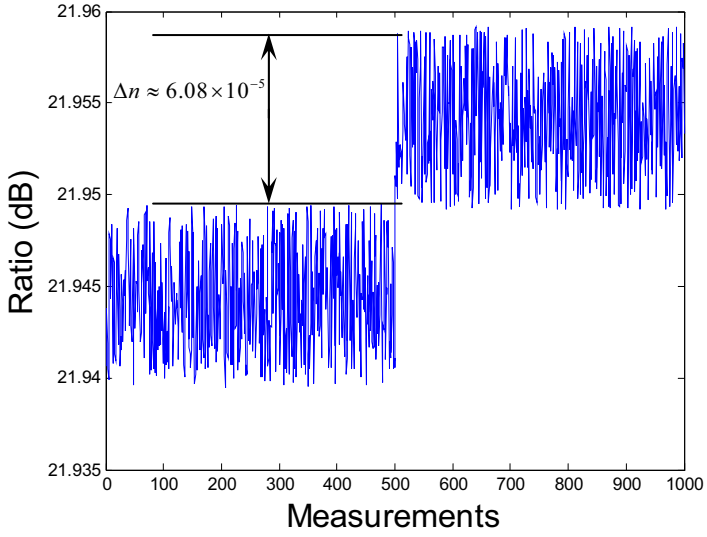

Figure 12. Calculated output power ratio, including receiver noise as in [179], showing that a refractive index increment equal to the estimated resolution is clearly detectable at a refractive index of 1.50.

Conclusion

In conclusion, we have proposed and presented a novel all-fiber macrobending refractometer sensor for measuring the unknown refractive index of liquid sample. The well-known scalar approximation method for predicting the macrobending loss of singlemode fiber has been utilized for numerical simulation. A possible ratiometric measurement system implementation is also investigated theoretically. By adjusting the cladding radius, an improved estimated resolution of 6.08×10^{-5} over a measureable refractive index range from 1.46 to 1.56 can be achieved, for a cladding radius of 31 μm. Corresponding experimental work for this refractometer sensor is ongoing.

References

[166]. T. Wei, Y. Han, Y. Li, H-L. Tsai and H. Xiao, "Temperature-insensitive miniaturized fiber inline Fabry-Perot interferometer for highly sensitive refractive index measurement." Opt. Express, Vol. 16, No. 8, pp. 5764-5769 (2008).

[167]. Z. Tian, S. S-H. Yam and H-P. Loock, "Refractive index sensor based on an abrupt taper Michelson interferometer in a single-mode fiber." Opt. Lett., Vol. 33, No. 10, pp. 1105-1107 (2008).

[168]. J. Villatoro and D. Monzón-Hernández, "Low-cost optical fiber refractive-index sensor based on core diameter mismatch." J. Lightwave Technol., Vol. 24, No. 3, pp. 1409–1413 (2006).

[169]. Q. Wang and G. Farrell, "All-fiber multimode-interference-based refractometer sensor: proposal and design." Opt. Lett., Vol. 31, No. 3, pp. 317-319 (2006).

[170]. Y. Murakami and H. Tsuchia, "Bending losses of coated single-mode optical fibres," IEEE J. Quant. Electron., Vol. QE-14, No. 7, pp. 495-501 (1978).

[171]. G. J. Veldhuis and P. V. Lambeck, "Highly-sensitive passive integrated

optical spiral-shaped waveguide refractometer," Appl. Phys. Lett., Vol. 71, No. 20, pp. 2895–2897, 1997.

[172]. G. J. Veldhuis, L. E. W. van der Veen, and P. V. Lambeck, "Integrated optical refractometer based on waveguide bend loss," J. Lightwave Technol., Vol. 17, No. 5, pp. 857–864, 1999.

[173]. D. Marcuse, "Curvature loss formula for optical fibers," J. Opt. Soc. Am., Vol. 66, No. 3, pp. 216-220 (1976).

[174]. I. Valiente and C. Vassallo, "New formalism for bending losses in coated single-mode optical fibres," Electron. Lett., Vol. 25, No. 22, pp. 1544-1545 (1989).

[175]. H. Renner, "Bending losses of coated single-mode fibers: a simple approach," J. Lightwave Technol., Vol. 10, No. 5, pp. 544-551 (1992).

[176]. L. Faustini and G. Martini, "Bend loss in single-mode fibers," J. Lightwave Technol., Vol. 15, No.4, pp. 671-679 (1997).

[177]. Q. Wang, G. Farrell, and T. Freir, "Theoretical and experimental investigations of macro-bend losses for standard single mode fibers," Opt. Exp., Vol. 13, No. 12, pp. 4476-4484 (2005).

[178]. Q. Wang, G. Farrell, T. Freir, G. Rajan and P. Wang, "Low-cost Wavelength Measurement based on a Macrobending Single-mode Fiber," Optics Letters, Vol. 31, No. 12, pp. 1785-1787, 2006.

[179]. Q. Wang, G. Rajan, G. Farrell, P. Wang, Y. Semenova and T. Freir, "Macrobending fiber loss filter, ratiometric wavelength measurement and application," Measurement Science and Technology, Vol. 18, pp. 3082-3088, 2007.